



AMERICAN UNIVERSITY OF BEIRUT

NOVEL ORGANIC DYES FOR DYE SENSITIZED SOLAR  
CELLS

by  
VANESSA ANTOINE EL BITAR NEHME

A thesis  
submitted in partial fulfillment of the requirements  
for the degree of Master of Science  
to the Department of Chemistry  
of the Faculty of Arts and Sciences  
at the American University of Beirut

Beirut, Lebanon  
April, 2019

AMERICAN UNIVERSITY OF BEIRUT

NOVEL ORGANIC DYES FOR DYE SENSITIZED SOLAR  
CELLS

by  
VANESSA ANTOINE EL BITAR NEHME

Approved by:

---

Dr. Tarek Ghaddar, Professor  
Department of Chemistry

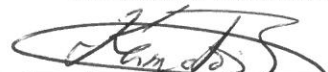
Advisor



---

Dr. Kamal Bouhadir, Professor  
Department of Chemistry


Member of Committee



---

Dr. Pierre Karam, Assistant Professor  
Department of Chemistry

Member of Committee



---

Date of thesis defense: April 5, 2019

# AMERICAN UNIVERSITY OF BEIRUT

## THESIS, DISSERTATION, PROJECT RELEASE FORM

Student Name:

El Riker Ndim

Last

Vanessa

First

Antoine

Middle

Master's Thesis  
Dissertation

Master's Project

Doctoral

I authorize the American University of Beirut to: (a) reproduce hard or electronic copies of my thesis, dissertation, or project; (b) include such copies in the archives and digital repositories of the University; and (c) make freely available such copies to third parties for research or educational purposes.

I authorize the American University of Beirut, to: (a) reproduce hard or electronic copies of it; (b) include such copies in the archives and digital repositories of the University; and (c) make freely available such copies to third parties for research or educational purposes

after : **One ---- year from the date of submission of my thesis, dissertation, or project.**

**Two ---- years from the date of submission of my thesis, dissertation, or project.**

**Three ---- years from the date of submission of my thesis, dissertation, or project.**

Vanessa

Signature

11-4-2019

Date

## ACKNOWLEDGMENTS

Firstly, I would like to express my heartiest and sincerest gratitude to my respected advisor Prof. Tarek Ghaddar. This work would not have been possible without his continuous support and undying guidance throughout my master's years. I consider myself more than lucky to have had the chance to be part of his research group.

Second, I would like to thank my committee members Prof. Kamal Bouhadir and Prof. Pierre Karam for their valuable suggestions and comments on my work.

I would also like to extend my regards to my classmates, lab mates and friends at AUB. The time we spent together is unforgettable. Also, a particular thank you goes to my friends outside AUB for always being by my side.

Furthermore, I am most indebted to my beloved parents for providing me with the love and support and most importantly the unlimited sacrifices you do for me and my sister. You mean the world to me.

Finally, I want to thank my twin sister Melissa, the closest person to my heart. I am more than blessed to have you as my sister and best friend and I'm beyond grateful that we stand by each other's side in every step of our lives. Thank you for always inspiring me and pushing me forward.

# AN ABSTRACT OF THE THESIS OF

Vanessa Antoine El Bitar Nehme for Master of Science  
- Major: Chemistry

Title: Novel Organic Dyes for Dye Sensitized Solar Cells

Interest in dye sensitized solar cells (DSSCs) has increased in the last 26 years because of their application in solar energy conversion. This photovoltaic device has attracted the attention of many researchers because of its relatively good efficiency, its eco-friendliness, and its low cost of fabrication.

Many attempts were made to synthesize organic dyes as sensitizers in a DSSC instead of metal-based ones because of their high molar extinction coefficients that become important in cobalt-based DSSCs. Hence, we plan to synthesize organic dyes having the form donor-  $\pi$  -acceptor- $\pi$  with either a terminal pyridine or carboxylic acid anchoring group, Scheme 1. The pyridyl-based dyes will be studied as co-adsorbents with commercially available carboxylic acid-based dyes and the effect of co-sensitization on the DSSCs' efficiencies. The usage of the proposed electron-acceptor units have never been studied in any organic sensitizer in DSSCs, and therefore the carboxylic and the pyridyl based dyes with these novel electron accepting units will be incorporated, one at a time, in a fully assembled DSSC, and the efficiencies of these cells will be measured and analyzed.

# CONTENTS

ACKNOWLEDGMENTS .....	v
ABSTRACT.....	vi
LIST OF ILLUSTRATIONS.....	x
LIST OF TABLES .....	xiv

## Chapter

1. INTRODUCTION .....	1
1.1. Light from the Sun.....	1
1.2. Brief Overview of Photovoltaics .....	2
1.3. Dye-Sensitized Solar Cells .....	3
1.3.1. Structure and Principle of Operation .....	3
1.3.2. Electron Transfer Processes.....	6
1.3.3. Basic Parameters of DSSCs.....	9
1.3.3.1. Incident Photon-to-Current Conversion Efficiency (IPCE) .....	9
1.3.3.2. Open-Circuit Voltage ( $V_{OC}$ ) .....	10
1.3.3.3. Short-Circuit Current ( $J_{SC}$ ) .....	10
1.3.3.4. Fill Factor ( $ff$ ) .....	11
1.3.3.5. Overall Conversion Efficiency ( $\eta$ ) .....	11
1.3.4. Basic Components of DSSCs .....	11
1.3.4.1. Working Electrode .....	11
1.3.4.2. Counter Electrode .....	13
1.3.4.3. Electrolyte .....	14
1.3.4.4. Sensitizer .....	19
1.4. Electrochemical Impedance Spectroscopy (EIS).....	28
1.5. Objective of thesis .....	30

2. EXPERIMENTAL SECTION.....	32
2.1. Materials and Instrumentation .....	32
2.2. Computational Studies.....	33
2.3. Dye Synthesis .....	33
2.3.1. Synthetic Procedure of T220 .....	33
2.3.1.1. Synthesis of 1-(2-Ethylhexyl)-1 <i>H</i> -pyrrole-2, 5-Dione <b>(1)</b> .....	33
2.3.1.2. Synthesis of 3, 6-Bis (5-bromo-2-thienyl)-1, 2, 4, 5- tetrazine <b>(2)</b> .....	34
2.3.1.3. Synthesis of 1, 4-Bis (5-bromo-2-thienyl)-6-(2- ethylhexyl)-5 <i>H</i> -pyrrolo [3, 4- <i>d</i> ] pyridazine-5,7(6 <i>H</i> )- dione <b>(3)</b> .....	34
2.3.1.4. Synthesis of T220 .....	35
2.3.2. Synthetic Procedure of T221 .....	36
2.3.2.1. Synthesis of 2, 5-Dihydro-3, 6-di-2-thienylpyrrolo [3, 4- <i>c</i> ] pyrrole-1, 4-dione <b>(4)</b> .....	36
2.3.2.2. Synthesis of 2, 5-Diethylhexyl-3, 6-dithiophen-2- ylpyrrolo [3, 4- <i>c</i> ] pyrrole-1, 4-dione <b>(5)</b> .....	36
2.3.2.3. Synthesis of 2,5-Diethylhexyl-3,6-bis(5- bromothiophen-2-yl)pyrrolo[3,4- <i>c</i> ]-pyrrole-1,4- dione <b>(6)</b> .....	37
2.3.2.4. Synthesis of T221 .....	38
2.3.3. Synthetic Procedure of T222 .....	39
2.3.3.1. Synthesis of (E)- 4-(5-Bromo-2-thienyl)-4-oxo-2- butenoic acid <b>(7)</b> .....	39
2.3.3.2. Synthesis of (E)-5,5-(5-bromo-2- thienyl)bifuranylidenedione <b>(8)</b> .....	39
2.3.3.3. Synthesis of 2 <i>H</i> -Pyrrol-2-one, 5-(5-bromo-2-thienyl)- 3-[5-(5-bromo-2-thienyl)-1-(2-ethylhexyl)-1,2- dihydro-2-oxo-3 <i>H</i> -pyrrol-3-ylidene]-1-(2-ethylhexyl)- 1,3-dihydro-, (3 <i>E</i> ) <b>(9)</b> .....	40
2.3.3.4. Synthesis of T222 .....	40
2.4. Solar Cell Fabrication .....	41
3. RESULTS AND DISCUSSION.....	44
3.1. Dye Design .....	44
3.1.1. Synthetic Procedure of T220 .....	44



3.1.2. Synthetic Procedure of T221 .....	46
3.1.3. Synthetic Procedure of T222 .....	47
3.2. Optical and Electrochemical Properties.....	49
3.3. Computational Studies.....	53
3.4. Photovoltaic Performance.....	57
3.4.1. Individual Dye Performance.....	57
3.5. Dye Loading Measurements .....	60
3.5.1. Co-adsorption with T220 and DB.....	61
3.5.2. Co-adsorption with T221 and D35 .....	64
3.6. Density Functional Theory Calculations (DFT) .....	66
3.7. Photovoltaic Performance.....	68
3.7.1. Co-adsorbed T220 and DB device.....	68
3.8. EIS of T220+DB-based device .....	70
3.9. Photovoltaic Performance .....	73
3.9.1. Co-adsorbed T221 and D35 device .....	73
 4. CONCLUSION.....	 76
 5. SUPPORTING INFORMATION.....	 78
 REFERENCES .....	 89

## ILLUSTRATIONS

Figure	Page
1. Basic components in a DSSC.....	4
2. Working principle of a DSSC.....	5
3. A schematic representation of the electron transfer processes in a DSSC.....	9
4. Optimized photoanode for DSSCs.....	13
5. Structures of NI6 and NI2, respectively.....	21
6. Structures of 1 and HKK-BTZ4, respectively.....	23
7. Molecular structure of <i>i</i> Pr-PMI with R=2, 6-diisopropylphenyl.....	24
8. Molecular structure of PT-2.....	24
9. Molecular structure of R6.....	25
10. Thienyl DPP chromophores with R as the attached alkyl chains.....	26
11. Structures of D35 and DB, respectively.....	27
12. Nyquist plot and the equivalent circuit of the DSSC.....	29
13. Molecular structure of the three proposed dyes.....	31
14. Structure of a thiophene containing Pechmann dye.....	48
15. UV-vis absorption (solid) and emission (dotted) spectra of a) T220, b) T221 and c) T222 in THF ( $\lambda_{ex}$ = 434 and 624 nm for T220 and T221, respectively).....	50
16. Differential pulse voltammetry of a) T220 b) T221 and c) T222.....	52
17. Schematic representation of the energy levels of T220, T221 and T222.....	53
18. Energy level diagram of T220, T221, and T222.....	56

19.	A) <i>I-V</i> curve of the DSSCs based on the individual T220, T221 and T222 dyes under illumination and in darkness, B) incident photon-to-current conversion efficiency spectra.....	59
20.	Molecular structures of D35 and DB.....	61
21.	Absorption spectra of T220, BD, and T220-BD anchored on the TiO <sub>2</sub> film.....	62
22.	Absorbance spectra of the desorbed films of the individual T220 and DB and the co-sensitized T220-DB dyes.....	63
23.	Absorption spectra of T221, D35, and T221-D35 anchored on the TiO <sub>2</sub> film.....	64
24.	Absorbance spectra of the desorbed films of the individual T221 and D35 and the co-sensitized T221-D35 dyes.....	65
25.	The calculated vertical distances in T220 and DB.....	67
26.	The calculated vertical distances in D35 and T221 dyes.....	67
27.	A) <i>I-V</i> curve of the DSSCs based on the individual T220, DB, and the co-sensitized T220-DB under illumination and in darkness, B) incident photon-to-current conversion efficiency spectra.....	69
28.	A) Charge transfer resistance values obtained from EIS and B) chemical capacitance values of T220, DB and the co-sensitized T220-DB cells.....	72
29.	Electron lifetime values obtained from EIS for the T220, DB and the co-sensitized T220-DB cells.....	73
30.	A) <i>I-V</i> curve of the DSSCs based on the individual T221, D35, and the co-sensitized T221-D35 under illumination and in darkness, B) incident photon-to-current conversion efficiency spectra.....	74
31.	<sup>1</sup> H NMR of 1-(2-ethylhexyl)-1 <i>H</i> -pyrrole-2, 5-dione in CDCl <sub>3</sub> ( <b>1</b> ).....	77
32.	<sup>1</sup> H NMR of 3, 6-Bis (5-bromo-2-thienyl)-1, 2, 4, 5-tetrazine in CDCl <sub>3</sub> ( <b>2</b> )...	78
33.	<sup>1</sup> H NMR of 1,4-Bis(5-bromo-2-thienyl)-6-(2-octyldodecyl)-5 <i>H</i> -pyrrolo[3,4- <i>d</i> ]pyridazine-5,7(6 <i>H</i> )-dione in CDCl <sub>3</sub> ( <b>3</b> ).....	79

34.	<sup>1</sup> H NMR of T220 in DMSO.....	80
35.	<sup>1</sup> H NMR of 2, 5-Dihydro-3, 6-di-2-thienylpyrrolo [3, 4-c] pyrrole-1, 4-dione_in CDCl <sub>3</sub> (5).....	81
36.	<sup>1</sup> H NMR of 2,5-Diethylhexyl-3,6-bis(5-bromothiophen-2-yl)pyrrolo[3,4-c]-pyrrole-1,4-dione in CDCl <sub>3</sub> (6).....	82
37.	<sup>1</sup> H NMR of T221 in Acetone- <i>d</i> <sub>6</sub> .....	83
38.	<sup>1</sup> H NMR of (E)- 4-(5-Bromo-2-thienyl)-4-oxo-2-butenic acid in CDCl <sub>3</sub> (7).....	84
39.	<sup>1</sup> H NMR of 2 <i>H</i> -Pyrrol-2-one, 5-(5-bromo-2-thienyl)-3-[5-(5-bromo-2-thienyl)-1-(2-ethylhexyl)-1,2-dihydro-2-oxo-3 <i>H</i> -pyrrol-3-ylidene]-1-(2-ethylhexyl)-1,3-dihydro-, (3 <i>E</i> ) in CDCl <sub>3</sub> (9).....	85
40.	<sup>1</sup> H NMR of T222 in Acetone- <i>d</i> <sub>6</sub> .....	86
41.	Mass spectrometry of T220.....	87
42.	Mass spectrometry of T221.....	87
43.	Mass spectrometry of compound (9).....	88
44.	Mass spectrometry of T222.....	88

## SCHEMES

Scheme		Page
1.	Synthetic scheme of T220 where a) dichloromethane, acetic anhydride, sodium acetate; b) hydrazine, sulfur, ethanol, sodium nitrite, acetic acid; c) diphenyl ether at 150°C; d) C <sub>5</sub> H <sub>6</sub> BNO <sub>2</sub> , C <sub>52</sub> H <sub>66</sub> BNO <sub>2</sub> , Pd(OAc) <sub>2</sub> , PPh <sub>3</sub> , K <sub>2</sub> CO <sub>3</sub> , dioxane:THF:H <sub>2</sub> O.....	45
2.	Synthetic scheme of T221 where a) tertiary amyl alcohol, potassium tert-butoxide, diethyl succinate; b) K <sub>2</sub> CO <sub>3</sub> , 2-ethylbromohexane, 18-crown ether, DMF; c) NBS, acetic acid and chloroform; d) C <sub>5</sub> H <sub>6</sub> BNO <sub>2</sub> , C <sub>52</sub> H <sub>66</sub> BNO <sub>2</sub> , Pd(OAc) <sub>2</sub> , PPh <sub>3</sub> , K <sub>2</sub> CO <sub>3</sub> , dioxane:THF:H <sub>2</sub> O.....	47
3.	Synthetic scheme of T222 where a) AlCl <sub>3</sub> , dichloromethane; b) CuCl, NH <sub>4</sub> Cl, acetic anhydride; c) 2-ethyl-1-hexamine, dichloromethane; d) C <sub>5</sub> H <sub>6</sub> BNO <sub>2</sub> , C <sub>52</sub> H <sub>66</sub> BNO <sub>2</sub> , Pd(OAc) <sub>2</sub> , PPh <sub>3</sub> , K <sub>2</sub> CO <sub>3</sub> , dioxane:THF:H <sub>2</sub> O .....	48

## TABLES

Table	Page
1. Optical and electrochemical properties of T220, T221, and T222 dyes.....	53
2. Frontier molecular orbitals of T220, T221, and T222.....	55
3. Calculated spectra of T220, T221, and T222, respectively.....	56
4. Photovoltaic performance of T220, T221, and T222 devices obtained from the <i>I-V</i> curves.....	60
5. Dye loading measurements of the individual and co-sensitized TiO <sub>2</sub> films <sup>a</sup> .....	63
6. Dye loading measurements of the individual and co-sensitized TiO <sub>2</sub> films <sup>a</sup> .....	65
7. Photovoltaic performance of the T220, BD, and co-sensitized T220-DB based devices obtained from the <i>I-V</i> curves.....	70
8. Photovoltaic performance of the T221, D35, and co-sensitized T221-D35 based devices obtained from the <i>I-V</i> curves.....	75

# CHAPTER 1

## INTRODUCTION

### 1.1. Light from the Sun

With the rapid technological advancements and the constantly growing world population, the demand of energy is gradually rising and the global consumption is expected to double in the next 50 years.<sup>1</sup> Currently, an estimate of 17.7 Terawatts is being consumed from different sources of energy, namely fossil fuel (oil, coal, natural gas). The combustion of fossil fuel causes irreversible environmental risks like the emission of greenhouse gases which might as well lead to climate changes and global warming. Meanwhile, the world will shortly come to an end of fossil fuel due to its limited supply and being non-renewable. Therefore, it is crucial to find a sustainable energy that could meet our daily energy needs, and a most likely possible alternative would be the solar energy.<sup>2</sup>

Among the many renewable sources of energy: sun, biomass, wind power, geothermal heat, and tidal power, energy from the sun is by far the most abundant and exploitable resource. The solar energy that strikes the earth's surface annually is almost  $3 \times 10^{24}$  J which is about  $10^4$  times more than the world's need to consume energy.<sup>3</sup> To this end, the main focus over the past decades is to make use of this renewable energy, and until now photovoltaic technologies are the potential candidates for solar energy conversions.

## 1.2. Brief Overview of Photovoltaics

Photovoltaic devices convert solar energy into electricity through the generation of an electron-hole pair at the interface of two different materials. Based on the material used, maximum power conversion efficiency and the cost of fabrication, photovoltaic solar cells can be categorized into three generations.

First generation PVs use high purity materials (single crystals) with expensive processing cost. It is dominated by a single p-n junction, mainly silicon, with a maximum power conversion efficiency of 25%.<sup>4</sup> Second generation PVs have lower conversion efficiency, however less material is used with a much reduced cost. Thin film PVs like amorphous silicon, CdTe (Cadmium telluride), and CIGS (Copper indium gallium selenide) fall in this group where the thickness of the semiconductor material is reduced to few micrometers. The major drawback of these two generations (single p-n junction cells) is that their conversion efficiency is limited by Shockley-Queisser theoretical limit of 30%.<sup>5</sup> The third generation PVs give efficiencies above Shockley-Queisser limit and include polymer-based cells, multi-junction cells, quantum dot based cells and dye-sensitized solar cells. Dye-sensitized solar cells are considered the most prominent third generation solar cells. In contrary to the conventional silicon-based solar cell, where the semiconductor has both tasks of absorbing light as well as charge transport; in DSSCs the two tasks are separated. Because of their low cost, ease of fabrication, and eco-friendliness, DSSCs have gained a great deal of attention and intensive research interest over the past few decades. The following section will provide more details on DSSCs.

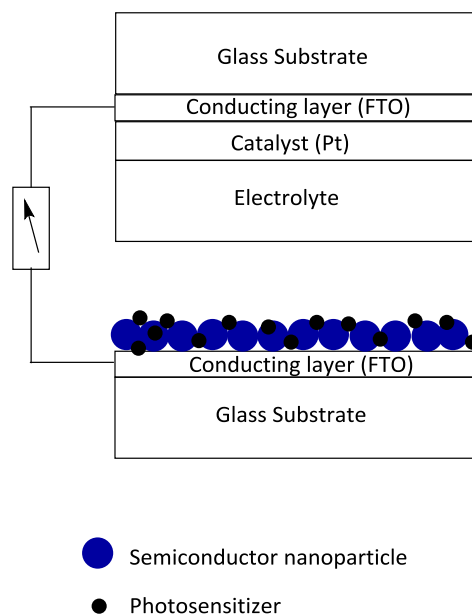


### 1.3. Dye-Sensitized Solar Cells

The concept and operating mechanism of dye-sensitized solar cells dates back to the 1960s when Gerischer and Tributsch first introduced a wide band gap metal-oxide semiconductor ZnO with dyes such as Rose Bengal as photosensitizers.<sup>6</sup> However, the efficiency of these cells remained low for several years. A breakthrough in this research field occurred in 1991 when O'Regan and Grätzel initiated the use of a mesoporous nanometer sized TiO<sub>2</sub> layer as the semiconductor together with a ruthenium based sensitizer giving an overall efficiency up to 7%.<sup>7</sup> This pioneering work opened up a new era in the field of DSSCs to find ways of improving its efficiency and stability. To date, thousands of different metal-based as well as metal free organic dyes have been molecularly designed and engaged in DSSCs with efficiencies reaching up to 15%.<sup>8-10</sup>

#### *1.3.1. Structure and Principle of Operation*

A typical DSSC consists of: 1) a transparent conductive oxide (TCO) glass substrate, usually fluorine-doped tin-oxide (FTO) which acts as the photoanode; 2) a wide band gap semiconductor material, typically TiO<sub>2</sub>, deposited on the glass substrate for electron transfer; 3) a layer of dye sensitizer adsorbed on the surface of the metal oxide layer for photon harvesting; 4) a counter electrode which is coated with a catalyst (usually, platinum) on a second TCO substrate; 5) and an electrolyte system consisting of an organic solvent and a redox couple (typically, I<sup>-</sup>/I<sub>3</sub><sup>-</sup>).<sup>11-12</sup> Figure 1 shows the basic components in a DSSC.



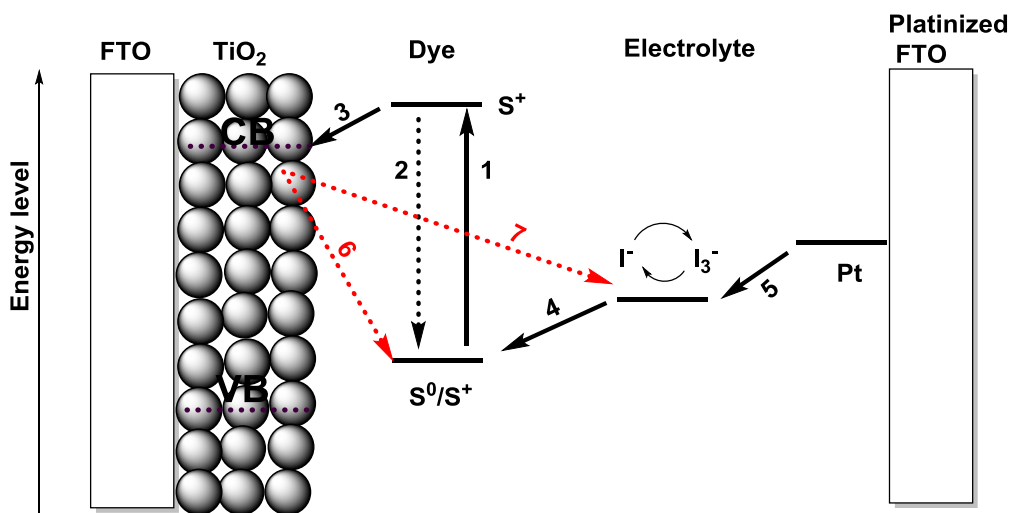
**Figure 1:** Basic components in a DSSC.

The working principle of a DSSC is illustrated in Figure 2. Under light illumination, the dye sensitizer (S) absorbs the incident photon where electrons are photoexcited from the HOMO to the LUMO of the dye leaving it in its electronically excited state ( $S^*$ ) (equation 1). The excited dye can relax back to the ground state (equation 2) or can undergo oxidative quenching by injecting the excited electron into the  $\text{TiO}_2$  conduction band to form the oxidized dye ( $D^+$ ) (equation 3). Afterwards, the oxidized dye restores back its ground state by electron donation from the redox couple ( $\text{I}/\text{I}_3^-$ ) in the electrolyte system (equation 4). This process is known as dye regeneration where iodide ion  $\text{I}^-$  is oxidized to triiodide ion  $\text{I}_3^-$ . This is followed by the migration of the electron through the semiconductor material and the external load till it reaches the counter electrode, thus completing the electrical circuit. At the counter electrode and with the help of the platinum catalyst the triiodide ion is reduced back to iodide ion by

capturing the migrating electron (equation 5), and the regenerative cycle is completed. Meanwhile, two recombination reactions known as back electron transfer reactions can take place in the cell. One reaction is the recombination of the electrons in the  $\text{TiO}_2$  conduction band with the oxidized dye (equation 6), and the other is the recombination with the oxidized redox couple  $\text{I}_3^-$  in the electrolyte (equation 7).

The reactions taking place in a DSSC are:

- (1) Photoexcitation:  $S + h\nu \rightarrow S^*$
- (2) Emission:  $S^* \rightarrow S + h\nu'$
- (3) Electron injection:  $S^* \rightarrow S^+ + e_{\text{CB}}^- (\text{TiO}_2)$
- (4) Dye regeneration:  $2S^+ + 3\text{I}^- \rightarrow 2S + \text{I}_3^-$
- (5) Electrolyte regeneration:  $\text{I}_3^- + 2e^- \rightarrow 3\text{I}^-$
- (6) Recombination with oxidized dye:  $S^+ + e_{\text{TiO}_2}^- \rightarrow S$
- (7) Recombination with oxidized electrolyte:  $\text{I}_3^- + e_{\text{TiO}_2}^- \rightarrow 3\text{I}^-$



**Figure 2:** Working principle of a DSSC.

### ***1.3.2. Electron Transfer Processes***

One of the most important features in a DSSC, unlike conventional photovoltaic devices, is that the task of light absorption and charge carrier transport are separated.

The first step in the charge separation process at the TiO<sub>2</sub> interface is electron injection. Charge separation results in the ultrafast injection of the electron from the photoexcited dye into the metal oxide conduction band and the hole into the electrolyte. The electron injection causes an upward shift in the TiO<sub>2</sub> Fermi level towards the conduction band, which under illumination generates the photovoltage in the circuit. This injection process is believed to occur in the femtosecond timescale.<sup>13-14</sup> Efficient electron injection requires a strong electronic overlap between the LUMO of the dye and the semiconductor conduction band. Therefore, it is important that the dye sensitizer has a binding group or an anchoring group that allows its attachment to the mesoporous TiO<sub>2</sub> layer to facilitate the electron injection process.

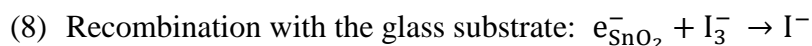
Radiative and non radiative decay of the excited state dye (S\*) to the ground state (equation 2), which varies from picoseconds to nanoseconds, compete with the electron injection process.<sup>15</sup> Therefore, it is important that the rate of injection to be faster relative to the dyes' decay to the ground state. The movement of electrons in the semiconductor conduction band is dominated by diffusion, mainly ambipolar diffusion, a process in which the charge compensating cations in the electrolyte and the electrons move through the film simultaneously.<sup>16</sup> On the other hand, it is evident that during the transport process the injected electrons might undergo trapping and detrapping process where they can be captured by trap states located in the semiconductor band gap,<sup>17</sup> or they can thermally detrap back to the conduction band. The origin of these traps are due

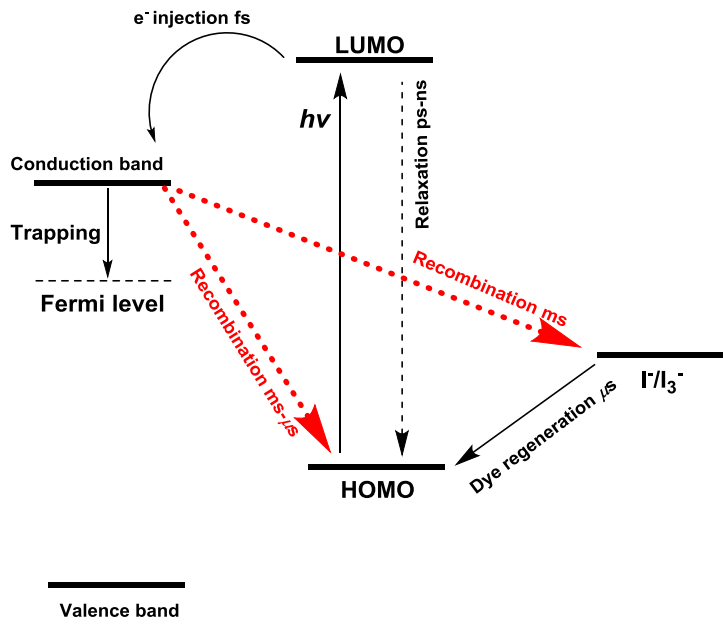
to structural defects like oxygen vacancies<sup>18</sup> that are located at the bulk or grain boundaries of TiO<sub>2</sub>. This trapping process will slow down the electron transport prior to recombination.

Dye regeneration is one of the most basic steps taking place in a DSSC. Generally, for effective dye regeneration the oxidation potential of the dye should be more positive than the redox potential of the electrolyte. Regarding kinetics, the rate of dye regeneration should be greater than the rate of recombination of the dye cation with the electrons in the semiconductor. During regeneration process, the resulting oxidized dye (S<sup>+</sup>) is restored back to its original state by the electron donor I<sup>-</sup> in the electrolyte (equation 4), which occurs in the microsecond timescale. The oxidation of I<sup>-</sup> occurs on the dye-TiO<sub>2</sub> surface and the formed oxidized ion I<sub>3</sub><sup>-</sup> migrates from the photoanode to the catalytically active counter electrode where it is reduced to I<sup>-</sup> (equation 5). At the same time, the reduced species diffuses back to the photoanode where it is depleted, and I<sub>3</sub><sup>-</sup> is depleted at the counter electrode. The transport between the two electrodes occur by diffusion, where the diffusion of I<sup>-</sup> is faster than I<sub>3</sub><sup>-</sup>, therefore, the current limitations in DSSC are due to the transport of I<sub>3</sub><sup>-</sup> to the counter electrode.<sup>19</sup>

On the other hand, a series of reaction pathways compete with the major charge transfer events taking place in the cell. One reaction is the recombination of the electrons with the dye cation (equation 6), which occurs in the microsecond to millisecond timescale and competes with the regeneration process. Hirata and coworkers<sup>20</sup> and Durrant and coworkers<sup>21</sup> demonstrated a possible way to retard charge recombination by increasing the physical separation between the dye cation and the TiO<sub>2</sub> surface through the addition of an electron donor group to the dye sensitizer.

Due to the ability of the redox mediator to penetrate through the semiconductor material reaching the FTO glass substrate two recombination reactions can occur between the  $\text{TiO}_2$  ( $e^-$ ) and the acceptors in the electrolyte (equation 7) and at the part of the FTO substrate that is exposed to the electrolyte (equation 8). The latter can be retarded by the deposition of a  $\text{TiO}_2$  blocking layer between the glass substrate and the  $\text{TiO}_2$  semiconductor layer.<sup>22</sup> The former occurs in the millisecond timescale, and is referred to as electron lifetime. A common way to suppress this recombination is by the incorporation of long alkyl chain to the dye structure. These long chains form an aliphatic network that blocks  $\text{I}_3^-$  from reaching the semiconductor surface, therefore, retarding recombination and increasing electron lifetime and the photovoltage ( $V_{OC}$ ).<sup>23</sup> Moreover, the presence of nitrogen-containing additives in the electrolyte such as *tert*-butylpyridine (TBP) which causes an upward shift in the conduction band, as well as adsorbs on the  $\text{TiO}_2$  surface blocking the approach of triiodide ion is also believed to suppress recombination.<sup>24-25</sup> Figure 3 summarizes the electron transfer in the cell with the relative time constants.





**Figure 3:** A schematic representation of the electron transfer processes in a DSSC.

### 1.3.3. Basic Parameters of DSSCs

The characterization of the cell depends on several photovoltaic parameters which are the open circuit voltage ( $V_{OC}$ ), short circuit current ( $J_{sc}$ ), incident photon to current efficiency (IPCE), fill factor ( $ff$ ), and the overall efficiency ( $\eta$ ). These parameters will be discussed below.

#### 1.3.3.1. Incident Photon-to-Current Conversion Efficiency (IPCE)

The incident photon-to-current conversion efficiency corresponds to the photocurrent density measured under monochromatic illumination generated in the external circuit divided by the photon flux that strikes the cell.

$$IPCE = LHE(\lambda)\phi_{inj}\eta_{coll} = 1240 \left( \frac{J_{sc}}{\lambda\phi} \right)$$

where LHE is the light harvesting efficiency,  $\phi_{inj}$  is the quantum yield of electron injection,  $\eta_{coll}$  is the collection efficiency of the injected electron,  $\lambda$  is the wavelength,  $J_{SC}$  is the short circuit current and  $\phi$  is the incident radiative flux.<sup>26</sup> Therefore, IPCE depends on the efficiency of charge injection from the dye sensitizer to the conduction band, on the amount of dye adsorbed on the semiconductor surface and on the collection efficiency in the circuit.

### 1.3.3.2. Open-Circuit Voltage ( $V_{OC}$ )

The  $V_{OC}$  corresponds to the potential of the cell when no external load is connected to the device and the current is zero. The voltage generated under light illumination is determined by the difference between the Fermi-level of the electron in the semiconductor ( $E_{F,n}$ ) and the redox potential of the electrolyte ( $E_{F,redox}$ ) and is expressed as follows:

$$V_{OC} = E_{F,redox} - E_{F,n}$$

$$E_{F,n} = E_{CB} + k_B T \ln\left(\frac{n_c}{N_C}\right)$$

where  $n_c$  is the number of electrons in the semiconductor,  $N_c$  is density of state in the conduction band,  $T$  is the temperature,  $k_B$  is the Boltzmann constant.

### 1.3.3.3. Short-Circuit Current ( $J_{SC}$ )

Short-circuit current ( $J_{SC}$ ) is the photocurrent per unit area ( $\text{mA}\cdot\text{cm}^{-2}$ ) measured when the voltage is zero. A high  $J_{SC}$  can be obtained by having a strong electronic coupling between the dye and the semiconductor, by using a sensitizer that absorbs light in the visible to the near-IR part of the spectrum, by efficient dye regeneration, and low



electron recombination reaction. From the  $I$ - $V$  (current-voltage) curve  $J_{SC}$  can be obtained at  $V=0$ , and  $V_{OC}$  at  $I=0$ .

#### 1.3.3.4. Fill Factor ( $ff$ )

The fill factor takes a value between 0 and 1 and it illustrates the shape of the  $I$ - $V$  curve. It is expressed by the following equation:

$$ff = \frac{P_{max}}{V_{OC}J_{SC}} = \frac{I_{max} V_{max}}{V_{OC}J_{SC}}$$

It is associated with the series resistance ( $R_S$ ) and shunt resistance ( $R_{SH}$ ) where increasing the shunt resistance and reducing the series resistance as well as decreasing the overvoltage for electron transfer and diffusion are required to achieve high  $ff$  value.

#### 1.3.3.5. Overall Conversion Efficiency ( $\eta$ )

The performance of the cell can be estimated by the overall sunlight-to-electric power conversion efficiency which is given by the ratio of the maximum power output ( $P_{max}$ ) over the power of incident light ( $P_{in}$ ). Usually it is tested under standard irradiation conditions (AM 1.5, 100 mW/cm<sup>2</sup>). For high  $\eta$  values the three parameters  $J_{SC}$ ,  $V_{OC}$ , and  $ff$  must be optimized.

$$\eta = \frac{P_{max}}{P_{in}} = \frac{J_{SC}V_{OC}ff}{P_{in}}$$

### **1.3.4. Basic Components of DSSCs**

#### 1.3.4.1. Working Electrode

The basic role of the photoanode is related to light harvesting by providing a large surface area for dye adsorption as well as transporting the injected electrons to the

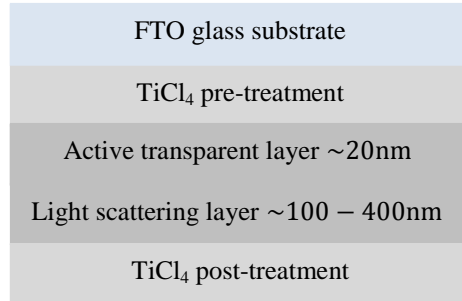
external circuit. The most commonly used wide-bandgap metal oxide semiconductor in DSSCs is the n-type  $\text{TiO}_2$ .  $\text{TiO}_2$  is present in nature in many crystalline forms: rutile, anatase and brookite. Despite the fact that rutile has the thermodynamically most stable form, anatase is the adopted structure in DSSCs since it has a higher bandgap 3.2 eV vs. rutile 3.0 eV as well as a higher conduction band energy leading to a higher photovoltage. Moreover, the photocurrent for the anatase-based cells is higher compared to the rutile ones; this is because the rutile film has a smaller surface area therefore less amount of dye adsorption.<sup>27</sup>

A typical DSSC consists of a  $\sim 10 \mu\text{m}$  thick  $\text{TiO}_2$  mesoporous layer with  $\sim 20$  nm-sized particles deposited on the FTO substrate. This is followed by a sintering process at  $500^\circ\text{C}$  to remove organic compounds and provide interconnection between the particles. One of the restrictions in the dye sensitizer is its poor absorbance in the near-IR region. A possible way to increase the optical path length and enhance the harvesting of light in the red part of the spectrum is by incorporating a layer of 100-400 nm sized light scattering  $\text{TiO}_2$  on top of the first mesoporous layer.<sup>28-29</sup> Therefore, combining two  $\text{TiO}_2$  layers one with small and the other with large particle size enhances the absorption of most dye in the red part of the spectrum.

Before and after the  $\text{TiO}_2$  deposition, the photoanode is treated with aqueous  $\text{TiCl}_4$  by chemical bath deposition, this is known as pre-treatment and post-treatment, respectively.<sup>30</sup> Pre-treatment of the glass substrate suppresses the recombination between the  $\text{I}_3^-$  in the electrolyte and the electron in the FTO, as well as it provides better interconnection between the glass substrate and the semiconductor layer. On the other hand, the  $\text{TiCl}_4$  post-treatment provides an extra ultrapure layer of  $\text{TiO}_2$  on top of the mesoporous  $\text{TiO}_2$  film which might contain some impurities. Moreover, it increases

the dye loading by increasing the surface roughness, thus enhancing the photocurrent.<sup>31</sup>

Figure 4 shows the optimized photoanode.



**Figure 4:** Optimized photoanode for DSSCs.

#### 1.3.4.2. Counter Electrode

The counter electrode (CE) provides the catalytic site for the reduction of the oxidized species in the electrolyte by capturing the migrating electrons from the external circuit. Usually, the counter electrode glass substrate is coated with a platinum layer; the choice of this catalyst is due to its catalytic properties, stability towards the redox couple, low resistance, and large surface area that provides more sites for the reduction of the triiodide ion. The transport of charges to the counter electrode is accompanied by a number of resistances including the charge transfer resistance ( $R_{CT}$ ) at the CE/electrolyte interface which functions as a series resistance in the cell.<sup>32-34</sup> An overpotential ( $\eta$ ) is required to drive the reaction at a current density ( $J$ ) which is related to the charge transfer resistance, where ideally the  $R_{CT}$  should have a value less than  $1 \Omega \cdot \text{cm}^2$  to avoid major losses. Therefore, it is crucial for the counter electrode to be catalytically active in order to assure a low overpotential ( $\eta$ ) and a quick reaction.

$$R_{CT} = \frac{RT}{nFJ}$$

#### 1.3.4.3. Electrolyte

The electrolyte system is one of the most important components in a DSSC. Its basic function is the transport of charges between the two electrodes as well as the regeneration of the oxidized dye.<sup>35</sup> In principle, the three photovoltaic parameters photovoltage, short-circuit current, and the fill factor are affected by the electrolyte system. Thus, several characteristics must be taken into account when choosing an electrolyte:<sup>36</sup> 1) it should exhibit a weak absorption in the visible light; 2) it should attain a long term stability and not cause desorption of the sensitizer; 3) the redox potential must be more negative than the HOMO of the dye to ensure an effective dye regeneration; 4) it must exhibit fast diffusion of the charge carrier with no mass-limitation problems; 5) and a fast electron transfer kinetics is required at the counter electrode. Electrolytes can be classified into liquid electrolytes, quasi-solid-state electrolytes, and solid-state ionic conductors. Ever since the pioneering work done by Grätzel, liquid electrolytes remain the most commonly used transport mediator in DSSCs owing to some of their important features, namely their low viscosity, high conductivity, and stability. In this section, the discussion will be narrowed to liquid electrolytes only. The basic components in a liquid electrolyte include: organic solvent, additives, and the redox couple.<sup>37</sup> These components will be further discussed in the following section.

- ***Organic Solvent***

The basic role of the solvent is the dissolution of the redox couple along with the other additives found in the electrolyte system. Typically, non-aqueous solvents are used in DSSCs given the fact that water might have some harmful effects on the cell.<sup>38</sup> The physical properties of the organic solvent like its melting point, boiling point,

viscosity, dielectric constant etc. influence the cell's photovoltaic parameters. The effect of the solvent on the performance of the cell is related to changes in the flatband potential ( $V_{fb}$ ) of the  $TiO_2$  surface which in turn affects  $V_{OC}$  and  $J_{SC}$ . Acetonitrile (ACN), a class of nitrile solvents, is considered as the best polar organic solvent used in DSSCs due to its good solubilizing ability, chemical stability as well as its low viscosity allowing a high diffusion coefficient of the redox couple. However, acetonitrile has a low boiling point ( $82^\circ C$ ) which might lead to the evaporation of the electrolyte under the cell's operating conditions. In order to increase the boiling point and avoid sealing problems, a mixture of nitrile solvents such as acetonitrile and valeronitrile is often used.<sup>39</sup> On another note, strong electron donating (basic) solvents such as DMSO and DMF decrease the number of protons on the  $TiO_2$  surface leading to a negative shift of the conduction band level. The  $V_{OC}$  is thus higher due to the increase in the potential difference between redox potential of the electrolyte and the  $TiO_2$   $V_{fb}$ , but  $J_{SC}$  will decrease due to the decrease in the driving force for the charge injection from the excited dye to the semiconductor.<sup>40</sup> A potential alternative for the volatile organic solvents are the ionic liquid-based electrolytes (ILs) which are salts in the liquid state and are entirely made of ions.<sup>41-42</sup> ILs afford some characteristics like: non-volatile, nonflammable, stable, and tunable viscosity making them a possible option in DSSCs.

- ***Additives***

Additives are usually added to the electrolyte system to optimize the photovoltaic performance of the cell. Their presence can cause changes in the semiconductor material, shift in the conduction band level, increase in the electron lifetime, modification in the redox couple potential, and changes in the rate of recombination reactions.<sup>24, 43-45</sup> Mainly, there are two kinds of additives used in

DSSCs: the nitrogen-containing heterocyclic compounds, such as 4-tert-butylpyridine (TBP), and the cations. In 1993, Grätzel et *al.* first reported the use of TBP as an additive which resulted in a remarkable increase in  $V_{OC}$  from 0.38 V to 0.72 V.<sup>30</sup> The basic pyridine additive is believed to adsorb on the Lewis acid sites of the  $TiO_2$  surface preventing the approach of  $I_3^-$ , thus decreasing the rate of back electron transfer at the  $TiO_2$ /electrolyte junction leading to an increase in the photovoltage. Moreover, TBP deprotonates the  $TiO_2$  surface causing an upward shift of the conduction band towards negative potentials, which also explains the dramatic increase in  $V_{OC}$ . Other nitrogen-containing additives have also been investigated in DSSCs such as pyridine, benzimidazole, pyrazole, and pyrimidine derivatives.<sup>46-48</sup>

Another class of additives contains the specific cations such as lithium ( $Li^+$ ) and guanidinium ( $G^+$ ) ions. The transport of the photo injected electrons into the mesoporous oxide film is strongly affected by the cations in the electrolyte. In order to achieve electro-neutrality in the  $TiO_2$  film, the transport of electrons in the film is followed by the simultaneous diffusion of the charge compensating cations in the electrolyte system. The contribution of both the electrons and cations is what is known as ambipolar diffusion.<sup>49-50</sup> The cations in the electrolyte tend to adsorb or accumulate on the titania surface and are expected to charge it positively leading to a positive movement of the conduction band, this results in an increase in the injection efficiency which in turn enhances the photocurrent density and drop in the photovoltage. Moreover, the size of the cation plays a significant role on the photovoltaic parameters in a cell. A series of ions,  $Li^+$ ,  $Na^+$ ,  $K^+$ ,  $Rb^+$ , and  $Cs^+$  were investigated by Liu and coworkers where they found that an increase in the cation radius (from  $Li^+$  to  $Cs^+$ , respectively) resulted in an increase in  $V_{OC}$  and decrease in  $J_{SC}$ .<sup>51</sup> This can be explained

by the ease of the small cations ( $\text{Li}^+$ ) to penetrate and combine with the electrons in the film to form an ambipolar  $\text{Li}^+ \cdot \text{e}^-$  which increases the electron's transport speed and thus the  $J_{\text{SC}}$ . On the contrary, the small-sized cations tend to increase recombination reactions and decrease  $V_{\text{OC}}$  by combining with the triiodide ions. Despite the fact that the two mentioned types of additives have opposite effects on the conduction band level, both are used simultaneously in the electrolyte system to ensure that the two photovoltaic parameters  $V_{\text{OC}}$  and  $J_{\text{SC}}$  are optimized.

Other types of additives are the dye additives such as chenodeoxycholic acid (CDCA) which is commonly used as a co-adsorbent in DSSCs. CDCA possesses an anchoring group that can bind to the  $\text{TiO}_2$ ; however it doesn't have light absorbing properties. In order to prevent dye aggregation on the  $\text{TiO}_2$  film, the dye sensitizer can be adsorbed in a solution containing CDCA, thus improving the cell's efficiency.

- ***Redox Couple***

The redox mediator in a liquid electrolyte system assumes both the task of dye regeneration and transport of charges between the working and the counter electrode. As mentioned in the previous section, a sufficient driving force is required for dye regeneration, whereby the energy level of the redox species should be relatively close to the energy level of  $\text{S}/\text{S}^+$ .<sup>19</sup> Ever since the introduction of DSSCs,  $\text{I}/\text{I}_3^-$  has been widely used as a redox mediator in the electrolyte system achieving conversion efficiencies greater than 11%.<sup>52-54</sup> Several mechanisms for the reduction of the dye cation by  $\text{I}/\text{I}_3^-$  have been proposed.<sup>19, 55</sup> One prevailing pathway which requires a large driving force for regeneration consists of the formation of an intermediate complex  $[\text{dye}^+ \cdots \text{I}^-]$

followed by the radical formation  $I_2^{\cdot-}$  in the second step and finally its disproportionation into  $I^-$  and  $I_3^-$ .

For the past 20 years this redox couple is considered as the high-performance electrolyte owing to some of its properties: ability to penetrate into the porous film, fast dye regeneration, and slow electron recombination events. Despite its remarkable performance,  $I^-/I_3^-$  redox electrolyte is limited by several drawbacks:<sup>19, 56</sup> 1) a high overpotential is required for dye regeneration causing losses in the photovoltage; 2) corrosiveness towards metal-based current collector (silver) and sealing materials in large-scale DSSCs; 3) ability of triiodide ions and other polyiodides to absorb light in the visible part of the spectrum (up to 450 nm) which competes with the dye sensitizer and reduces the photocurrent in the cell; 4) mismatch in the redox potential of the redox couple with that of the sensitizer causing significant losses in  $V_{OC}$ . Due to such limitations, considerable amount of effort has been made to find alternative iodine-free redox couples.<sup>57</sup> In 2010, Feldt *et al.* reported a highly efficient DSSC based on a transition-metal based cobalt tris(bipyridine) redox shuttle  $[Co(bpy)]^{3+/2+}$  together with a bulky triphenylamine-based organic dye sensitizer achieving an open-circuit potential up to 1V.<sup>58</sup> Following this work, promising efficiencies up to 12% were achieved with cobalt-based DSSCs in combination with organic dyes and metal-based dyes.<sup>10, 59</sup> Unlike iodine-based electrolytes, the one-electron outer-sphere cobalt complexes exhibit good stability, weak light absorption, higher redox potential and a tunable structure by modifying the ligands. However, these redox couples are limited by fast charge recombination of  $Co^{3+}$  complex with the photo injected electrons leading to shorter electron lifetimes, as well as mass transport problems associated to their large size and heavy mass leading to slow diffusion across the  $TiO_2$  film to the counter electrode.<sup>60-64</sup>



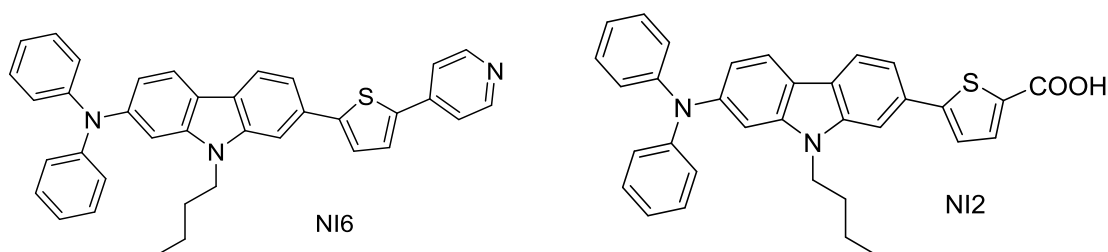
A significant way to suppress the undesirable recombination reaction is by increasing the steric bulkiness of the dye sensitizer by adding long insulating alkyl chains. Moreover, when working with diffusion-limited redox couples, the film thickness, pore size and the porosity of the TiO<sub>2</sub> layer should be controlled and optimized.<sup>65</sup> To minimize the diffusive problems of the relatively large cobalt complexes, a thin and more porous TiO<sub>2</sub> film is required which can be achieved by diluting the TiO<sub>2</sub> paste with ethyl cellulose.<sup>66</sup> Also, decreasing the TiCl<sub>4</sub> concentration during post-treatment can increase the pore size as well as the porosity of the film thus improving the transport rate of the cobalt species.<sup>67</sup> Other redox complexes that were investigated include Cu(I)/Cu(II), ferrocene/ferrocenium (Fc/Fc<sup>+</sup>), and thiolate/disulfide (T<sup>-</sup>/T<sub>2</sub>) with conversion efficiencies of 8%, 7.5% and 6.44%, respectively.<sup>68-70</sup>

#### 1.3.4.4. Sensitizer

The basic role of the dye sensitizer is to absorb the incident photon and convert it to current. In addition to light harvesting, the dye is responsible for charge injection and separation which occurs at the interface of the dye-TiO<sub>2</sub> surface and the electrolyte. An ideal sensitizer must have a broad absorption spectrum where it should be able to absorb light in the visible region and part of the near-IR region. A high molar extinction coefficient ( $\epsilon$ ) is also required especially when working with thin-film DSSCs. Moreover, for efficient dye regeneration the oxidized state level of the dye should be more positive than the redox potential of the electrolyte, and for a sufficient driving force for electron injection the excited state level of the sensitizer should be higher in energy than the TiO<sub>2</sub> conduction band (-0.5 V vs. NHE). In addition, the dye should not aggregate on the electrode surface, as well as its structure must be optimized

to minimize charge recombination at the  $\text{TiO}_2$ /electrolyte interface. Finally, the dye sensitizer must have a suitable anchoring group (carboxylate, phosphonate etc.) to bind on the  $\text{TiO}_2$  surface, thus providing a good electronic coupling between the LUMO of the dye and the conduction band.<sup>71</sup> Many dyes have been designed in the past couple decades that could meet these requirements. Generally, dye sensitizers can be metal-based such as porphyrins, ruthenium (II) complexes etc. and metal free organic dyes. The metal complex dyes consist of a central metal, ancillary ligands and anchoring groups. In particular, Ru complexes have been widely investigated due to their favorable electrochemical and photovoltaic properties as well as their broad absorption spectrum.<sup>72</sup> On the other hand, organic dyes have emerged as potential alternatives to the ruthenium dyes because they can be easily designed and synthesized, exhibit a high molar extinction coefficient, have a low cost, and finally DSSCs with organic dyes show higher efficiencies. The basic structure of an organic dye is D- $\pi$ -A where D is the donor group,  $\pi$  is a conjugated linker and A is the acceptor unit which also acts as the anchoring group. When the dye absorbs light an intramolecular charge transfer (ICT) occurs from the donor group to the acceptor through the  $\pi$  bridge. Also, by adopting this structure, the HOMO and LUMO energy levels of the dye can be adjusted by varying the donor,  $\pi$  and acceptor units, thus extending the absorption spectra. Typically, carboxylic acid and cyanoacrylic acid groups are the most commonly used anchors as well as electron accepting groups in dyes owing to their excellent electron withdrawing abilities. The carboxyl groups are believed to bind on the Brønsted acid sites of the  $\text{TiO}_2$  surface providing a good electronic communication between the dye and semiconductor. Despite the fact that cyanoacrylic acid-based anchoring groups combine both the strong electron withdrawing capacity of the cyano-group as well as

the binding abilities of the carboxyl group, these groups tend to desorb from the semiconductor surface as well as degrade and convert to aldehyde in the presence of water.<sup>73</sup> In 2011, Ooyama and co-workers reported the use of a pyridine ring as an anchoring and electron acceptor group on a number of carbazole-based organic dyes instead of the traditional carboxyl groups.<sup>74</sup> Their work was based on the design of an effective pyridine-based organic dye NI6 with  $J_{SC} = 5.63 \text{ mA}\cdot\text{cm}^{-2}$  and  $\eta = 1.84\%$  compared to a conventional carboxyl-based dye NI2 with  $J_{SC} = 3.07 \text{ mA}\cdot\text{cm}^{-2}$  and  $\eta = 0.97\%$ .<sup>74</sup> This suggested that the pyridine ring provides efficient electron injection from the dye to the semiconductor material. The structures of NI6 and NI2 are shown in figure 5. Unlike the carboxyl groups, the pyridine's binding mode on the  $\text{TiO}_2$  surface occurs through a coordinate bonding between the Lewis acid sites of  $\text{TiO}_2$  ( $\text{Ti}^{n+}$  cations) and the lone pair of electrons on the nitrogen atom of the pyridine ring.



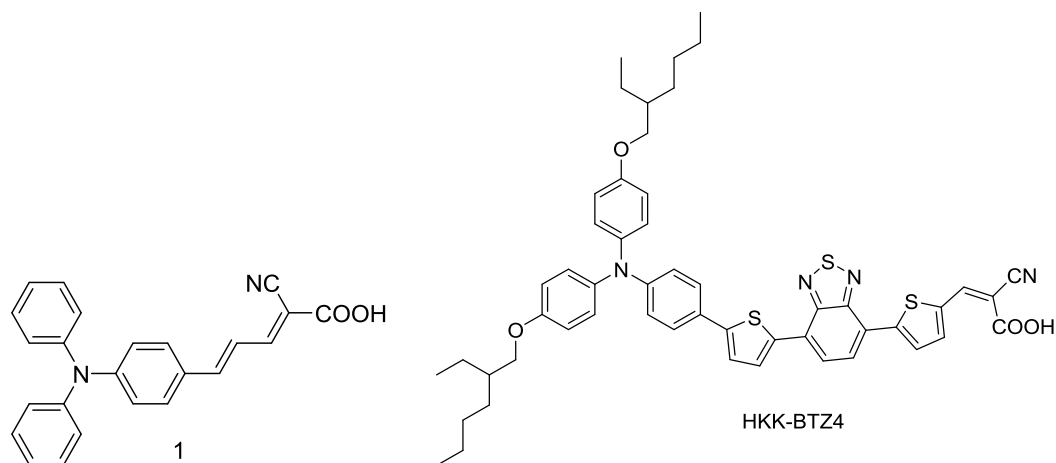
**Figure 5:** Structures of NI6 and NI2, respectively.

A possible way to extend the absorption spectra in DSSCs is by adsorbing on the  $\text{TiO}_2$  film two dyes with complementary spectra (blue and red absorbing dyes).<sup>75</sup> This is known as co-sensitization, where it also requires compatibility between the dyes to prevent mutual interactions. A successful co-sensitization was reported in 2015

between a carboxy-anchor organic dye and an alkoxy-silyl-anchor dye resulting in a record conversion efficiency of 14.3% and  $V_{OC}$  above 1 V.<sup>8</sup>

- ***Triphenylamine Dyes***

Triphenylamine-based organic sensitizers (TPA) have been widely investigated due to their electron donating abilities and hole transporting capability. These donor groups have achieved high power conversion efficiencies up to 10.3% over the past few years.<sup>52</sup> In addition to their donating ability, the non-planar TPAs can suppress aggregation and charge recombination as well as increase the molar extinction coefficient of the dye sensitizer.<sup>76-78</sup> Yanagida and co-workers first reported the synthesis of a triphenylamine donor group in a dye sensitizer (1) with methine unit as a spacer to expand the  $\pi$ -conjugated system, achieving a PCE of 5.3%.<sup>79</sup> Moreover, Ellis and co-workers showed that the introduction of thiophene units on the  $\pi$ -conjugated moiety of a series of TPA-based organic dyes extended their spectral response into the red region of the spectrum.<sup>80</sup> In addition, it was demonstrated by Lee and co-workers that the addition of a bulky alkoxy group onto to the triphenylamine donor moiety (dye HKK-BTZ4) red-shifts the absorption spectrum, mainly due to the destabilization of the donor's HOMO and the reduction of the HOMO-LUMO energy gap, as well as these groups prevent dye aggregation.<sup>81</sup> The structures of dye 1 and HKK-BTZ4 are shown in figure 6.

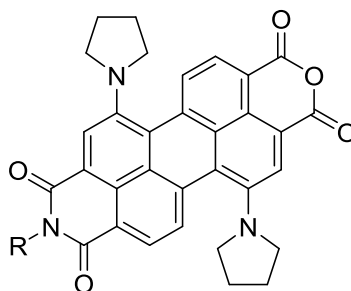


**Figure 6:** Structures of 1 and HKK-BTZ4, respectively.

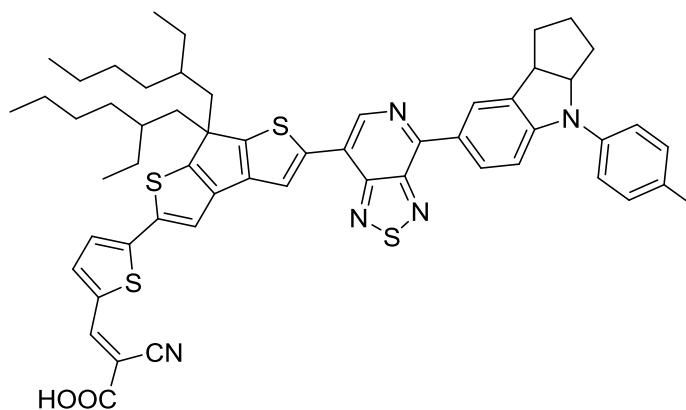
- **Blue Dyes**

Near-infrared absorbing dyes, in particular blue and green dyes, are of great interest due to their ability of absorbing the incident photon in the red and near-IR part of the spectrum. Compared to red sensitizers, very few efficient blue sensitizers have been developed over the past years and it is noteworthy to mention that a great effort is being made to molecularly synthesize efficient near IR dyes for DSSCs. Squaraine-based sensitizers are well known for their sharp and intense absorption in the near-IR region yielding blue colored solar cells; however the device's performance with these dyes was always poor yielding low efficiencies which is mainly due to dye aggregation and poor electron injection.<sup>82-87</sup> Another blue organic dye belonging to the perylene imide derivatives (*iPr-PMI* dye) was also reported; this dye displays an intense absorption in the near-IR part of the spectrum at around 700 nm.<sup>88</sup> However, the perylene-sensitized solar cell exhibits a limited cell performance with a power conversion efficiency reaching up to 2.6%.<sup>88</sup> The structure of the electron donating perylene tetracarboxylic acid derivative dye *iPr-PMI* is shown in figure 7. In 2014, Grätzel and coworkers synthesized a promising blue [1,2,5]thiadiazolo[3,4-c]pyridine-

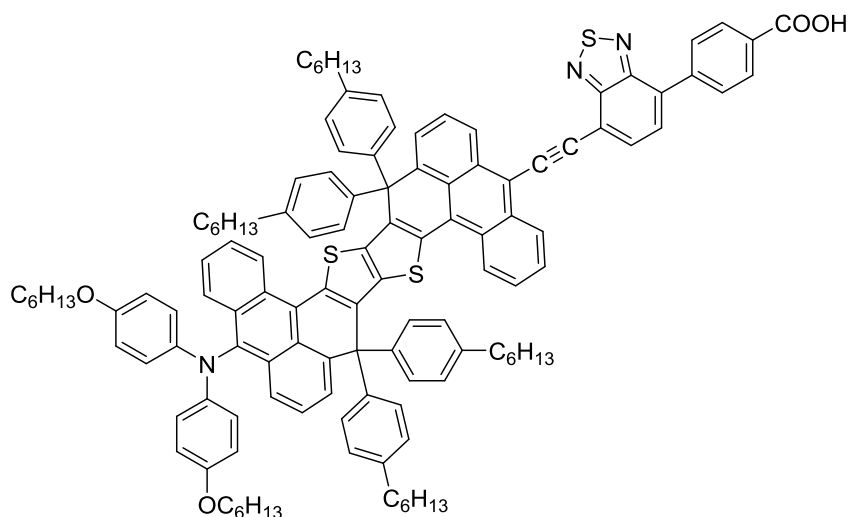
containing organic dye (PT-2) exhibiting a reduced HOMO-LUMO band gap and consisting of a strong electron acceptor group and thiophene as a  $\pi$ -bridging unit.<sup>89</sup> The PT-2-based DSSC using iodine as an electrolyte achieved a conversion efficiency of around 6.7%.<sup>89</sup> The molecular structure of PT-2 is shown in figure 8. Very recently, in 2018, a novel and stable dye R6 was designed which when adsorbed on the TiO<sub>2</sub> film gave a very bright sapphire color. The DSSC with this dye achieved a remarkable efficiency of 12.6% in the presence of Co(II/III) tris(bipyridyl) redox couple which is by far the highest performance in the family of blue dyes.<sup>90</sup> R6 is based on strong electron donating polycyclic aromatic hydrocarbon (PAH) group along with diarylamine as an electron donor and benzoic acid electron acceptor. Its structure is shown in figure 9.



**Figure 7:** Molecular structure of *iPr*-PMI with R=2, 6-diisopropylphenyl.



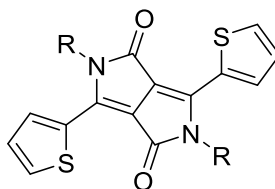
**Figure 8:** Molecular structure of PT-2.



**Figure 9:** Molecular structure of R6.

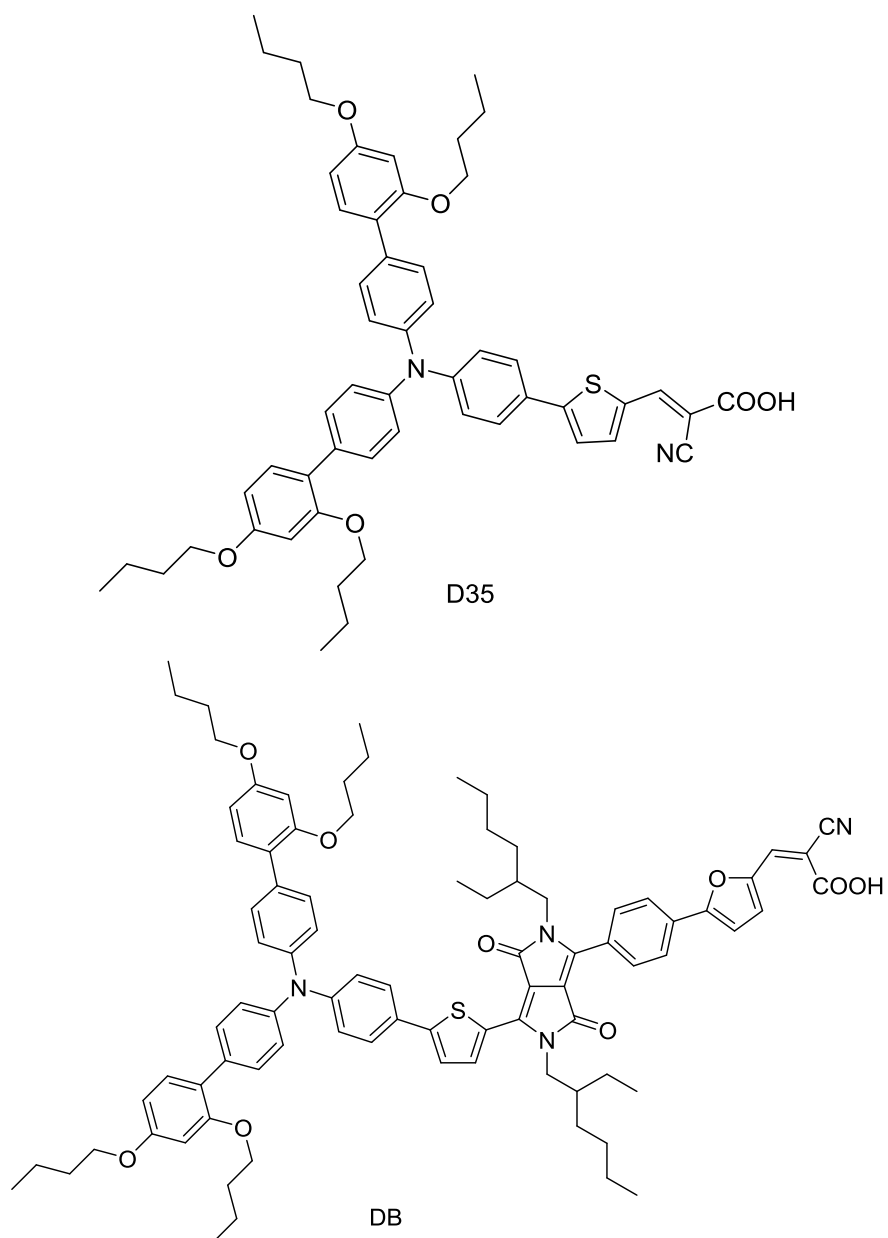
Over the past few years, diketopyrrolopyrrole (DPP)-based polymers have been commonly used as organic building blocks in optoelectronic applications, mainly organic field-effect transistors (FET), and photovoltaic applications.<sup>91-92</sup> 1,4-diketopyrrolopyrrole (DPP) with pyrrole[3,4-c]pyrrole-1,4-dione as the core chromophore unit were first reported and synthesized by Farnum and coworkers in 1974.<sup>93</sup> The conjugated and planar bicyclic structure of the DPP moiety as well as its electron withdrawing abilities makes it a suitable chromophore in low band gap donor-acceptor materials. Recently, DPP-based sensitizers have been introduced to DSSCs as blue-colored dyes yielding satisfactory efficiencies reaching up to 10%.<sup>94-102</sup> DPPs are characterized by a planar conjugated bicyclic structure, which particularly consists of two electron withdrawing cyclic amide groups, making it a successful  $\pi$ -conjugated unit in organic dyes. However, the big conjugated system has a tendency to form  $\pi$ - $\pi$  stacking aggregation on the TiO<sub>2</sub> film which increases charge recombination; this can be suppressed by attaching long alkyl chains on the lactams nitrogen atom. Moreover,

N-alkylation can increase the solubility of the DPP chromophores in organic solvents. The DPP core is usually substituted with a strong electron donating thienyl group  $\text{DPP}(\text{Th})_2$ <sup>103-104</sup> which shifts the absorption towards longer wavelengths due to enhanced intramolecular charge transfer transitions. The structure of the DPP moiety with the attached thiophene units is shown in figure 10. In 2016, Grätzel and co-workers reported the synthesis of a DPP sensitizer with a triphenylamine donor group and a cyanoacrylic acid electron acceptor group (Dyename Blue DB) which when assembled with a cobalt-based electrolyte achieved an efficiency of 7.3%. In order to extend the absorption spectra and improving the device's performance, this blue dye was successfully co-sensitized with a red organic dye D35 having a complementary absorption spectra resulting in an efficiency of 8.7% with the cobalt redox couple.<sup>105</sup> . The structures of DB and D35 are shown in figure 11.



**Figure 10:** Thienyl DPP chromophores with R as the attached alkyl chains.

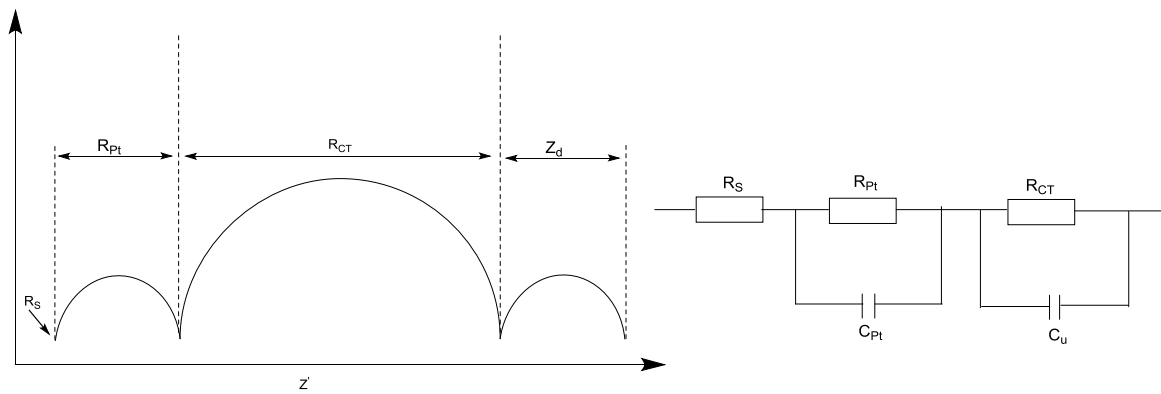




**Figure 11:** Structures of D35 and DB, respectively.

#### 1.4. Electrochemical Impedance Spectroscopy (EIS)

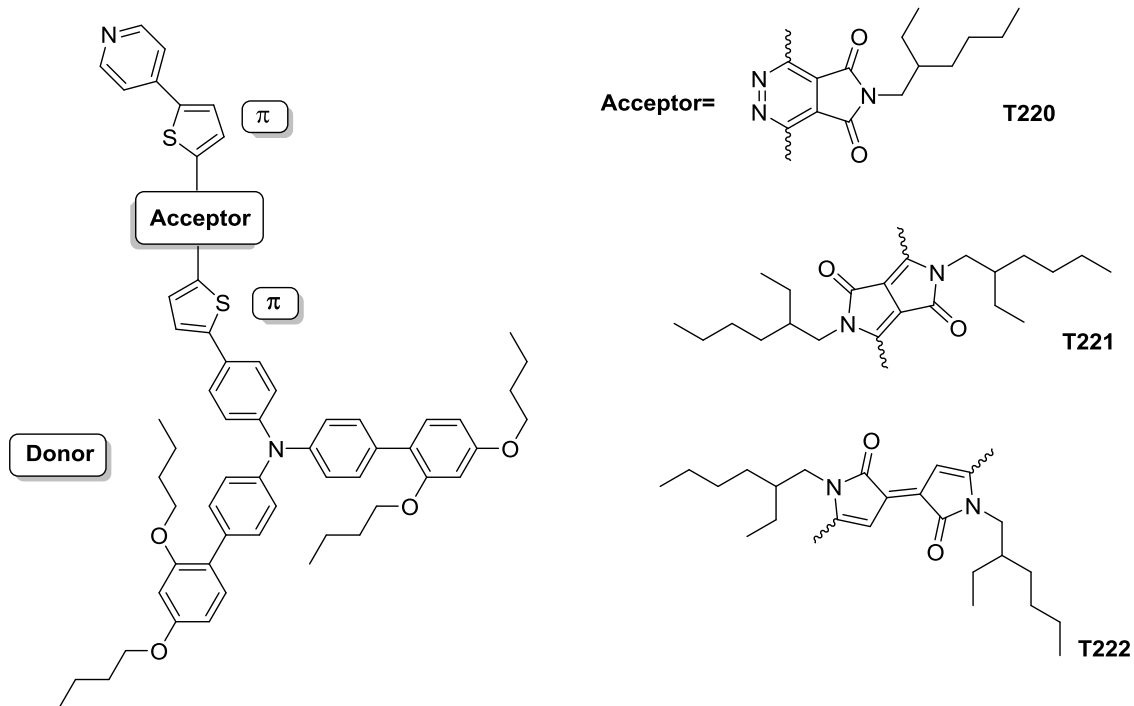
EIS is a useful tool to study the transport and charge transfer processes taking place in a DSSC. It measures the current response by applying an AC voltage as a function of frequency.<sup>106</sup> The impedance response of a DSSC is related to different internal resistance elements that can be fitted into an equivalent circuit which include: series resistance, charge transfer resistance at the counter electrode, resistance of electron transport, diffusion resistance of the electrolyte and the chemical capacitance at the TiO<sub>2</sub> interface.<sup>107-110</sup> Under open circuit voltage, the impedance spectrum of a DSSC is represented in the form of Nyquist plot where  $Z''$  the imaginary impedance is plotted as a function of  $Z'$  the real impedance. Typically, it features three semicircles; the first semicircle (left) at the high frequency region is attributed to the charge transfer resistance ( $R_{Pt}$ ) and the double layer capacitance ( $C_{Pt}$ ) at the platinized counter electrode, the middle frequency region corresponds to the charge transfer resistance of the recombination reaction between electrons in the TiO<sub>2</sub> film and the electrolyte ( $R_{CT}$ ) and the chemical capacitance of the metal oxide film ( $C_{\mu}$ ), and the low frequency semicircle demonstrates the diffusion resistance of ions in the electrolyte ( $Z_d$ ). In the Nyquist plot, the distance between the origin of the x-axis ( $Z'$ ) and the intercept of the high frequency semicircle corresponds to the series resistance ( $R_S$ ) which is related to the sheet resistance in the FTO. Moreover, from the charge transfer resistance and the chemical capacitance, the electron lifetime ( $\tau$ ) can be obtained  $\tau=R_{CT}\cdot C_{\mu}$ . The typical Nyquist plot and the electrical equivalent circuit of a DSSC are shown in figure 12.



**Figure 12:** Nyquist plot and the equivalent circuit of the DSSC.

## 1.5. Objective of thesis

Highly efficient DSSCs with remarkable photovoltaic performance have been attained by employing metal-free organic dyes with different electrolyte systems, particularly, great efforts have been made to molecularly design and synthesize efficient organic blue dyes where the ultimate goal is to reach efficiencies as high as 15%. The fact that many red sensitizers with absorptions below 500 nm have been synthesized and successfully used in DSSCs over the past years while leaving a great part of the incident photon in the near-IR part of the spectrum unused is the main reason why many efforts are being done to design efficient blue-colored dyes to be employed in DSSCs. Among the most promising blue sensitizers that have been recently reported are the DPP-based dyes consisting of a cyanoacrylic anchoring group achieving remarkable efficiencies. Inspired by the fact that the number of blue dye is still somehow scarce, we aim on synthesizing three novel pyridine-based organic dyes T220, T221 and T222 (two of which turned out to be blue and one orange in color) and study them in fully assembled DSSCs as the sole dyes or when co-adsorbed with dyes that complements their absorption spectra. These dyes have the form donor- $\pi$ -acceptor- $\pi$  with a terminal pyridine anchoring group which also acts as an electron acceptor, a bulky triphenylamine as a donor group, and thiophene as the  $\pi$ -conjugated system while varying the middle acceptor moiety between the three dyes which shifts the absorption towards the red part of the spectrum. T221 and T222 belong to the family of diketopyrrolopyrrole (DPP) and Pechmann-based dyes, respectively. The proposed dyes will be studied for the conversion of light into electricity in fully assembled DSSC using cobalt (II/III) redox couple which has been proved to be efficient for structurally similar dyes.<sup>80</sup> The structure of the three dyes is shown in figure 13.



**Figure 13:** Molecular structure of the three proposed dyes.

# CHAPTER 2

## EXPERIMENTAL SECTION

### 2.1. Materials and Instrumentation

All organic chemicals were purchased from Sigma-Aldrich and used as supplied. The DB, D35 dye and 2',4'-dibutoxy-N-(2',4'-dibutoxy-[1,1'-biphenyl]-4-yl)-N-(4-(4,4,5,5-tetramethyl-1,3,2-dioxaborolan-2-yl)phenyl)-[1,1'-biphenyl]-4-amine were purchased from Dyenamo (Sweden). FTO glass "Tec15" and "Tec8" were purchased from Pilkington (USA). TiO<sub>2</sub> colloids 30NR-D and WER2-O were purchased from Dyesol (Australia). The NMR spectra (<sup>1</sup>H and <sup>13</sup>C) were measured on a Bruker AM 500 MHz spectrometer. UV-vis spectra were recorded on a Jasco V-570 UV/vis/NIR spectrometer. Steady state emission spectra were measured on a JobinYvon Horiba Fluorolog-3 spectrofluorometer. The electrochemical setup consisted of a three-electrode cell, with a platinum rod as the working electrode, a Pt wire ~ 1 mm diameter as the counter electrode, and Ag/Ag<sup>+</sup> (10 mM AgNO<sub>3</sub>) as the reference electrode. The electrochemical measurements were performed in 0.1 LiClO<sub>4</sub> in DMF, and Fc/Fc<sup>+</sup> standard (0.69 vs NHE in DMF) was used as an internal reference. Electrochemical impedance spectra of the DSSCs were performed with CH Instruments 760B (USA). The obtained impedance spectra were fitted with the Z-view software (v2.8b, Scribner Associates Inc.). The spectra were performed in the frequency range 0.1 Hz - 10<sup>5</sup> Hz with oscillation potential amplitudes of 10 mV at RT under open circuit conditions at different light levels. IPCE% spectra were recorded using a Newport 74000 Cornerstone™ monochromator. Photocurrent vs. Voltage characteristics were

measured with a Keithley 2400 sourcemeter and a solar simulator illuminated by a Xenon arc lamp (Oriel) through an AM1.5 simulation filter (ScienceTech). The irradiated area of the cell was 0.5 x 0.5 cm<sup>2</sup> with a 0.6 x 0.6 cm<sup>2</sup> black mask.

## 2.2. Computational Studies

Calculations were carried out using *Gaussian 03*.<sup>111</sup> Geometries were optimized using the 6-31G\* basis set with (CAM-B3LYP) in water (C-PCM algorithm).<sup>112</sup>

## 2.3. Dye Synthesis

### 2.3.1. Synthetic Procedure of T220

#### 2.3.1.1. Synthesis of 1-(2-ethylhexyl)-1*H*-pyrrole-2, 5-dione (**1**)<sup>113</sup>

Maleic anhydride (10.0 g, 101.9 mmol) was dissolved in 30 mL dichloromethane. 16 mL of 2-ethyl-1-hexamine in 64 mL dichloromethane were added drop wise to the mixture over 10 minutes. After the addition was complete, the reaction was allowed to stir and left overnight after which the organic solvent was removed under reduced pressure. 100 mL acetic anhydride and 10.1 g of sodium acetate were added to the flask and the mixture was stirred at 40°C for 2 hours. After 2 hours, the reaction mixture was poured into 400 mL cold water and extracted with hexane. The combined organic layer was washed with aqueous sodium bicarbonate and dried over magnesium sulfate. The solvent was then evaporated and a yellow oil was obtained which was further purified by column chromatography using hexane as eluent to get the pure 1-(2-ethylhexyl)-1*H*-pyrrole-2, 5-dione (10.5 g, 50% yield). <sup>1</sup>H NMR (500 MHz, CDCl<sub>3</sub>) δ 6.62 (s, 2H), 3.36 (d, *J* = 7Hz, 2H), 1.63-1.66 (m, 1H), 1.12-1.24 (m, 8H),

0.80-0.83 (m, 6H).  $^{13}\text{C}$  NMR (125 MHz,  $\text{CDCl}_3$ )  $\delta$  171.18, 133.98, 41.74, 38.21, 30.41, 28.45, 23.75, 23.00, 14.05, 10.38.

#### 2.3.1.2. Synthesis of 3, 6-bis (5-bromo-2-thienyl)-1, 2, 4, 5-tetrazine (2)<sup>114</sup>

5.3 mL hydrazine monohydrate was added drop wise to 5-bromo-2-thiophenecarbonitrile (4.72 g, 25.1 mmol) and sulfur (0.48g, 15 mmol) in 10 mL ethanol. The mixture was heated at reflux for 2 hours and the cooled mixture was filtered to obtain a light brown solid. The obtained solid was dissolved in dichloromethane and a solution of sodium nitrite (3.9 g, 56.5 mmol) and water was added to the mixture. Acetic acid was added drop wise and the reaction mixture was allowed to stir overnight. The solvent was then removed under reduced pressure and the precipitate was filtered and washed with water and ethanol. The crude product was then recrystallized from ethanol to afford 3, 6-bis (5-bromo-2-thienyl)-1, 2, 4, 5-tetrazine as a pure red solid (3.59 g, 35% yield).  $^1\text{H}$  NMR (500 MHz,  $\text{CDCl}_3$ )  $\delta$  7.95 (d,  $J = 4\text{Hz}$ , 2H), 7.17 (d,  $J = 4\text{Hz}$ , 2H).  $^{13}\text{C}$  NMR (125 MHz,  $\text{CDCl}_3$ )  $\delta$  160.73, 137.01, 132.14, 131.33, 121.01.

#### 2.3.1.3. Synthesis of 1,4-bis(5-bromo-2-thienyl)-6-(2-octyldodecyl)-5H-pyrrolo[3,4-d]pyridazine-5,7(6H)-dione (3)<sup>115</sup>

Compound 1-(2-ethylhexyl)-1*H*-pyrrole-2, 5-dione (1.04 g, 4.96 mmol), compound 3, 6-Bis (5-bromo-2-thienyl)-1, 2, 4, 5-tetrazine (1.0 g, 2.48 mmol) and diphenyl ether were mixed together and the reaction mixture was heated to 150°C for 24 hours. The mixture was then cooled and the obtained solid was filtered and washed with hexane to get 1,4-bis(5-bromo-2-thienyl)-6-(2-octyldodecyl)-5H-pyrrolo[3,4-d]pyridazine-5,7(6H)-dione as a pure yellow solid (1.13 g, 78% yield).  $^1\text{H}$  NMR (500



MHz, CDCl<sub>3</sub>)  $\delta$  8.65 (d,  $J$  = 4.5Hz, 2H), 7.22 (d,  $J$  = 4.5Hz, 2H), 3.70 (d,  $J$  = 7Hz, 2H), 1.83-1.88 (m, 1H), 1.31-1.41 (m, 8H), 0.90-0.96 (m, 6H). <sup>13</sup>C NMR (125 MHz, CDCl<sub>3</sub>)  $\delta$  167.40, 147.97, 139.35, 133.99, 131.71, 122.14, 121.08, 43.01, 38.26, 30.97, 28.46, 23.85, 22.98, 14.07, 10.36.

#### 2.3.1.4. Synthesis of T220

In a 50 mL round bottom flask, 1,4-bis(5-bromo-2-thienyl)-6-(2-octyldodecyl)-5H-pyrrolo[3,4-d]pyridazine-5,7(6H)-dione (0.40 g, 0.68 mmol), 4-pyridinyl boronic acid (0.092 g, 0.75 mmol, 1.1 eqv) and 2',4'-dibutoxy-N-(2',4'-dibutoxy-[1,1'-biphenyl]-4-yl)-N-(4-(4,4,5,5-tetramethyl-1,3,2-dioxaborolan-2-yl)phenyl)-[1,1'-biphenyl]-4-amine (0.61 g, 0.75 mmol, 1.1 eqv) were added along with triphenyl phosphine C<sub>18</sub>H<sub>15</sub>P (0.08 g, 0.28 mmol), potassium carbonate K<sub>2</sub>CO<sub>3</sub> (1.38 g, 9.98 mmol) and palladium acetate Pd(OAc)<sub>2</sub> (0.012 g, 0.054 mmol). A mixture of 25 mL dioxane: THF: water (3:2:1) was added and the solution was purged with argon and refluxed for 48 hours. The reaction mixture was cooled, and the solvent was removed under reduced pressure. The obtained solid was then extracted with dichloromethane washed with water and dried with sodium sulfate. The resulting solid was purified by column chromatography with dichloromethane and 5% methanol as mobile phase. T220 was then isolated as a pure orange solid (0.22 g, 26% yield). Mp: 210.5-213 °C. <sup>1</sup>H NMR (500 MHz, DMSO-*d*<sub>6</sub>)  $\delta$  8.68 (d,  $J$  = 6.0 Hz, 2H), 8.13 (d,  $J$  = 4.1 Hz, 1H), 7.91 (d,  $J$  = 4.1 Hz, 1H), 7.79 (d,  $J$  = 6.1 Hz, 2H), 7.72 (d,  $J$  = 8.4 Hz, 2H), 7.52 (d,  $J$  = 8.5 Hz, 5H), 7.48 (d,  $J$  = 4.0 Hz, 1H), 7.30 (d,  $J$  = 8.3 Hz, 2H), 7.16 (d,  $J$  = 8.2 Hz, 6H), 6.69 (d,  $J$  = 2.4 Hz, 2H), 6.64 (dd,  $J_1$  = 8.6,  $J_2$  = 2.3 Hz, 2H), 4.07 (dt, 9H), 3.18 (t, 3H), 1.79 – 1.68 (m, 9H), 1.55 – 1.37 (m, 11H), 1.09 (t, 7H), 0.99 (t, 7H), 0.88 (t, 7H). <sup>13</sup>C NMR (125 MHz,

DMSO)  $\delta$  206.99, 166.04, 159.75, 157.01, 150.97, 149.64, 148.29, 147.75, 146.65, 145.26, 142.50, 140.80, 138.30, 133.77, 131.00, 130.67, 127.96, 127.68, 127.60, 127.10, 124.18, 123.32, 122.28, 119.99, 106.41, 100.72, 68.12, 67.68, 31.28, 31.17, 30.73, 28.87, 23.81, 23.03, 19.29, 14.50, 14.13, 11.01. MALDI-TOF MS (m/z): calculated for  $C_{73}H_{79}N_5O_6S_2$ , 1186.6; found, [M + H<sub>2</sub>O] 1204.5.

### 2.3.2. Synthetic Procedure of T221

#### 2.3.2.1. Synthesis of 2, 5-dihydro-3, 6-di-2-thienylpyrrolo [3, 4-c] pyrrole-1, 4-dione (4)<sup>116</sup>

50 mL of Tertiary amyl alcohol was dissolved in potassium tert-butoxide (5.45 g, 48.6 mmol) under argon and the mixture was heated up to 100°C. 2-thiophenecarbonitrile (5.30 g, 48.6 mmol) and diethyl succinate (2.94 g, 16.9 mmol) were added at the same temperature and left for 3 hours. The reaction mixture was then cooled and poured into 85 mL methanol and 35 mL acetic acid and the precipitate was filtered and washed with water and methanol to obtain 2, 5-dihydro-3, 6-di-2-thienylpyrrolo [3, 4-c] pyrrole-1, 4-dione as a purple solid (1.10 g, 8% yield).

#### 2.3.2.2. Synthesis of 2, 5-diethylhexyl-3, 6-dithiophen-2-ylpyrrolo [3, 4-c] pyrrole-1, 4-dione (5)<sup>116</sup>

Compound 2, 5-dihydro-3, 6-di-2-thienylpyrrolo [3, 4-c] pyrrole-1, 4-dione (0.88 g, 2.93 mmol), K<sub>2</sub>CO<sub>3</sub> (1.62 g, 11.72 mmol, 4 eqv) and 2-ethylbromohexane (1.69 g, 8.79 mmol, 3 eqv) were dissolved in 25 mL DMF with a small amount of 18-crown ether at 145°C under argon and the reaction was left overnight. The reaction mixture was cooled and poured into ice-water and extracted with dichloromethane. The combined organic layer was dried over sodium sulfate and the organic solvent was removed under reduced pressure. The obtained solid was purified by column

chromatography using hexane, 30% DCM as eluent. The obtained solid was poured into methanol and suction filtration was performed. A pure purple solid 2, 5-diethylhexyl-3, 6-dithiophen-2-ylpyrrolo [3, 4-c] pyrrole-1, 4-dione was obtained (0.10 g, 7% yield).  $^1\text{H}$ NMR (500 MHz,  $\text{CDCl}_3$ )  $\delta$  8.81 (d,  $J = 5$  Hz, 2H), 7.55 (d,  $J = 3$  Hz, 2H), 7.21 (d,  $J = 3.5$  Hz, 2H), 4.00 (p, 4H), 1.79-1.77 (m, 2H), 1.30-1.16 (m, 16H), 0.82-0.76 (m, 13H)  $^{13}\text{C}$  NMR (125 MHz,  $\text{CDCl}_3$ )  $\delta$  160.74, 139.41, 134.27, 129.52, 128.79, 127.41, 106.88, 44.82, 38.04, 29.17, 27.32, 22.48, 22.04, 13.01, 9.45.

### 2.3.2.3. Synthesis of 2,5-diethylhexyl-3,6-bis(5-bromothiophen-2-yl)pyrrolo[3,4-c]-pyrrole-1,4-dione (6)<sup>116</sup>

Compound 2, 5-diethylhexyl-3, 6-dithiophen-2-ylpyrrolo [3, 4-c] pyrrole-1, 4-dione (0.25 g, 0.48 mmol) and NBS (0.18 g, 1 mmol, 2.1 eqv) were dissolved in acetic acid and chloroform. The mixture was stirred at room temperature for 24 hours. The organic solvent was removed under reduced pressure, and the residue was washed with methanol and filtered to obtain 2,5-diethylhexyl-3,6-bis(5-bromothiophen-2-yl)pyrrolo[3,4-c]-pyrrole-1,4-dione as a pure purple solid (0.10 g, 31% yield).  $^1\text{H}$  NMR (500 MHz,  $\text{CDCl}_3$ )  $\delta$  8.57 (d,  $J = 4\text{Hz}$ , 2H), 7.16 (d,  $J = 4\text{Hz}$ , 2H), 3.84 (p, 4H), 1.77-1.75 (m, 2H), 1.31-1.20 (m, 16H), 0.83-0.74 (m, 13H).  $^{13}\text{C}$  NMR (125 MHz,  $\text{CDCl}_3$ )  $\delta$  161.56, 138.33, 134.38, 130.46, 130.13, 118.06, 107.02, 44.96, 38.06, 28.68, 28.60, 22.52, 22.01, 13.00, 9.42.

#### 2.3.2.4. Synthesis of T221

In a 50 mL round bottom flask, 3,6-bis(5-bromo-2-thienyl)-2,5-bis(2-ethylhexyl)-2,5-dihydropyrrolo[3,4-c]pyrrole-1,4-dione (0.20 g, 0.29 mmol), 4-pyridinyl boronic acid (0.034 g, 0.32 mmol, 1.1 eqv) and 2',4'-dibutoxy-*N*-(2',4'-dibutoxy-[1,1'-biphenyl]-4-yl)-*N*-(4-(4,4,5,5-tetramethyl-1,3,2-dioxaborolan-2-yl)phenyl)-[1,1'-biphenyl]-4-amine (0.26 g, 0.32 mmol, 1.1 eqv) were added along with triphenyl phosphine C<sub>18</sub>H<sub>15</sub>P (0.034 g, 0.12 mmol), potassium carbonate K<sub>2</sub>CO<sub>3</sub> (0.58 g, 4.2 mmol) and palladium acetate Pd(OAc)<sub>2</sub> (0.0051 g, 0.023 mmol). A 25 mL mixture of dioxane: THF: water (3:2:1) was added and the solution was purged with argon and refluxed for 48 hours. The solvent was then removed under reduced pressure and the obtained solid was extracted with dichloromethane, washed with water dried with sodium sulfate. The resulting crude solid was purified by column chromatography with dichloromethane and 3% methanol as eluent. T221 was isolated as a pure blue solid (0.10 g, 27% yield). Mp: 66.8-67.5 °C. <sup>1</sup>H NMR (500 MHz, Acetone-*d*<sub>6</sub>) δ 9.05 (d, *J* = 4 Hz, 1H), 8.86 (d, *J* = 4 Hz, 1H), 8.53 (d, *J* = 6 Hz, 2H), 7.84 (d, *J* = 4 Hz, 1H), 7.61 (d, *J* = 2.5 Hz, 2H), 7.60 (s, 2H), 7.55 (d, *J* = 4 Hz, 1H), 7.42 (d, *J* = 8.5 Hz, 4H), 7.16 (d, *J* = 8.5 Hz, 2H), 7.07 (d, *J* = 8.5 Hz, 4H), 7.02 (d, *J* = 9 Hz, 2H), 6.53 (d, *J* = 2.5 Hz, 2H), 6.48 (dd, *J*<sub>1</sub> = 8.5, *J*<sub>2</sub> = 2.5 Hz, 2H), 4.02 – 3.94 (m, 4H), 3.92 (td, 10H), 1.65 – 1.52 (m, 12H), 1.36 (dq, 14H), 0.87 (t, 8H), 0.82 (t, 14H), 0.74 – 0.71 (m, 8H). <sup>13</sup>C NMR (125 MHz, Acetone-*d*<sub>6</sub>) δ 207.40, 207.25, 207.08, 161.77, 158.88, 152.52, 136.30, 132.23, 126.20, 121.47, 107.64, 102.02, 69.68, 69.22, 33.06, 32.93, 25.29, 24.61, 20.95, 20.84, 15.24, 15.06, 15.04, 11.74. MALDI-TOF MS (*m/z*): calculated for C<sub>81</sub>H<sub>96</sub>N<sub>4</sub>O<sub>6</sub>S<sub>2</sub>, 1285.8; found 1285.6.

### 2.3.3. Synthetic procedure of T222

#### 2.3.3.1. Synthesis of (E)- 4-(5-bromo-2-thienyl)-4-oxo-2-butenic acid (7)<sup>117</sup>

2-Bromothiophene (20.00 g, 0.12 mol) and maleic anhydride (12.02 g, 0.12 mol, 1 eqv) were dissolved in 500 mL dichloromethane in an ice bath. AlCl<sub>3</sub> (32.70 g, 0.24 mol, 2 eqv) were then added in small portions and the mixture turned from colorless to dark brown. The reaction was allowed to stir at room temperature for 24 hours. The mixture was then poured into 500 mL ice cold 1M HCl. The organic layer was separated and washed with water and dried over magnesium sulfate. After solvent evaporation, the obtained residue was suspended in hexane and filtered to obtain a pure light brown solid (E)- 4-(5-bromo-2-thienyl)-4-oxo-2-butenic acid (14.00 g, 47% yield). <sup>1</sup>H NMR (500 MHz, CDCl<sub>3</sub>)  $\delta$  7.71 (d,  $J$  = 15.5 Hz, 1H), 7.55 (d,  $J$  = 4 Hz, 1H), 7.12 (d,  $J$  = 4 Hz, 1H), 6.89 (d,  $J$  = 15.5 Hz, 1H). <sup>13</sup>C NMR (125 MHz, CDCl<sub>3</sub>)  $\delta$  179.62, 169.69, 144.07, 136.51, 136.12, 133.90, 133.81, 133.00.

#### 2.3.3.2. Synthesis of (E)-5,5-(5-bromo-2-thienyl)bifuranylidenedione (8)<sup>117</sup>

In a 50 mL round bottom flask, (E)- 4-(5-bromo-2-thienyl)-4-oxo-2-butenic acid (8.7 g, 35.49 mmol), CuCl (1.26 g, 12.77 mmol, 0.35 eqv) and NH<sub>4</sub>Cl (1.86 g, 34.42 mmol, 0.97 eqv) were dissolved in 50 mL acetic anhydride and refluxed for 2 hours during which the mixture turned dark purple. The mixture was cooled and the solid was collected by filtration and washed with acetic acid and ethanol. The purple solid was placed in a soxhlet thimble and extracted for 5 days using boiling chloroform to yield (E)-5,5-(5-bromo-2-thienyl)bifuranylidenedione (2.25 g, 13% yield).

2.3.3.3. Synthesis of 2*H*-pyrrol-2-one, 5-(5-bromo-2-thienyl)-3-[5-(5-bromo-2-thienyl)-1-(2-ethylhexyl)-1,2-dihydro-2-oxo-3*H*-pyrrol-3-ylidene]-1-(2-ethylhexyl)-1,3-dihydro-, (3*E*) (9)<sup>118</sup>

Compound (E)-5,5-(5-bromo-2-thienyl)bifuranylidenedione (1.25 g, 2.57 mmol) and 2-ethyl-1-hexamine (1.16 g, 8.99 mmol, 3.5 eqv) were dissolved in 150 mL dichloromethane at room temperature and the mixture was left to stir for 24 hours to form a dark brown clear solution. Then TsOH.H<sub>2</sub>O (2.47 g, 14.13 mmol, 5.5 eqv) and the solution turned green-blue and was allowed to stir for 3 hours. The organic layer was then washed with water and NaHCO<sub>3</sub> and dried over sodium sulfate. The residue was subjected to chromatography with 70% hexane and 30% DCM as eluent to afford 2*H*-pyrrol-2-one, 5-(5-bromo-2-thienyl)-3-[5-(5-bromo-2-thienyl)-1-(2-ethylhexyl)-1,2-dihydro-2-oxo-3*H*-pyrrol-3-ylidene]-1-(2-ethylhexyl)-1,3-dihydro-, (3*E*) as a pure blue solid (0.17 g, 9% yield). <sup>1</sup>H NMR (500 MHz, CDCl<sub>3</sub>) δ 7.14 (d, *J* = 5 Hz, 2H), 7.10 (d, *J* = 3.5 Hz, 1H), 7.02 (d, *J* = 4 Hz, 1H), 6.96 (d, *J* = 5 Hz, 3H), 6.89 (d, *J* = 4 Hz, 2H), 3.67 (p, 8H), 1.21-1.14 (m, 36H), 0.79-0.74 (m, 24H). <sup>13</sup>C NMR (125 MHz, CDCl<sub>3</sub>) δ 169.70, 143.31, 133.63, 132.24, 130.77, 130.06, 127.17, 126.78, 126.34, 43.79, 37.86, 29.21, 27.28, 22.58, 21.94, 13.00, 9.47. MALDI-TOF MS (*m/z*): calculated for C<sub>32</sub>H<sub>40</sub>Br<sub>2</sub>N<sub>4</sub>O<sub>6</sub>S<sub>2</sub>, 708.6; found 709.1.

2.3.3.4. Synthesis of T222

In a 50 mL round bottom flask, 2*H*-pyrrol-2-one, 5-(5-bromo-2-thienyl)-3-[5-(5-bromo-2-thienyl)-1-(2-ethylhexyl)-1,2-dihydro-2-oxo-3*H*-pyrrol-3-ylidene]-1-(2-ethylhexyl)-1,3-dihydro-, (3*E*) (0.15 g, 0.21 mmol), 4-pyridinyl boronic acid (0.028 g, 0.23 mmol, 1.1 eqv) and 2',4'-dibutoxy-*N*-(2',4'-dibutoxy-[1,1'-biphenyl]-4-yl)-*N*-(4-(4,4,5,5-tetramethyl-1,3,2-dioxaborolan-2-yl)phenyl)-[1,1'-biphenyl]-4-amine (0.19 g,

0.23 mmol, 1.1 eqv) were added along with triphenyl phosphine  $C_{18}H_{15}P$  (0.030 g, 0.11 mmol), potassium carbonate  $K_2CO_3$  (0.50 g, 3.61 mmol) and palladium acetate  $Pd(OAc)_2$  (0.045 g, 0.20 mmol). A mixture of 25 mL dioxane: THF: water (3:2:1) was added and the solution was purged with argon and refluxed for 48 hours. The reaction mixture was cooled, and the solvent was removed under reduced pressure. The obtained solid was then extracted with dichloromethane washed with water and dried with sodium sulfate. The resulting solid was purified by column chromatography with dichloromethane as mobile phase. T222 was isolated as a pure blue solid (0.10 g, 37 % yield). Mp: 85.3-88.2 °C.  $^1H$  NMR (500 MHz, Acetone- $d_6$ )  $\delta$  8.51 (d,  $J = 6.0$  Hz, 2H), 7.74 (d,  $J = 4.0$  Hz, 1H), 7.58 (d,  $J = 9.0$  Hz, 5H), 7.42 (d,  $J = 9.0$  Hz, 4H), 7.16 (d,  $J = 8.5$  Hz, 3H), 7.06 – 7.02 (m, 9H), 6.52 (d,  $J = 2.5$  Hz, 2H), 6.49 (dd,  $J_1 = 8.5$ ,  $J_2 = 2.5$  Hz, 2H), 3.92-3.89 (m, 10H), 3.80-3.76 (m, 4H), 1.65-1.59 (m, 12H), 1.41-1.31 (m, 12H), 0.87 (t, 8H), 0.79 (t, 8H), 0.73-0.69 (m, 14H).  $^{13}C$  NMR (125 MHz, Acetone- $d_6$ )  $\delta$  170.49, 170.17, 159.94, 157.08, 145.13, 134.32, 130.68, 130.40, 126.77, 124.26, 123.94, 122.45, 105.80, 102.59, 100.21, 67.87, 67.42, 44.41, 44.27, 38.91, 23.45, 22.78, 22.75, 19.16, 19.06, 13.44, 13.40, 13.27, 9.92. MALDI-TOF MS (m/z): calculated for  $C_{83}H_{98}N_4O_6S_2$ , 1311.8; found 1311.8.

## 2.4. Solar Cell Fabrication

The preparations of the DSSC photoanodes as well as the solar cell assembly were done according to known literature procedures. The fluorine-doped tin oxide (FTO) conductive glass substrates “TEC15” were cleaned with detergent solution, followed by rinsing with distilled water and ethanol in an ultrasonic bath for 10 minutes.

The clean FTOs were pretreated in a 40 mM  $\text{TiCl}_4$  aqueous solution at 70 °C for 1 hour, then rinsed with water and ethanol, and sintered at 500°C for 30 mins. Then, compact titania layer (Ti-Nanoxide BL/SP, Solaronix, Switzerland) was first spin-coated on the clean conductive glass substrate, followed by treatment with 40 mM  $\text{TiCl}_4$  aqueous solution at 70 °C for 30 min. A 4  $\mu\text{m}$  thick titania layer was then printed by the doctor blading method from a diluted  $\text{TiO}_2$  paste (60%  $\text{TiO}_2$  Dyesol 30NR-D, 34% terpeneol and 6% ethyl cellulose) for the T-series dyes and/or with DB and a 6  $\mu\text{m}$  thick layer for T221 with D35. The obtained  $\text{TiO}_2$  films were gradually heated at 200 °C for 10 mins, 300 °C for 10 mins, 400 °C for 10 mins and 550 °C for 15 mins, and then were sintered at 500 °C for 30 mins using a furnace. Next, a 4  $\mu\text{m}$  scattering layer of Dyesol WER2-O  $\text{TiO}_2$  paste was applied and the same procedure of sintering was applied. The thickness of the films was measured with Profilometer. The films were then immersed in a 40 mM  $\text{TiCl}_4$  aqueous solution at 70 °C for 30 mins, rinsed with water and ethanol and sintered at 500 °C for mins. The electrodes were further sintered at 500 °C for 30 mins, after reaching a temperature of almost 80 °C dye sensitization was performed where the films were dipped in a dye bath solution of 0.2 mM for the three individual dyes and/or with 0.03 mM Dyeblue (DB) in THF: t-butanol: acetonitrile (1:1:1) and a solution of 0.2 mM D35 dye in THF: ethanol (1:4) for 24 hours. The counter electrodes were fabricated by applying a 2-3  $\mu\text{l}/\text{cm}^2$  of 5 mM  $\text{H}_2\text{PtCl}_6$  in 2-propanol to the “Tec8” FTO glass, followed by heating in an oven at 400 °C for 20 minutes. Cell assembly was performed by sealing the counter electrode to the  $\text{TiO}_2$  electrode with a 25  $\mu\text{m}$  Surlyn (Dupont) spacer at ~ 100 °C for 3 mins. The cobalt electrolyte (the electrolyte consisted of 0.25 M  $\text{Co}^{\text{(II)}}(\text{bpy})_3\cdot 2\text{PF}_6$ , 0.06 M  $\text{Co}^{\text{(III)}}(\text{bpy})_3\cdot 3\text{PF}_6$ , 0.1 M  $\text{LiClO}_4$  and 0.6 M or 0.2 M *t*-butyl pyridine (TBP) in acetonitrile) was introduced



through two small holes, previously drilled through the counter electrode, which were then sealed with Surlyn®.

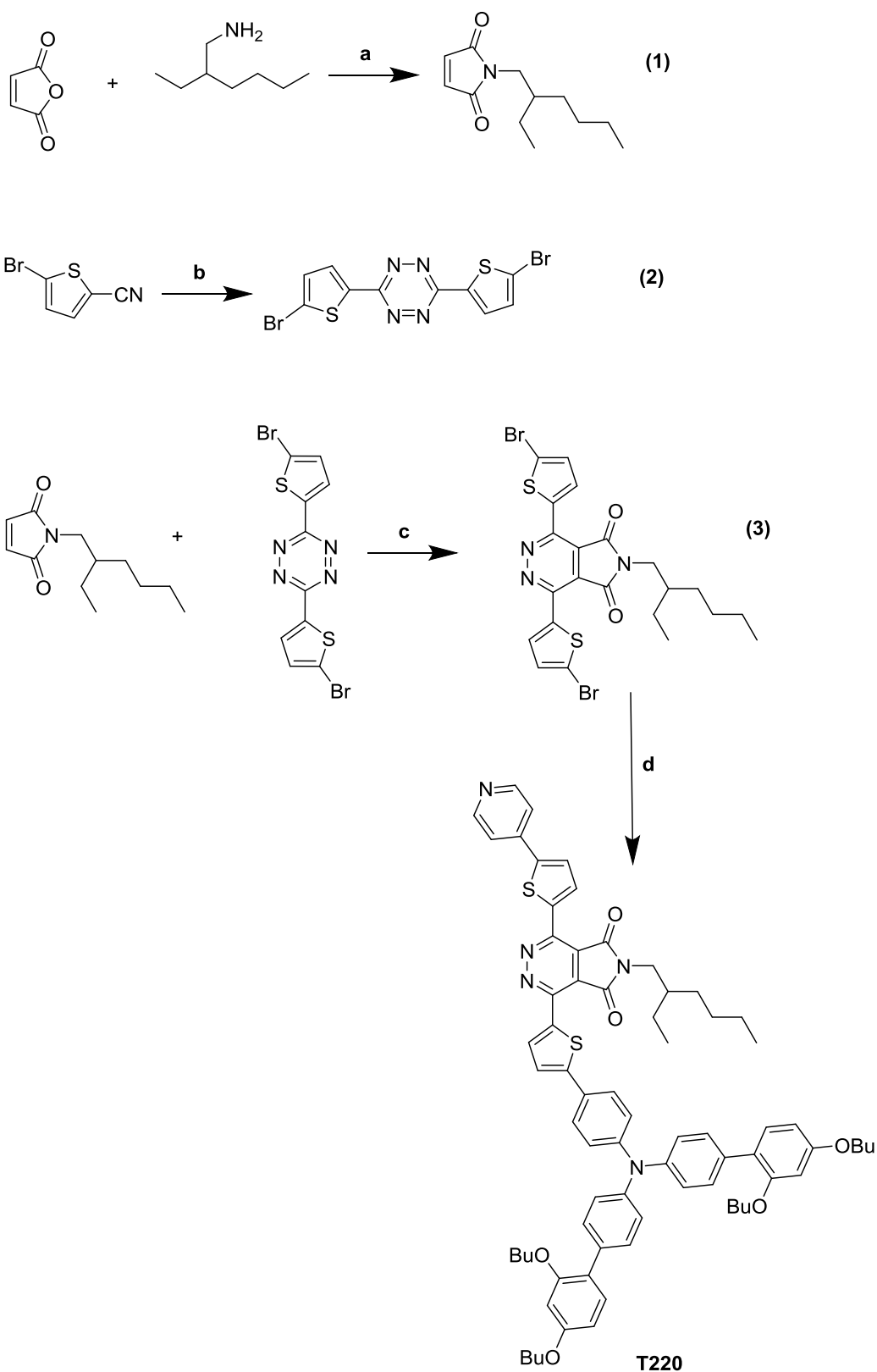
# CHAPTER 3

## RESULTS AND DISCUSSION

### 3.1. Dye Design

#### 3.1.1. *Synthetic Procedure of T220*<sup>113-115</sup>

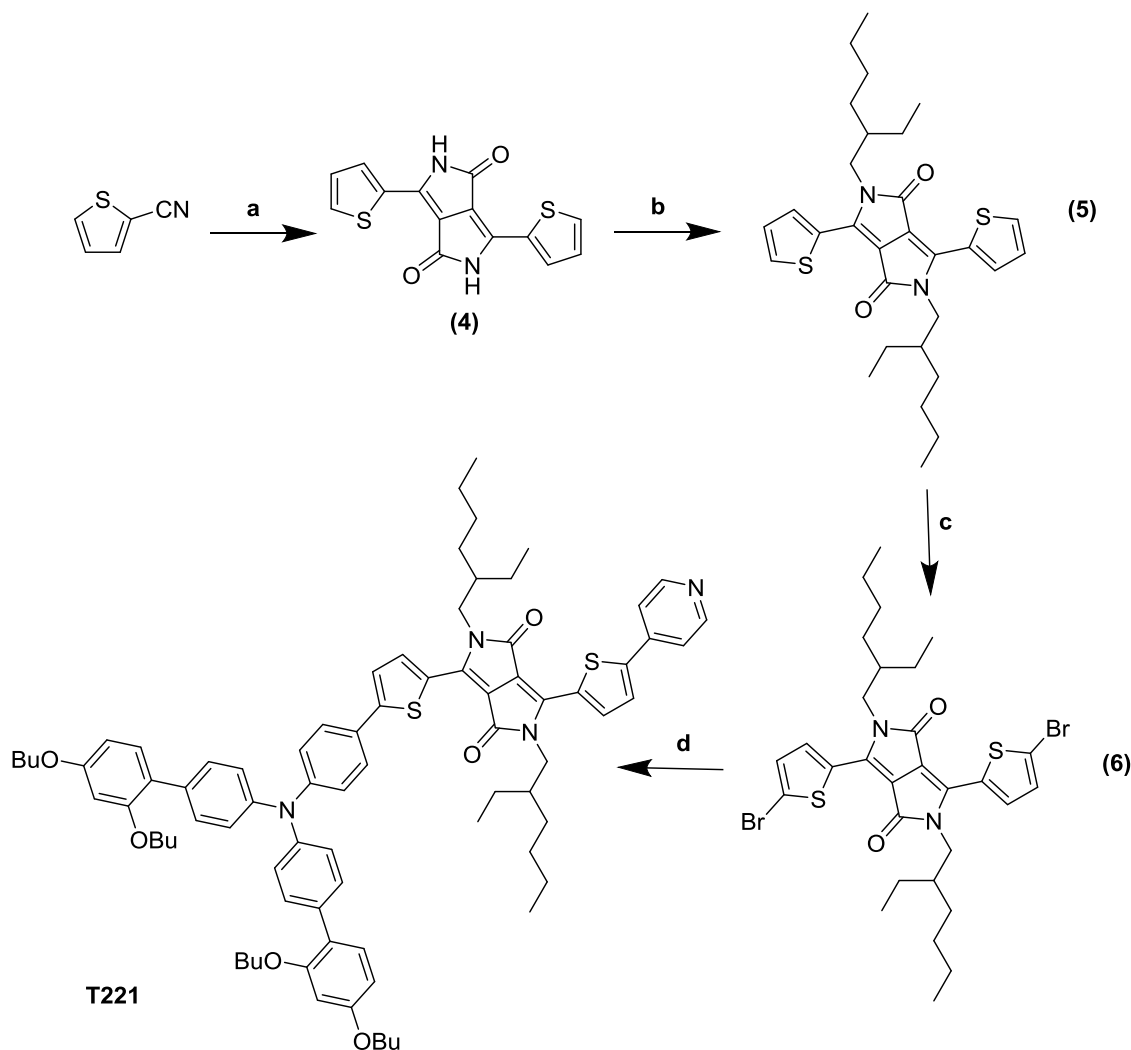
T220 was successfully designed and synthesized and its synthetic route is shown in scheme 1. The dye was prepared in four steps where the first step consists of the formation of the dienophile by the addition of the 2-ethylhexylamine chain to maleic anhydride; this alkyl chain is believed to suppress the recombination reaction between the oxidized electrolyte and the electrons in the TiO<sub>2</sub> conduction band as well as it prevents dye aggregation. This is followed by the formation of the di-bromo substituted tetrazine unit which acts as the diene. Afterwards, the tetrazine group reacts with the dienophile through a [4+2] Diels-Alder cycloaddition yielding the [4+2] Diels-Alder adduct which then undergoes an irreversible retro Diels-Alder step which is responsible for the release of nitrogen to give the middle pyridazine dibromo acceptor group. Finally a Suzuki coupling reaction was performed where the linking of the large triphenylamine donor group and the pyridine anchoring group to the middle acceptor unit was accomplished simultaneously in one-pot synthesis to give the desired orange dye T220. The structure of the dye was confirmed by <sup>1</sup>H NMR, <sup>13</sup>C NMR and mass spectrometry.



**Scheme 1:** Synthetic scheme of T220 where a) dichloromethane, acetic anhydride, sodium acetate; b) hydrazine, sulfur, ethanol, sodium nitrite, acetic acid; c) diphenyl ether at 150°C; d) C<sub>5</sub>H<sub>6</sub>BNO<sub>2</sub>, C<sub>52</sub>H<sub>66</sub>BNO<sub>2</sub>, Pd(OAc)<sub>2</sub>, PPh<sub>3</sub>, K<sub>2</sub>CO<sub>3</sub>, dioxane:THF:H<sub>2</sub>O

### 3.1.2. Synthetic Procedure of T221<sup>119</sup>

T221 was successfully designed and synthesized and its synthetic route is shown in scheme 2. The first step consists of a condensation reaction of diethylsuccinate with thiophene-2-carbonitrile in the presence of a strong base to give the pyrroline ester which further reacts with another thiophene-2-carbonitrile group where the subsequent ring closure affords the diketopyrrolopyrrole (DPP) moiety. Subsequently, a double *N*-alkylation is accomplished using potassium carbonate as a base to deprotonate the lactam units and thus attaching the 2-ethylbromohexane alkyl chain on the amide positions, yielding the soluble dialkyl-DPP compound. Then, the corresponding *N, N*-disubstituted DPP undergoes bromination with *N*-bromosuccinimide (NBS) to give the dibromo compounds which will undergo a Suzuki coupling reaction to attach the donor and pyridine anchoring group on the DPP core to finally give the desired blue dye T221. The structure of the dye was confirmed by <sup>1</sup>H NMR, <sup>13</sup>C NMR and mass spectrometry.

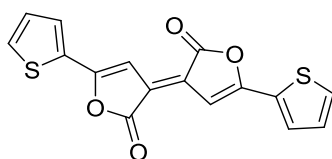


**Scheme 2:** Synthetic scheme of T221 where a) tertiary amyl alcohol, potassium tert-butoxide, diethyl succinate; b)  $K_2CO_3$ , 2-ethyl-1-bromohexane, 18-crown ether, DMF; c) NBS, acetic acid and chloroform; d)  $C_5H_6BNO_2$ ,  $C_{52}H_{66}BNO_2$ ,  $Pd(OAc)_2$ ,  $PPh_3$ ,  $K_2CO_3$ , dioxane:THF:H<sub>2</sub>O

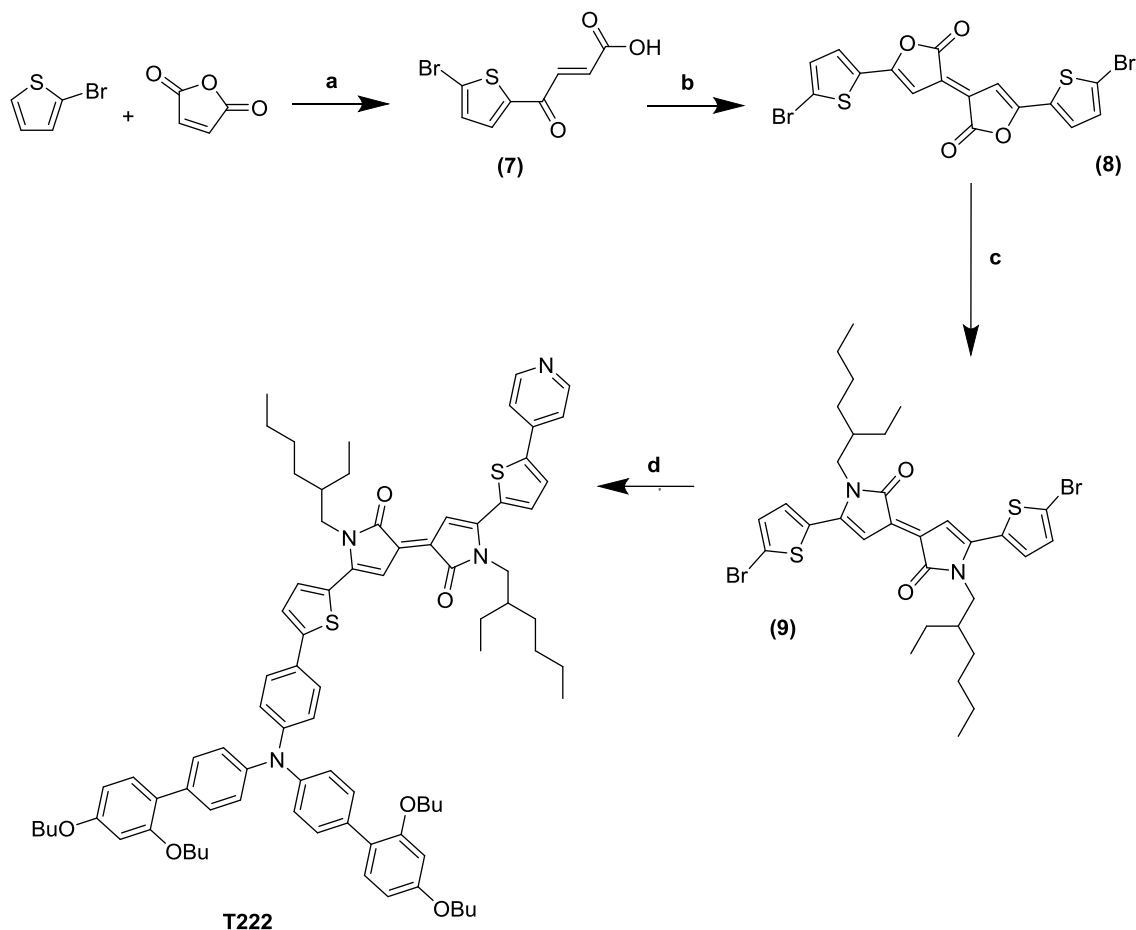
### 3.1.3. Synthetic Procedure of T222<sup>117-118</sup>

T222 was successfully designed and synthesized and its synthetic route is shown in scheme 3. T222 is a thiophene containing Pechmann-based dye. The basic structure of the Pechmann dye consists of a butenolide dimer with two lactones joined by an *exo* double bond in a *trans* manner, the structure of thiophene-based Pechmann dye is shown in figure 14. The first step in its synthesis corresponds to a Friedel-Crafts

acylation which is followed by the formation of the Pechmann chromophore and then the addition of the 2-ethylhexylamine chain and finally Suzuki coupling reaction for the addition of the donor and anchoring group to give our desired blue dye. The structure of the dye was confirmed by  $^1\text{H}$  NMR,  $^{13}\text{C}$  NMR and mass spectrometry.



**Figure 14:** Structure of a thiophene containing Pechmann dye.

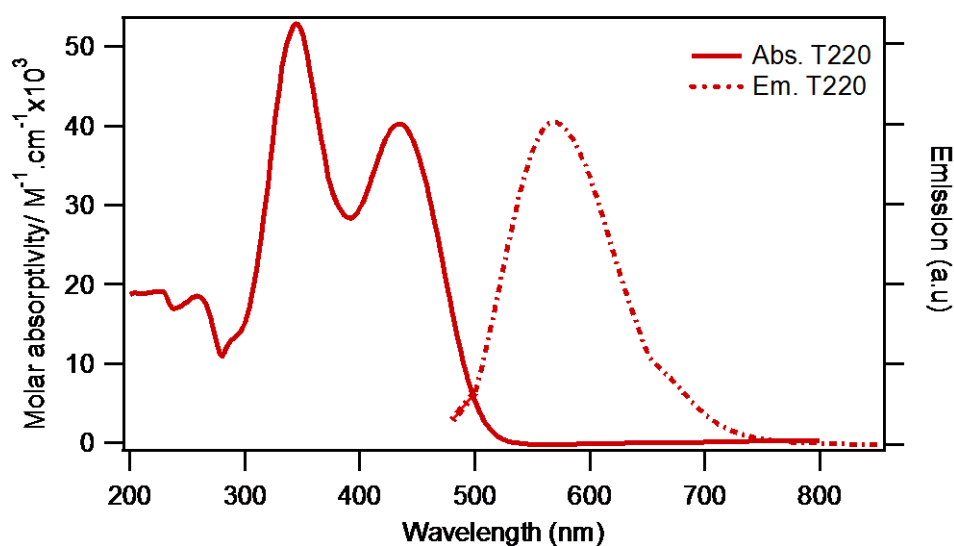


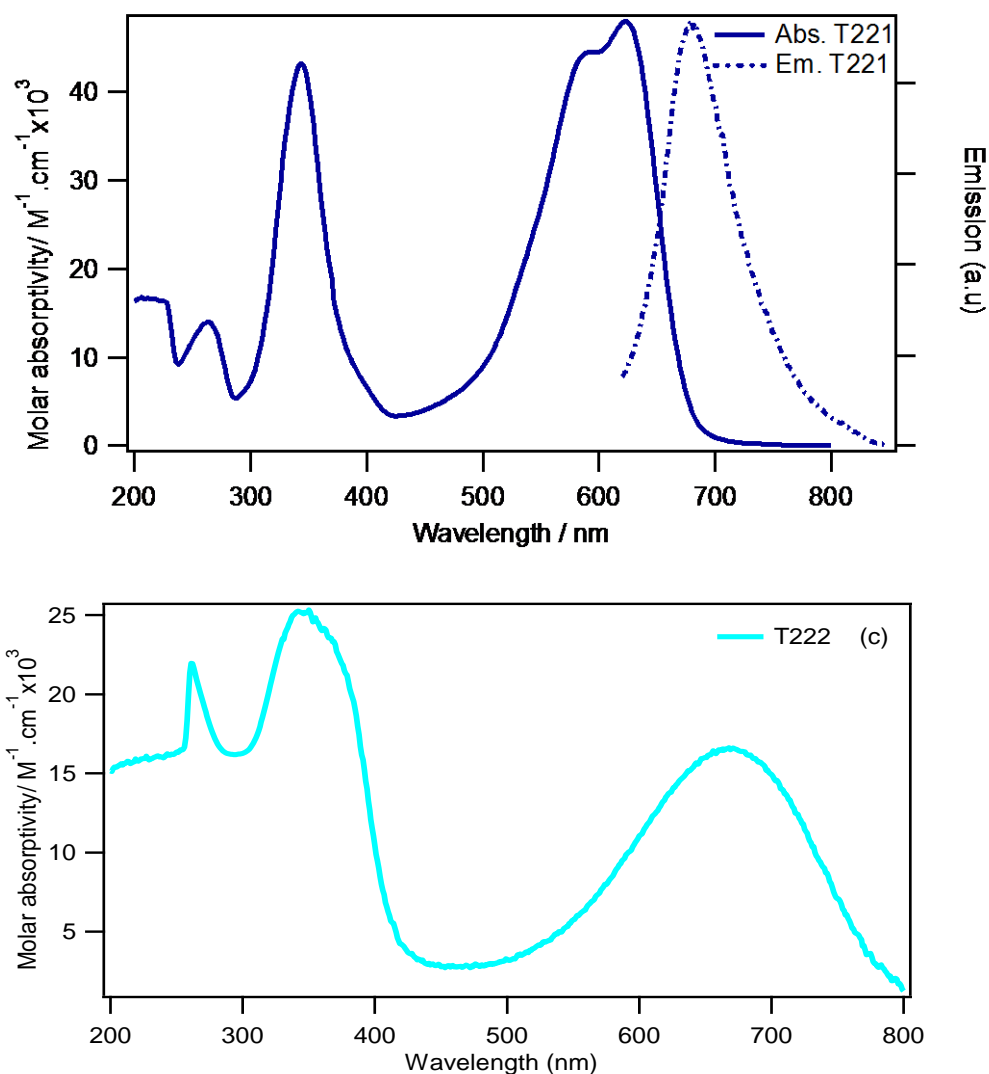
**Scheme 3:** Synthetic scheme of T222 where a)  $\text{AlCl}_3$ , dichloromethane; b)  $\text{CuCl}$ ,  $\text{NH}_4\text{Cl}$ , acetic anhydride; c) 2-ethylhexylamine, dichloromethane; d)  $\text{C}_5\text{H}_6\text{BNO}_2$ ,  $\text{C}_{52}\text{H}_{66}\text{BNO}_2$ ,  $\text{Pd}(\text{OAc})_2$ ,  $\text{PPh}_3$ ,  $\text{K}_2\text{CO}_3$ , dioxane:THF: $\text{H}_2\text{O}$

### 3.2. Optical and Electrochemical Properties

The UV-Vis absorption spectra of T220, T221 in THF and T222 dyes in DMF solution are shown in figure 15 (a, b, c).

As shown in figure 15, all dyes exhibit two major broad absorption peaks; a band located at a shorter wavelength at around 300-380 nm and a band at a longer wavelength at around 400-650 nm. The absorption maxima ( $\lambda_{\text{max}}$ ) were observed at 434, 624, and 670 nm for T220, T221 and T222, respectively. The corresponding molar extinction coefficient ( $\epsilon$ ) for T220, T221 and T222 are  $4.0 \times 10^4$ ,  $4.8 \times 10^4$ , and  $1.7 \times 10^4 \text{ M}^{-1} \text{ cm}^{-1}$ , respectively. T222 has a relatively lower extinction coefficient compared to the other two dyes, which will certainly affect the light harvesting efficiency of the device. As expected the two blue dyes T221 and T222 exhibited a light harvesting ability above 600 nm allowing a photo response in the red region of the spectra.



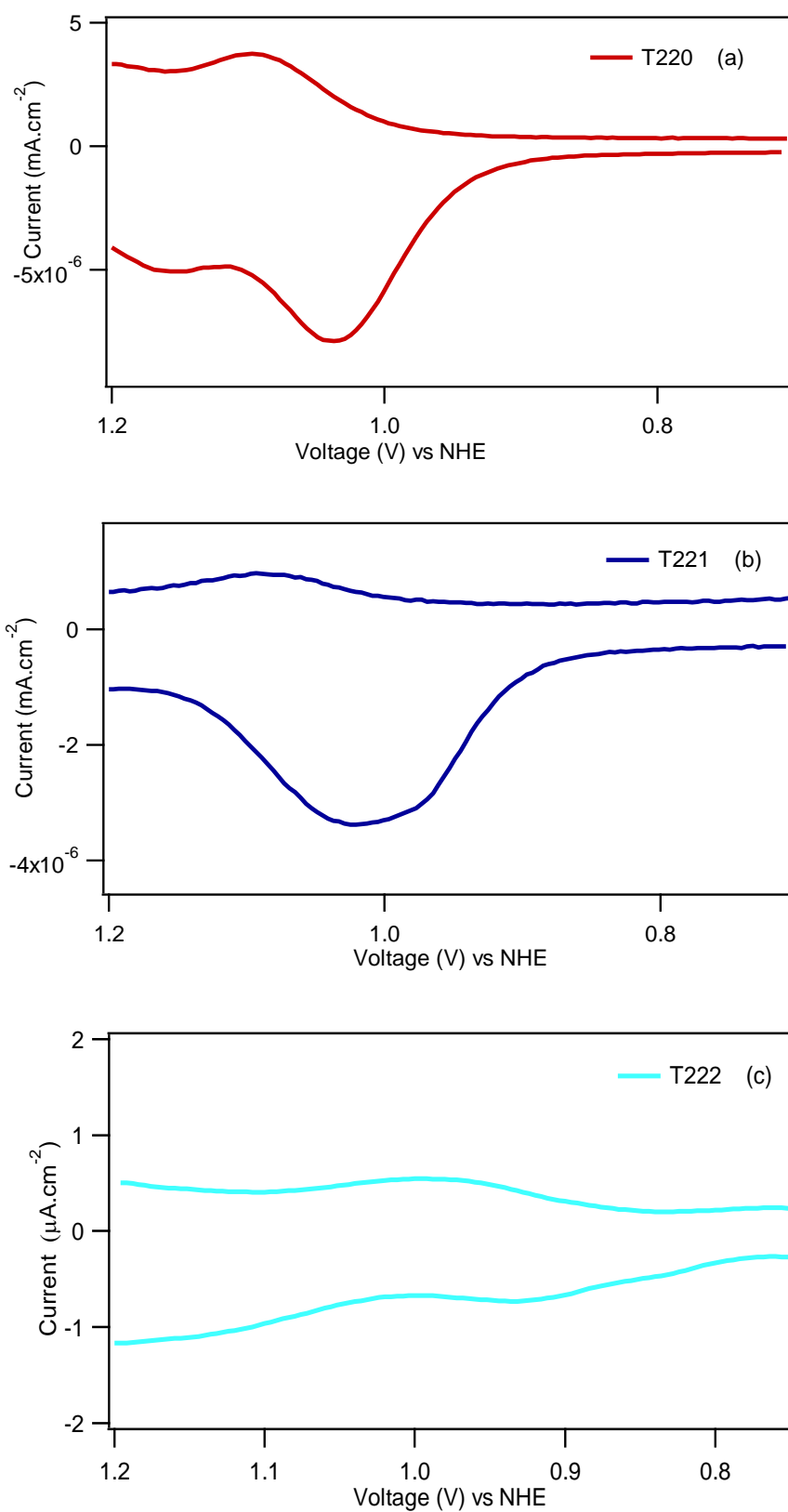


**Figure 15:** UV-vis absorption (solid) and emission (dotted) spectra of a) T220, b) T221 and c) T222 in THF ( $\lambda_{\text{ex}} = 434$  and  $624$  nm for T220 and T221, respectively).

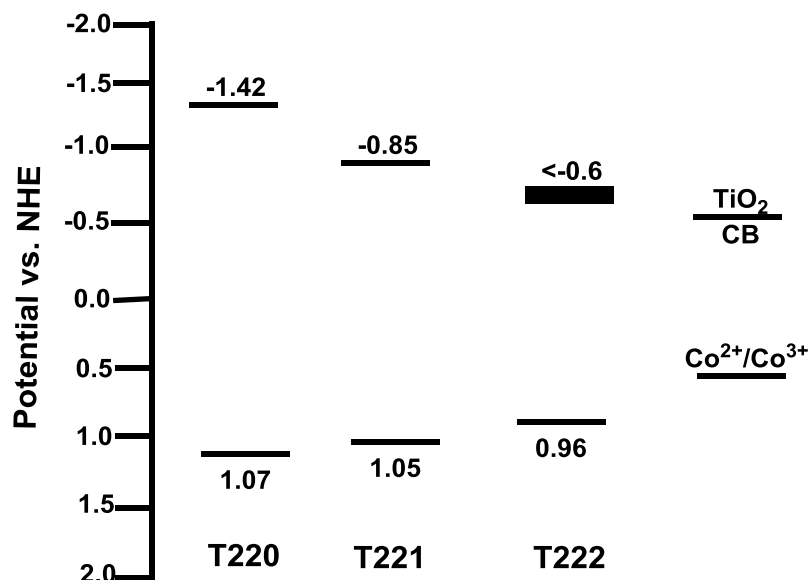
The fluorescence emission spectra of T220, and T221 in THF are also shown in figures 15 (a, b), correspondingly. The fluorescent maximum ( $\lambda_{\text{em}}$ ) occurs at  $570$  nm for T220,  $679$  nm for T221. However, the emission of T222 was not detected.



In order to investigate the possibility of energy level matching of the dye sensitizers with respect to the TiO<sub>2</sub> semiconductor and the electrolyte, the electrochemical properties of the three mentioned dyes were carried out using differential pulse voltammetry (DPV) measurements in a typical three-electrode cell. The measurements were performed in a dimethyl formamide solution containing 0.1 M TBAPF<sub>6</sub> (tetrabutylammonium hexafluorophosphate) as supporting electrolyte, an Ag/Ag<sup>+</sup> reference electrode which is calibrated with ferrocene/ferrocenium (Fc/Fc<sup>+</sup>) redox couple as an internal standard and a platinum counter electrode. The ground state redox potentials  $E_{ox}$  of T220, T221, and T222 were determined to be 1.07, 1.05 and 0.96 V vs. NHE, respectively. These values are more positive than [Co(bpy)<sub>3</sub>]<sup>2+/3+</sup> redox potential (+0.56 V vs. NHE), thus providing sufficient driving force for dye regeneration. The excited state redox potentials  $E_{ox}^*$  of the dye sensitizers were estimated from the equation  $E_{ox} - E_{0-0}$ , where  $E_{0-0}$  corresponds to the optical energy gap which is calculated from the intersection of the absorption and emission spectra.  $E_{ox}^*$  for T220 and T221 were found to be -1.42, and -0.85 V vs. NHE, respectively, which are more negative than the TiO<sub>2</sub> conduction band edge (-0.5 V vs. NHE) suggesting an efficient and fast electron injection. In the case of T222, we estimated the  $E_{ox} - E_{0-0}$  to be less than -0.6 V vs. NHE, which is barely above the CB of TiO<sub>2</sub>. The differential pulse voltammograms of T220, T221, and T222 are shown in Figure 16 (a, b, c), and the corresponding photophysical and electrochemical properties of the dyes are summarized in table 1. The energy levels of the three dyes with respect to TiO<sub>2</sub> conduction band and the redox couple are summarized in figure 17.



**Figure 16:** Differential pulse voltammetry of a) T220 b) T221 and c) T222 in DMF.



**Figure 17:** Schematic representation of the energy levels of T220, T221 and T222.

**Table 1.** Optical and electrochemical properties of T220, T221, and T222 dyes

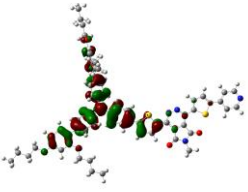
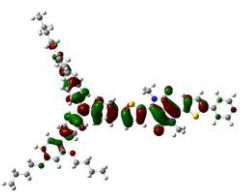
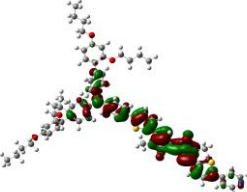
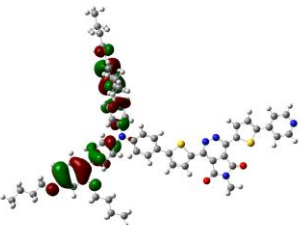
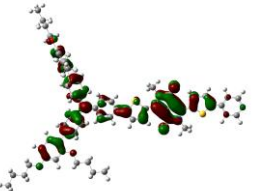
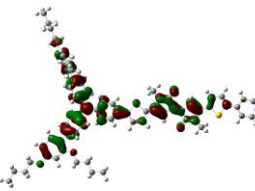

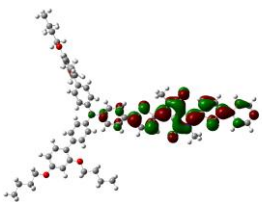
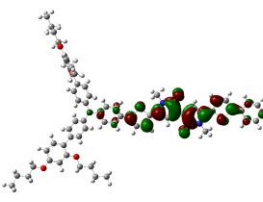
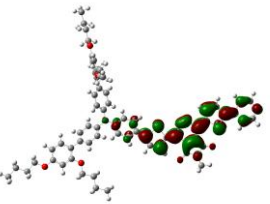
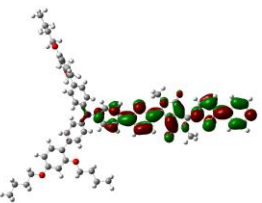
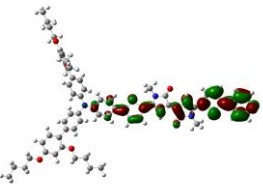
Dye	Abs. ( $\epsilon \times 10^4 \text{ M}^{-1} \text{ cm}^{-1}$ )	$\lambda_{\text{em}}$ ( $\lambda_{\text{ex}}$ ), nm	$E_{\text{ox}}$ , V vs NHE	$E_{\text{ox}} - E_{0-0}$ V vs NHE
T220	344 (5.3), 434 (4.0)	570 (434)	1.07	-1.42
T221	342 (4.3), 624 (4.8)	679 (624)	1.05	-0.85
T222	347 (2.5), 670 (1.7)	N.D.	0.96	< -0.6

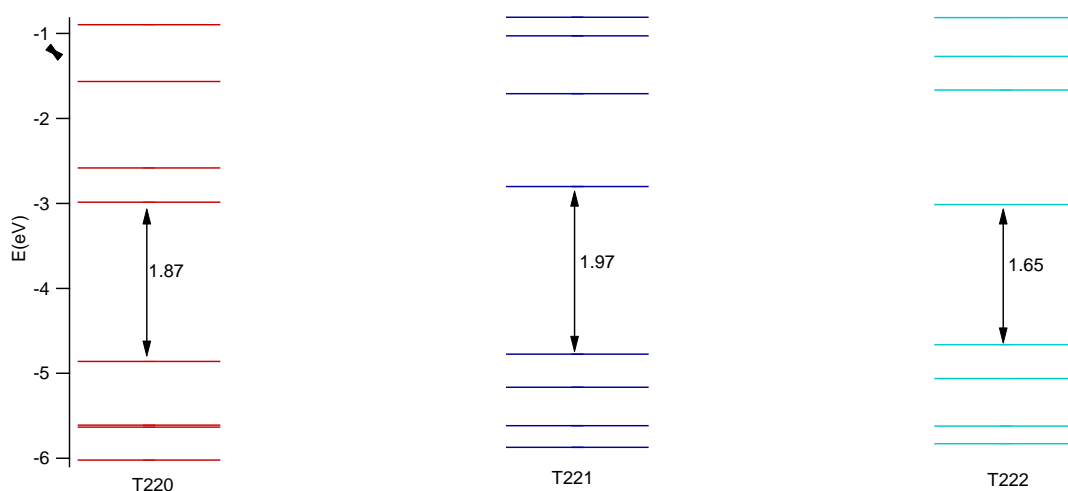
### 3.3. Computational Studies

In order to understand the electronic properties as well as the electronic transitions of the three dyes, DFT and time dependent density functional (TD-DFT) calculations were carried out using *Gaussian 03*. The electronic distributions of the frontier molecular orbitals of the three dyes are shown in table 2, and the corresponding energy levels are shown in figure 18. Usually, the HOMO electron density is mainly distributed over the triphenylamine donor group and the LUMO is localized over the

middle acceptor unit, the conjugated thiophene spacer, and the electron withdrawing pyridine anchoring group in each dye. This, under illumination, would result in a strong intramolecular charge transfer between the excited dyes and the TiO<sub>2</sub> conduction band. From table 2, the HOMO orbital of T220 is basically concentrated on the donor group; however its LUMO is solely located on the middle acceptor unit only isolated from the pyridine anchoring group, whereas the LUMO+1 is located on the middle acceptor group and shifted towards the pyridine anchoring group, suggesting that the injection occurs from the LUMO+1 level. Except for T220, the LUMO are concentrated in all dyes on the acceptor- $\pi$ -pyridine moiety which is favorable for electron injection into the valence band of TiO<sub>2</sub>. For T221, the HOMO is delocalized mostly over the donor- $\pi$  triphenylamine-thiophene moiety and extends to the middle acceptor- $\pi$ . However, in the case of T222 the HOMO extends all the way to the pyridine moiety and concentrated over the middle acceptor. Such a shift in electron density in the case of T222 might have a profound effect on the electron recombination from TiO<sub>2</sub> to the oxidized T222 dye, and consequently this could be an additional reason, besides its low LUMO level, for its bad performance in a DSSC. From figure 18, T222 dye exhibits a reduced HOMO-LUMO energy gap (1.65 eV) shifting the absorption spectrum towards longer wavelengths, which is consistent with the experimental UV-vis spectrum in figure 15 c). On the other hand, T220 shows a more reduced band gap (1.87 eV) compared to T221 (1.97 eV); these calculated results imply that T220 should exhibit a more red shifted absorption spectrum when compared to T221, however experimentally from the UV-vis spectra the opposite case was seen. The calculated electronic transitions with oscillator strength  $f \geq 0.02$  of the three dyes in water are shown in Table 3 (a, b, c).

**Table 2.** Frontier molecular orbitals of T220, T221, and T222

Dye	T220	T221	T222
HOMO			
HOMO-1			
LUMO			
LUMO+1			



**Figure 18:** Energy level diagram of T220, T221, and T222.

**Table 3.** Calculated spectra of T220, T221, and T222, respectively

**a)**

Dye	Excitation energy, nm	Oscillator strength	Assignment
<b>T220</b>	454.1	0.9364	HOMO→LUMO (35%), HOMO-1→LUMO (22%), HOMO→LUMO+1 (22%), HOMO-1→LUMO+1 (10%)
	438.6	1.1820	HOMO→LUMO+1 (34%), HOMO→LUMO (18%), HOMO-1→LUMO+1 (17%), HOMO-1→LUMO (15%)
	402.9	0.0024	HOMO-10→LUMO (79%), HOMO-9→LUMO (9%)
	354.7	0.0604	HOMO-3→LUMO (29%), HOMO→LUMO (29%), HOMO-1→LUMO (22%), HOMO-6→LUMO (6%), HOMO-4→LUMO (5%)
	349.7	0.2426	HOMO-1→LUMO+1 (31%), HOMO-3→LUMO+1 (26%), HOMO→LUMO+2 (11%), HOMO→LUMO+1 (10%)
	308.8	0.1532	HOMO-6→LUMO (22%), HOMO-1→LUMO (14%), HOMO→LUMO (13%), HOMO→LUMO+4 (10%), HOMO-4→LUMO (10%), HOMO-3→LUMO (8%), HOMO-17→LUMO (7%)
	308.6	0.8268	HOMO→LUMO+4(68%)
	305.9	0.2482	HOMO→LUMO+2 (29%), HOMO→LUMO+1 (27%), HOMO→LUMO+3 (16%), HOMO-1→LUMO+2 (8%), HOMO-1→LUMO+1 (7%)
	300.0	0.1967	HOMO-6→LUMO+1 (21%), HOMO-1→LUMO+2 (12%), HOMO→LUMO+3 (11%), HOMO-4→LUMO+1 (9%), HOMO-1→LUMO+1 (8%), HOMO-3→LUMO+1 (8%)

**b)**

Dye	Excitation energy, nm	Oscillator strength	Assignment
<b>T221</b>	575.4	1.7170	HOMO→LUMO (74%), HOMO-1→LUMO (21%)
	404.7	0.2867	HOMO-1→LUMO (54%), HOMO→LUMO+1 (13%), HOMO→LUMO (10%), HOMO-3→LUMO (10%)
	352.7	0.0244	HOMO→LUMO+1 (37%), HOMO-9→LUMO (22%), HOMO-1→LUMO+1 (18%), HOMO-1→LUMO (6%)
	313.8	0.9077	HOMO-6→LUMO (28%), HOMO-7→LUMO (21%), HOMO→LUMO+2 (17%), HOMO-1→LUMO+1 (6%)
	308.3	0.9680	HOMO→LUMO+3 (50%), HOMO-1→LUMO+3 (32%)
	305.8	0.0748	HOMO-7→LUMO (30%), HOMO-3→LUMO (26%), HOMO→LUMO+2 (8%)
	303.0	0.0479	HOMO-6→LUMO (23%), HOMO→LUMO+2 (14%), HOMO-3→LUMO (13%), HOMO-1→LUMO+1 (11%), HOMO-1→LUMO (9%)

**c)**

Dye	Excitation energy, nm	Oscillator strength	Assignment
<b>T222</b>	708.3	1.6737	HOMO→LUMO (87%), HOMO-1→LUMO (10%)
	449.3	0.0854	HOMO-1→LUMO (31%), HOMO-4→LUMO (29%), HOMO-3→LUMO (20%), HOMO-8→LUMO (6%)
	413.1	0.3803	HOMO-1→LUMO (37%), HOMO-4→LUMO (25%), HOMO-8→LUMO (15%), HOMO→LUMO (5%)
	336.4	1.1403	HOMO→LUMO+2 (52%), HOMO-7→LUMO (12%), HOMO-1→LUMO (10%), HOMO-1→LUMO+1 (6%)
	318.1	0.0212	HOMO-8→LUMO (35%), HOMO-3→LUMO (29%), HOMO-7→LUMO (12%)
	315.9	0.0588	HOMO-7→LUMO (39%), HOMO→LUMO+2 (16%), HOMO-3→LUMO (13%)
	309.1	0.9147	HOMO-1→LUMO+3 (50%), HOMO→LUMO+3 (30%)

### 3.4. Photovoltaic Performance

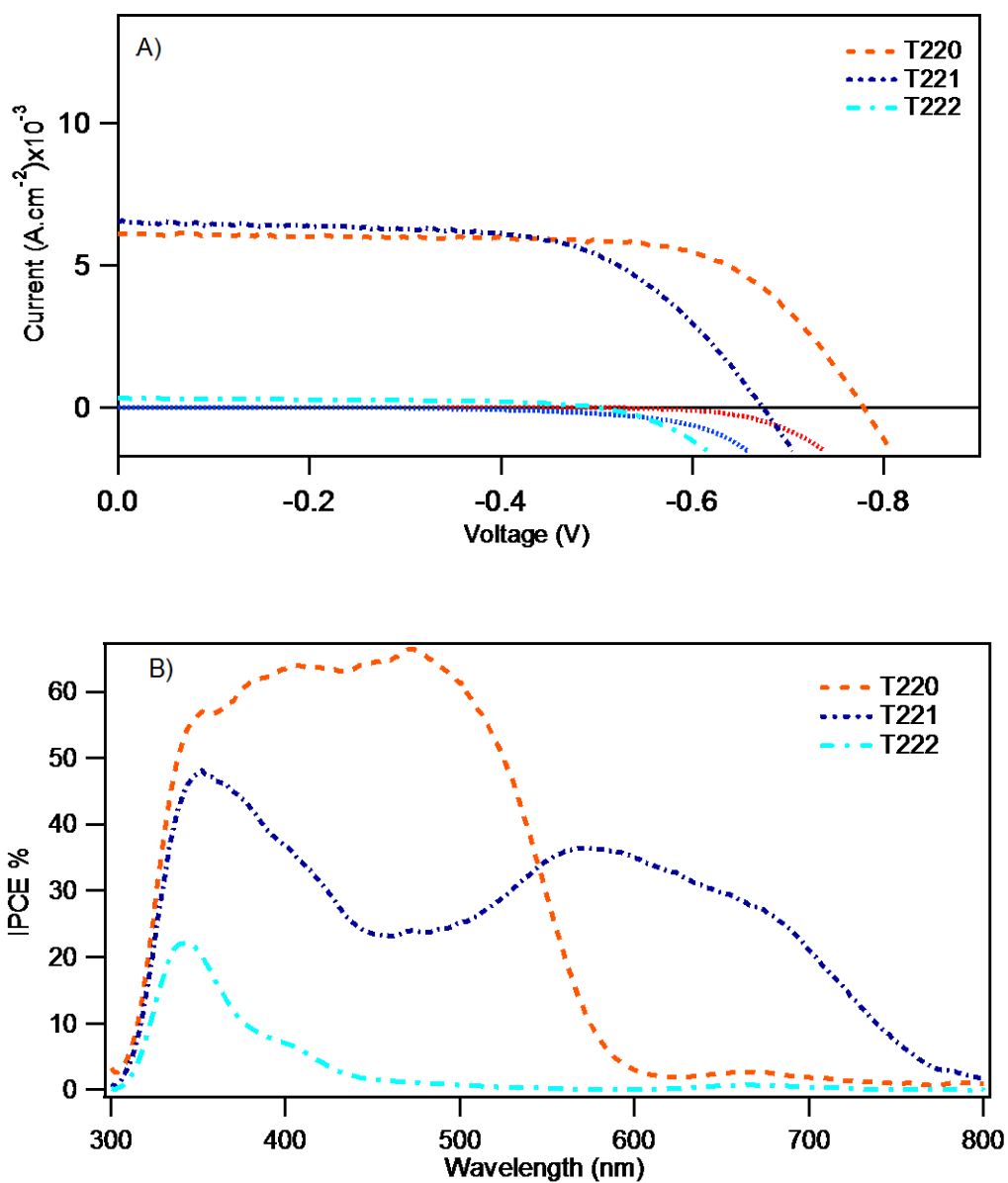
#### 3.4.1. Individual Dye Performance

In order to study the performance of the three dyes in DSSCs, 0.2 mM of each dye was sensitized individually on a 4 μm thick active transparent TiO<sub>2</sub> layer and a 4 μm scattering layer. The performance of the three dyes in fully functional DSSCs was evaluated by fabricating cobalt-based DSSC devices whereby the electrolyte system

consisted of 0.6 M tert-butyl pyridine (TBP) additive for T220 and T221 and 0.2 M TBP for T222. The *I-V* curves measured under standard AM 1.5 Global conditions are shown in figure 19 A). The corresponding photovoltaic parameters are summarized in Table 4. Among the three dyes, T220 showed the highest photovoltaic performance with a short-circuit current of  $6.1 \text{ mA.cm}^{-2}$ , an open circuit voltage of 773 mV, and an overall efficiency PCE% of 3.3 %. The DSSC based on T222 as a sensitizer showed the poorest performance with a  $J_{SC} = 0.3 \text{ mA.cm}^{-2}$ , a  $V_{OC} = 498 \text{ mV}$  and a  $FF = 0.47$ , corresponding to an overall conversion efficiency of 0.1 %. The low performance of the device can be attributed to its low molar extinction coefficient, poor electron injection due to its low LUMO level and high recombination processes in the DSSC as can be inferred from the low  $V_{oc}$ .

Action spectra of monochromatic incident to photon current efficiency (IPCE%) for the three DSSCs are shown in figure 19 B). The onset wavelength of the IPCE spectrum for the DSSC based on T220 was 610 nm with IPCE values of around 65%. With a starting wavelength of 770 nm, a maximum of around 47% at 350 nm was observed for the T221-based device as well as a shoulder is seen at around 690 nm. T222 demonstrated the lowest IPCE% among all of the three dyes as predicted from its *I-V* performance. The low IPCE value of the DSSC based on T222 might be due to the reduced LUMO level leading to a smaller energy gap between the LUMO the dye and the conduction band edge of  $\text{TiO}_2$ , which in turn decreases the charge injection kinetics and therefore lower  $J_{sc}$ .





**Figure 19:** A) *I-V* curve of the DSSCs based on the individual T220, T221 and T222 dyes under illumination and in darkness, B) incident photon-to-current conversion efficiency spectra.

**Table 4.** Photovoltaic performance of T220, T221, and T222 devices obtained from the *I-V* curves

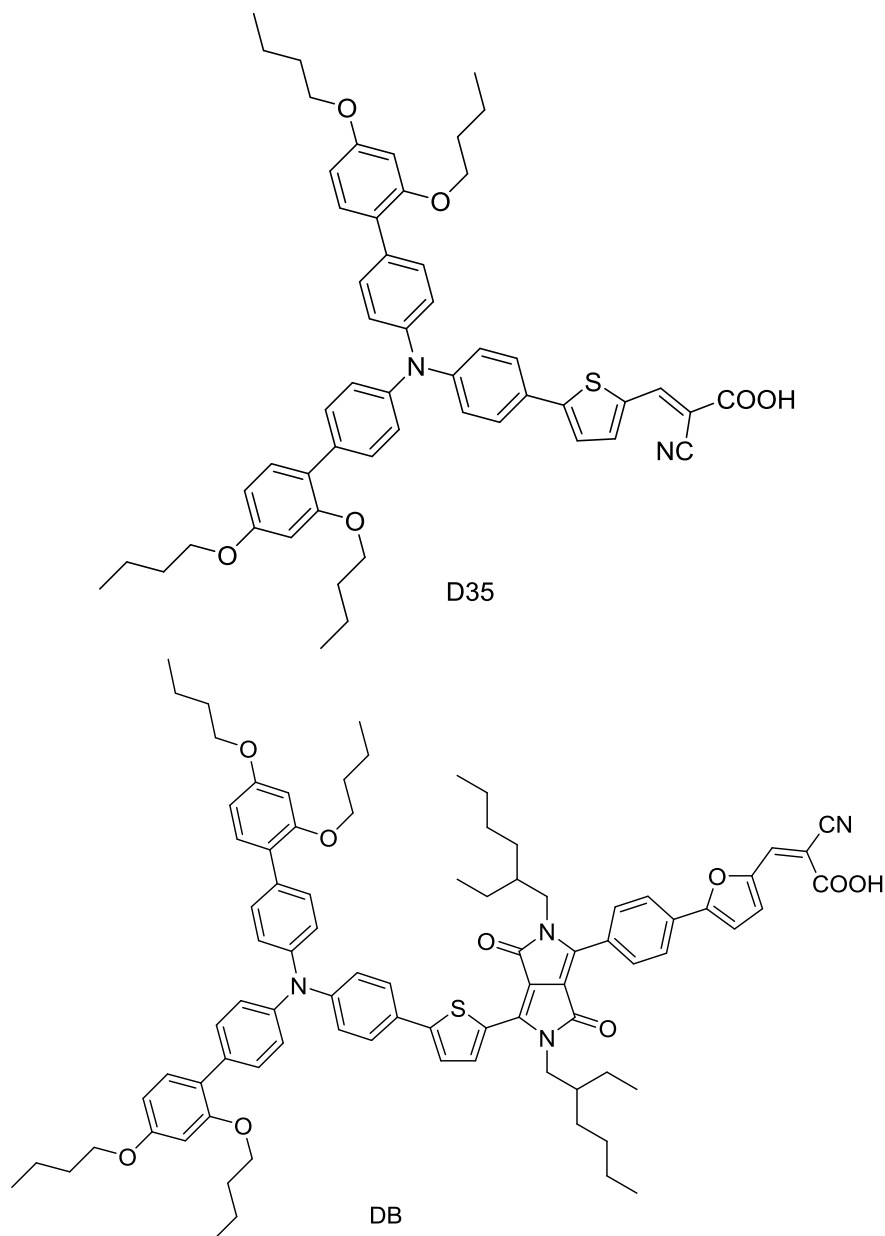
Dye	$J_{SC}$ (mA.cm <sup>-2</sup> )	$V_{OC}$ (mV)	FF	PCE (%) <sup>a</sup>
T220	6.1	773	0.68	3.3
T221	6.7	669	0.60	2.7
T222	0.3	498	0.47	0.1

<sup>a</sup> Measured under 100 mW.cm<sup>-2</sup> simulated AM1.5 spectrum with an active area 0.5 x 0.5 cm<sup>2</sup> and a black mask (0.6 x 0.6 cm<sup>2</sup>); the electrolyte consisted of 0.25 M Co(II), 0.06 M Co(III), 0.1 M LiClO<sub>4</sub>, 0.6 M TBP for T220 and T221 and 0.2 M TBP for T222

### 3.5. Dye Loading Measurements

Due to the fact that the pyridine-based T220 and T221 dyes exhibited the highest photovoltaic performance, these two dyes were chosen to further study their performance in DSSCs as co-sensitizing dyes.

In order to study the effect of co-adsorbing pyridine-anchor dyes with carboxyl-anchor based dyes, the orange dye T220 was co-sensitized with a commercially available blue cyanoacrylic-based dye DB (dyenamo blue), and the blue dye T221 was co-sensitized with an orange cyanoacrylic-based sensitizer D35 (dyenamo orange). The selection of DB and D35 dyes was solely based on matching of their absorption spectra with that of T220 and T221, respectively. The molecular structures of DB and D35 dyes are shown in figure 20.

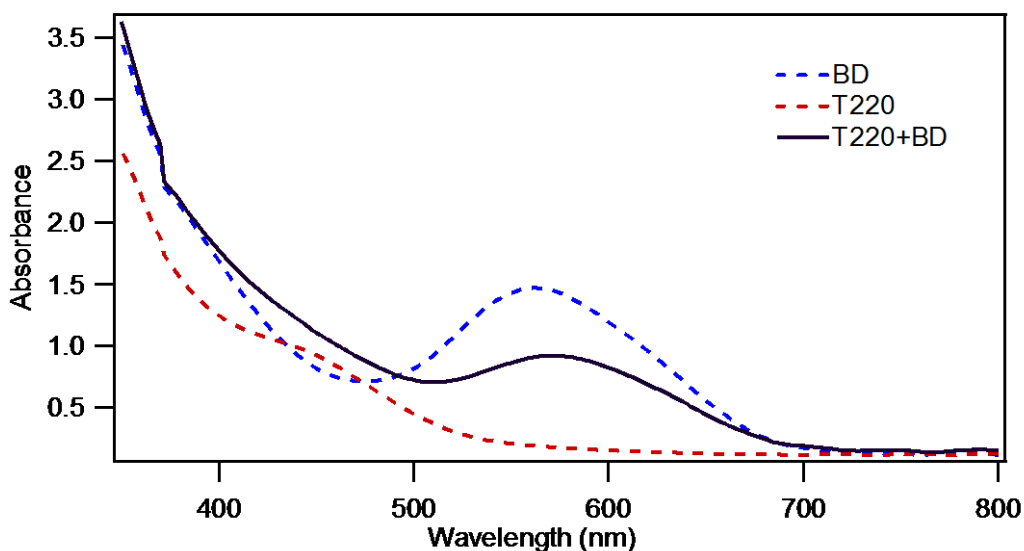


**Figure 20:** Molecular structures of D35 and DB.

### 3.5.1. Co-adsorption with T220 and DB

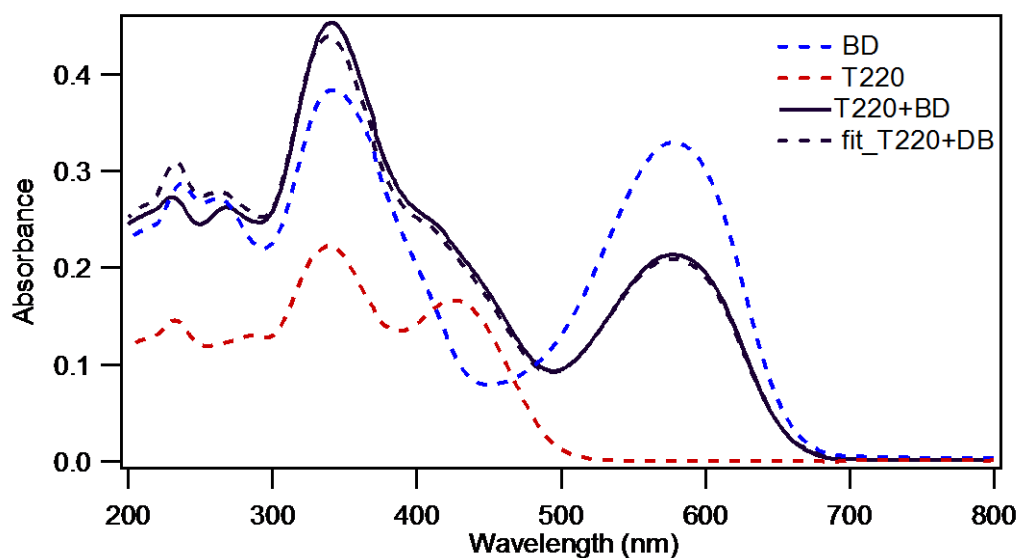
To begin with, in order to check the total dyes' loading on the TiO<sub>2</sub> film, we performed absorbance measurements on the adsorbed and co-adsorbed films in addition to the corresponding desorbed solutions for both pairs of dyes. Three TiO<sub>2</sub> films with 4 μm thickness were immersed in 0.2 mM solution of T220, 0.03 mM solution of DB, and

a mixture of T220 and DB with the same concentrations in a THF: t-butanol: acetonitrile (1:1:1) solution for 24 hours. The absorption spectra of the dyes attached to the TiO<sub>2</sub> films are shown in figure 21.



**Figure 21:** Absorption spectra of T220, BD, and T220-BD anchored on the TiO<sub>2</sub> film.

Moreover, desorption of the dye sensitizers from the loaded TiO<sub>2</sub> electrodes was performed. The individual T220 and BD as well as the co-sensitized T220+BD TiO<sub>2</sub> films were dipped in an alkaline KOH solution with a mixture of THF: ethanol: water. In order to determine the dyes' loading amount of the sensitizers, the absorption spectra of the desorbed solutions were measured, followed by the fitting of the co-sensitized spectrum as shown in figure 22. The dye loading measurements are summarized in table 5.



**Figure 22:** Absorbance spectra of the desorbed films of the individual T220 and DB and the co-sensitized T220-DB dyes.

**Table 5.** Dye loading measurements of the individual and co-sensitized TiO<sub>2</sub> films<sup>a</sup>

Dye bath concentrations	$n_{T220}$ (moles)	$n_{DB}$ (moles)	Total dye loading (moles)
T220 (0.2 mM)	$4.16 \times 10^{-8}$	-	$4.16 \times 10^{-8}$
DB (0.03 mM)	-	$6.73 \times 10^{-8}$	$6.73 \times 10^{-8}$
T220 (0.2 mM)+ DB (0.03 mM)	$3.68 \times 10^{-8}$	$4.23 \times 10^{-8}$	$7.91 \times 10^{-8}$

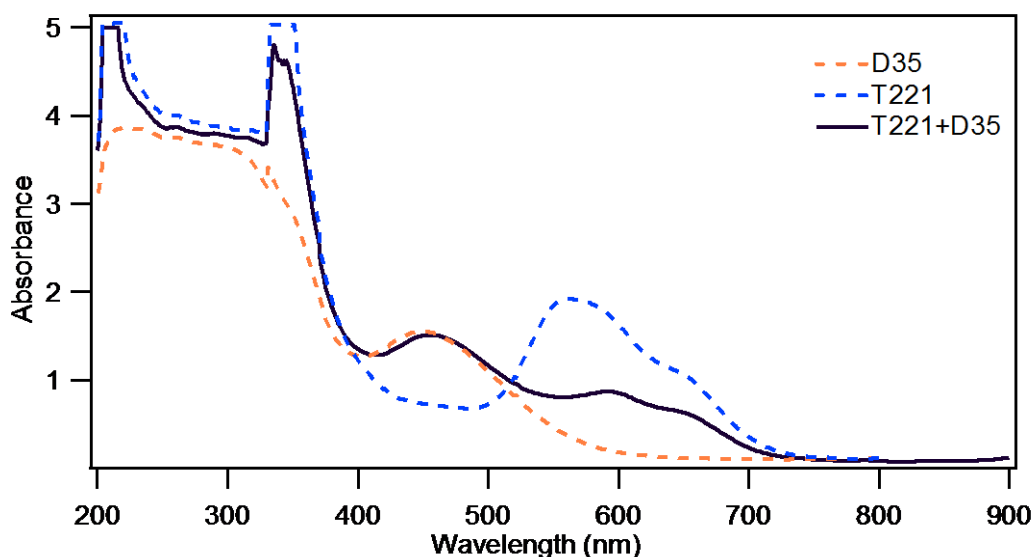
<sup>a</sup>4  $\mu$ m TiO<sub>2</sub> film thickness was used with an area of 2.56 cm<sup>2</sup>

From the curve fitting, the relative amounts of adsorbed T220 and DB in the co-sensitized film compared to the individually sensitized films were found to be 88% and 63%, respectively. The T220-DB co-sensitized film dye loading amounts (T220  $4.16 \times 10^{-8}$  moles and DB  $6.73 \times 10^{-8}$  moles) are less than the individual non co-sensitized dyes (T220  $3.68 \times 10^{-8}$  moles and DB  $4.23 \times 10^{-8}$  moles), suggesting that co-adsorbing these 2 dyes resulted in a decrease in the dye loading on the TiO<sub>2</sub> film. Ideally, these

values should be around 100% for both dyes since the anchoring sites are of different nature on TiO<sub>2</sub>, however, a very important factor is of relevance here; which is the respective sizes of each dye and its footprint on TiO<sub>2</sub> which will be elaborated in section 3.6.<sup>120-121</sup>

### 3.5.2. Co-adsorption with T221 and D35

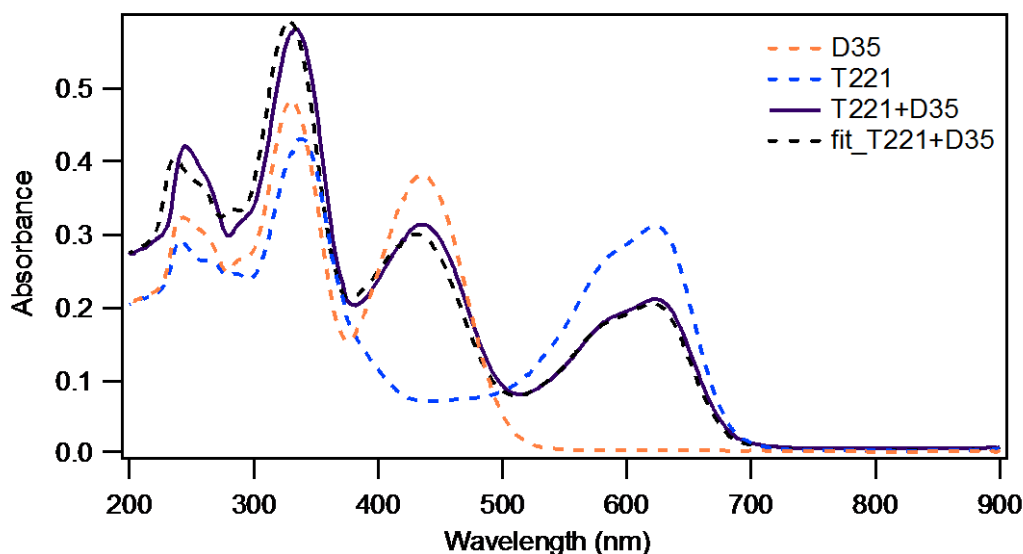
In a second study, the blue dye T221 was co-sensitized with a commercially available D35 dye. The three 6 μm TiO<sub>2</sub> electrodes were immersed in 0.2 mM solution T221, 0.2 mM solution D35, and T221 with D35 having the same concentration in a solution THF: ethanol (1:4) for 24 hours. The corresponding UV-vis spectra of the three adsorbed electrodes are shown in figure 23.



**Figure 23:** Absorption spectra of T221, D35, and T221-D35 anchored on the TiO<sub>2</sub> film.

Dye desorption was then performed where the pure and the mixed TiO<sub>2</sub> films were dipped in an alkaline KOH solution in a mixture of THF: ethanol: water. The

absorbance spectra of the desorbed films of T221, D35 and T221 mixed with D35 are shown in figure 24. The dye loading measurements are summarized in table 6.



**Figure 24:** Absorbance spectra of the desorbed films of the individual T221 and D35 and the co-sensitized T221-D35 dyes.

**Table 6.** Dye loading measurements of the individual and co-sensitized TiO<sub>2</sub> films<sup>a</sup>

Dye bath concentrations	$n_{T221}$ (moles)	$n_{D35}$ (moles)	Total dye loading (moles)
T221 (0.2 mM)	$6.49 \times 10^{-8}$	-	$6.49 \times 10^{-8}$
D35 (0.2 mM)	-	$1.23 \times 10^{-7}$	$1.23 \times 10^{-7}$
T221 (0.2 mM)+ D35 (0.2 mM)	$4.15 \times 10^{-8}$	$8.11 \times 10^{-8}$	$1.22 \times 10^{-7}$

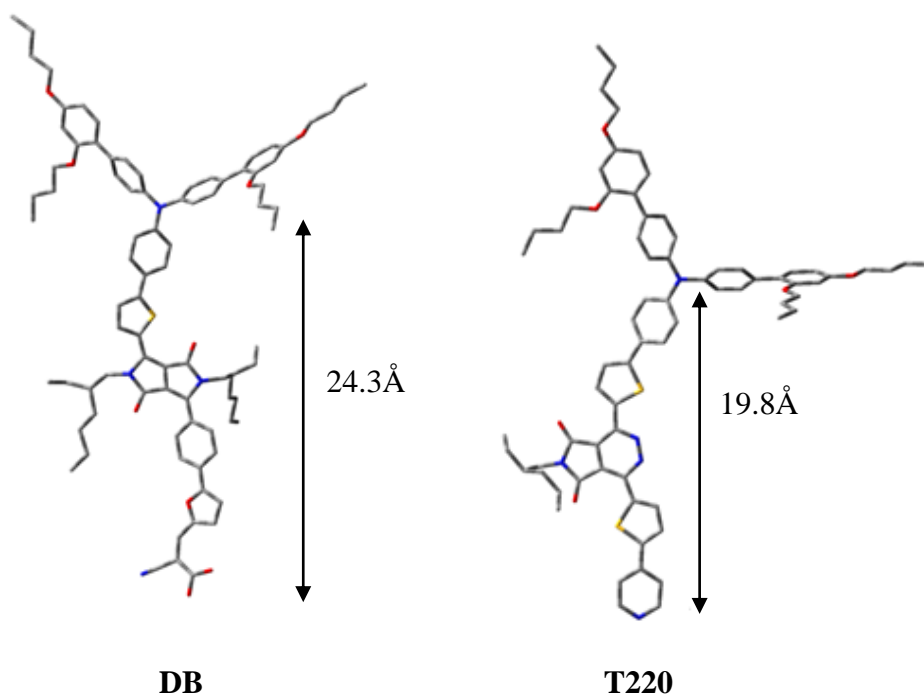
<sup>a</sup> 6  $\mu$ m TiO<sub>2</sub> film thickness was used with an area of 2.56 cm<sup>2</sup>

The coefficients of the adsorbed T221 and D35 in the co-sensitized film, which are obtained from the curve fitting, are 0.647 and 0.663, respectively. Both values are less than 1. Again, this could be due to mismatch in the sizes of the two dyes when adsorbed on TiO<sub>2</sub>.

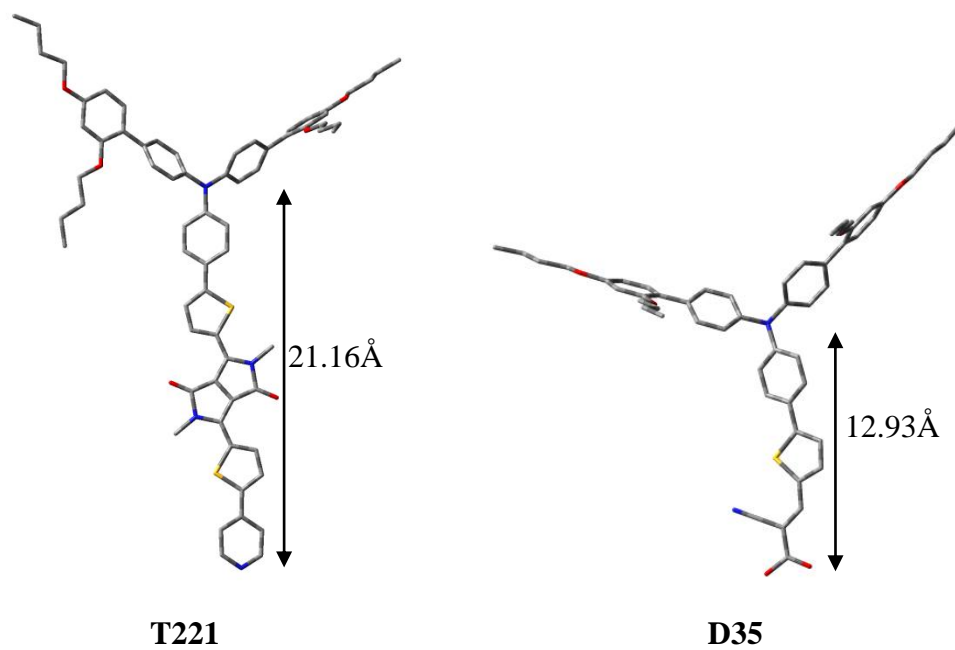
### 3.6. Density Functional Theory Calculations (DFT)

The dye loading amount of the co-sensitized T220-DB and T221-D35 dyes can be associated with the dyes' respective sizes, therefore density functional theory calculations were performed on the two dyes to further elucidate the relevance of the lower dyes' loading on the TiO<sub>2</sub> film with their relative sizes. Figure 25 and 26 show the sizes of T220-DB and T221-D35, respectively. In the case of T220 and DB, both dyes have very similar calculated vertical distances. In T220 the distance between the N atom of the triphenylamine donor moiety to the N atom of the pyridyl moiety is 19.75 Å, and in the case of DB the distance between the triphenylamine N atom and the O atom of the carboxylic acid moiety is 24.34 Å. As can be seen in figure 25 the bulky donor group of T220 can't fit within the groove right below the DB's triphenyl amine donor group, and consequently co-adsorbing of these 2 dyes results in a decrease in the theoretical total dye loading on the TiO<sub>2</sub> film. However, T221 and D35 have different vertical sizes (figure 26). For D35 the calculated vertical distance between the N atom of the donor group and the O atom of the carboxylic acid group is 12.93Å compared to T221 with a distance of 21.16Å. Ideally, from the difference in their respective sizes, T221 and D35 should perfectly fit together on the TiO<sub>2</sub> surface. However, this was not the case as seen from the coefficient values obtained in table 6. The decrease in dye coverage on the titania film for T221 and D35 might be due to the bulkiness of T221 and the presence of the bulky ethylhexyl chains on the two nitrogen atoms in the cyclic amide rings (not shown in figure).





**Figure 25:** The calculated vertical distances in DB and T220 dyes.



**Figure 26:** The calculated vertical distances in T221 and D35 dyes.

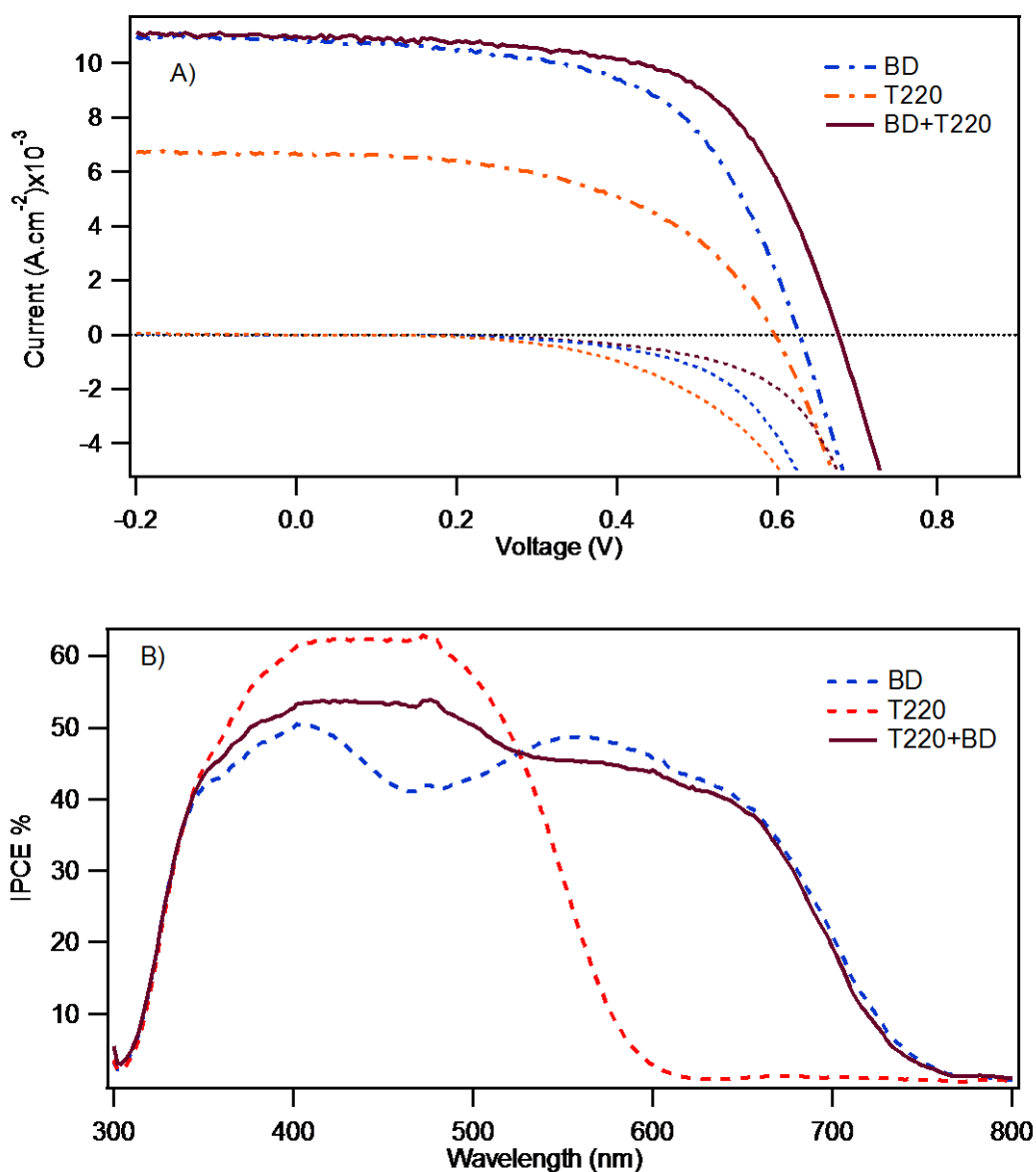
### 3.7. Photovoltaic performance

#### 3.7.1. Co-adsorbed T220 and DB device

Liquid cobalt-based DSSCs were fabricated to test the photovoltaic performance of the device upon co-sensitizing T220 with DB. The electrolyte system consisted of 0.2 M TBP as an additive. The pure T220 and BD with 0.2 mM and 0.03 mM concentration, respectively, as well as the co-sensitized T220-DB with the same concentrations were adsorbed on a 4  $\mu\text{m}$  thick active transparent  $\text{TiO}_2$  film with a scattering  $\text{TiO}_2$  layer having the same thickness. The  $I$ - $V$  curves of the devices as well as incident photon-to-current conversion efficiency (IPCE) plots are shown in figure 27 (A and B). The corresponding photovoltaic parameters of the cells are summarized in table 7.

The individually sensitized DB cell exhibits better photovoltaic performance parameters compared to the individual T220 dye. The greater difference in the photocurrents between the non co-sensitized BD  $10.9 \text{ mA}\cdot\text{cm}^{-2}$  and T220  $6.7 \text{ mA}\cdot\text{cm}^{-2}$  is due to the fact that T220's absorption is limited to the visible region of the spectrum as can be seen from the IPCE curve in figure 27 B). Upon co-sensitization, the T220-DB based devices showed notable improvement in the open circuit voltage and the photocurrent, as well as a remarkable increase in the power conversion efficiency for the co-sensitized device. Regarding the photovoltage, the co-sensitized device showed an increase in  $V_{\text{OC}}$  by 49 mV when compared to DB alone which is also seen in the dark currents where the co-sensitized cell exhibits a lower dark current with respect to the individual devices. Furthermore, the increase in  $J_{\text{SC}}$  for the co-sensitized cell ( $11.1 \text{ mA}\cdot\text{cm}^{-2}$ ) is probably due to the complementary absorption spectra between T220 and DB. Also, this increase in photocurrent compared to the individual DB is reflected in

the IPCE plots where T220-BD has a higher IPCE % compared to DB alone. The IPCE of the DSSCs based on T220 and DB individually are present in the range 300-600 nm and 300-800 nm, respectively. The IPCE spectrum of the co-sensitized DSSC, which provides the complementary behavior of the individual dyes, is remarkably broad covering the whole visible region, which is consistent with the absorption spectra of the co-adsorbed dyes on the TiO<sub>2</sub> film shown in figure 21.



**Figure 27:** A) *I-V* curve of the DSSCs based on the individual T220, DB, and the co-sensitized T220-DB under illumination and in darkness, B) incident photon-to-current conversion efficiency spectra.

**Table 7.** Photovoltaic performance of the T220, BD, and co-sensitized T220-DB based devices obtained from the *I-V* curves

Dye	$J_{SC}$ (mA.cm <sup>-2</sup> )	$V_{OC}$ (mV)	FF	PCE (%) <sup>a</sup>
T220	6.7	597	0.51	2.04
BD	10.9	625	0.58	3.94
T220+BD	11.1	674	0.54	4.07

<sup>a</sup> Measured under 100 mW.cm<sup>-2</sup> simulated AM1.5 spectrum with an active area 0.5 x 0.5 cm<sup>2</sup> and a black mask (0.6 x 0.6 cm<sup>2</sup>); the electrolyte consisted of 0.25 M Co(II), 0.06 M Co(III), 0.1 M LiClO<sub>4</sub>, and 0.2 M TBP

### 3.8. EIS of T220+DB-based Device

In an effort to understand the increase in  $V_{OC}$  for the co-sensitized T220-DB device, electrochemical impedance measurements (EIS) were carried out on the individual T220 and DB as well as on the mixed devices at open-circuit voltage using different light intensities. The fitting results of the impedance spectra are represented in figures 28 (A and B) and 29. Figures 28 (A and B) and 29 reveal, respectively, the plots of the charge transfer resistance between the electrons in the TiO<sub>2</sub> conduction band and the oxidized electrolyte  $R_{CT}$ , the TiO<sub>2</sub>/electrolyte chemical capacitance  $C_{\mu}$ , and the electron lifetime which is given by the equation  $\tau_n = R_{CT} \cdot C_{\mu}$ . For the three devices, the  $R_{CT}$  and  $C_{\mu}$  values were extracted from the EIS experiments versus the applied voltage ( ${}_nE_F - E_{F,redox}$ ), where  ${}_nE_F$  is the electron quasi-Fermi energy level in the TiO<sub>2</sub> film and  $E_{F,redox}$  is the electrolyte redox Fermi level.

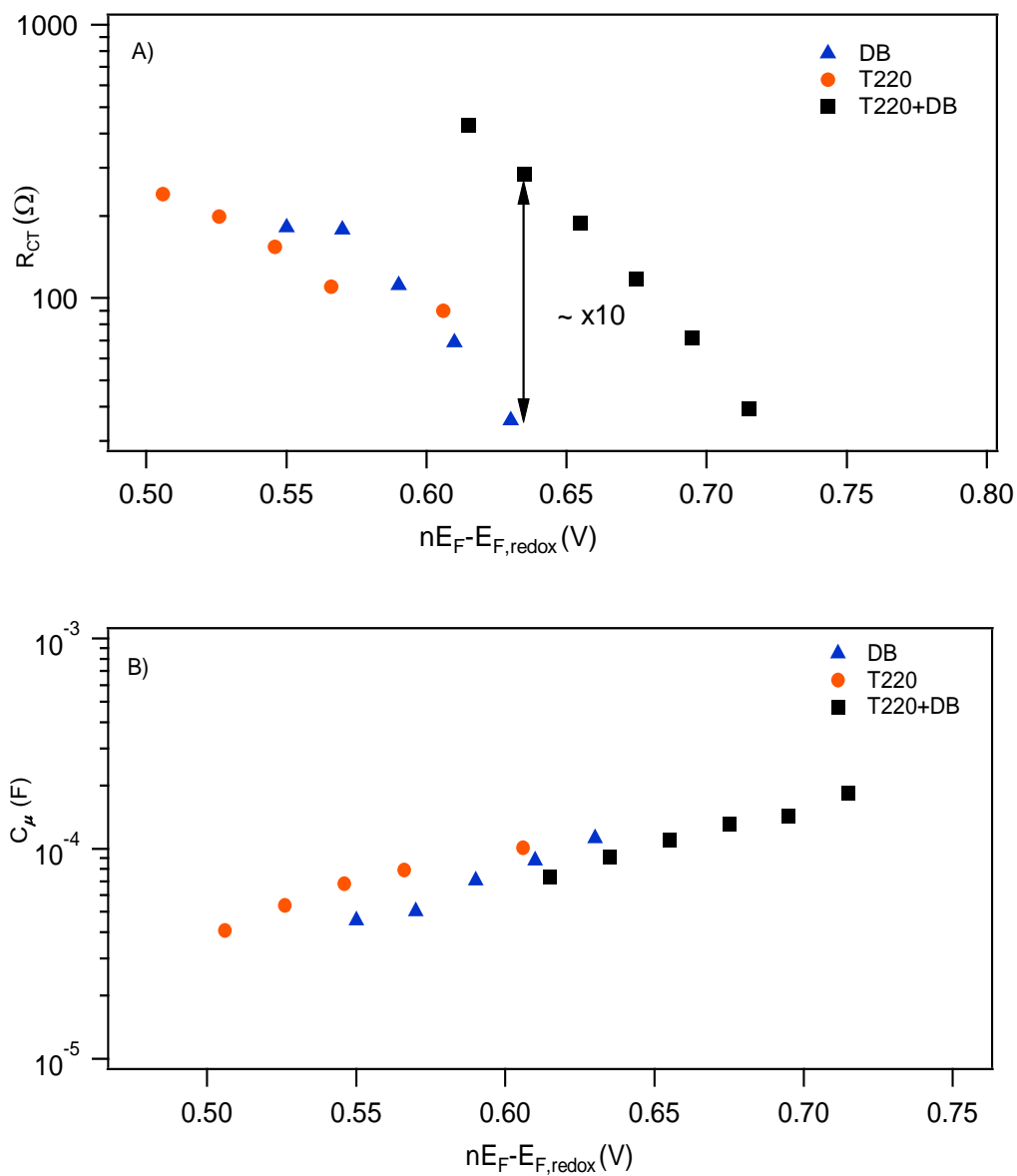
In Figure 28A, the  $R_{CT}$  values of the T220-DB co-sensitized cell are way higher than that of the DB device (~ 10 times higher). A higher  $R_{CT}$  value suggests a lower electron recombination in the co-sensitized T220-DB cell, and this is probably due to the blockage of the cobalt electrolyte from reaching the titania film. This effect is most

probably due to the close arrangement of the two dyes in the T220-DB cell, where the alkoxy arms on the donor groups would retard the approach of the Co(III) ions in the electrolyte to TiO<sub>2</sub>.

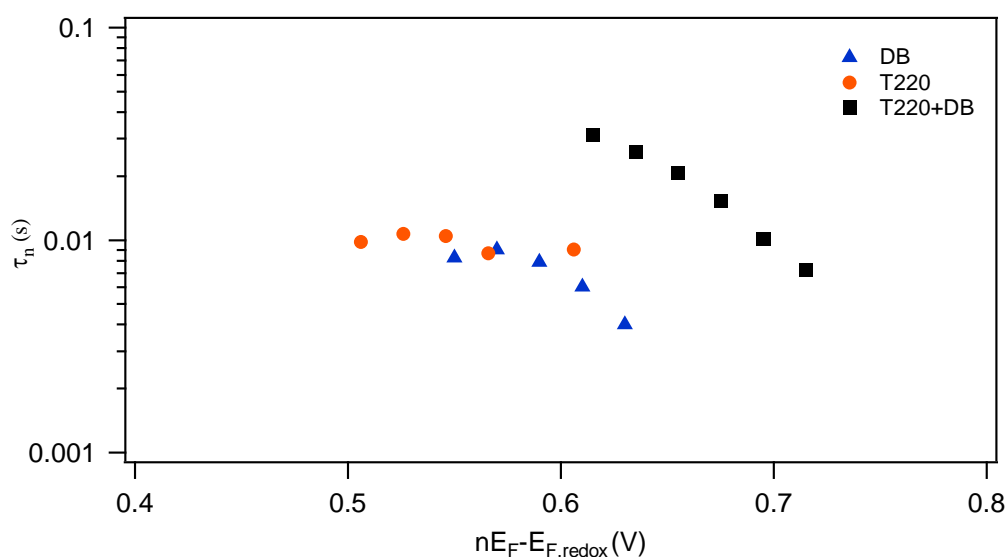
In Figure 28B, the co-sensitized T220-DB device shows a shift  $\Delta(nE_F - E_{F,redox})$  of  $\sim 20$  mV higher than the DB device at a certain  $C_{\mu}$  value. A shift in the  $(nE_F - E_{F,redox})$  toward higher or lower values is attributed to an upward or downward shift in the  $nE_F$  with respect to the electrolyte  $E_{F,redox}$ , respectively, since the same electrolyte composition is used in all DSSCs.<sup>122-123</sup> The upward shift in the  $nE_F$  in the co-sensitized cell could be one of the reasons behind the higher  $V_{oc}$  values of T220-DB than the individual ones. However, this upward shift of  $nE_F$  in the two co-sensitized cell is counter intuitive, since the DB dye contains one carboxylic acid proton that would usually result in a  $\sim 20$  mV downward shift of the conduction band, and one would expect a decrease in the  $V_{oc}$  values upon co-sensitizing T220 with DB. On the other hand, Boschloo et al. have showed before that the dye loading has pronounced effect on the photo-voltage in the case of cobalt electrolyte,<sup>124</sup> where in their EIS experiments they showed that a similar upward shift in the  $nE_F$  is seen with increasing dye loading amounts.

Therefore, we speculate that the above mentioned  $\Delta(nE_F - E_{F,redox})$  shift is rather due to the differences in the total dyes' coverage on TiO<sub>2</sub> between the individual and co-sensitized cells. A lower dye coverage, such as in the case of the DB and T220 cells when compared to the co-sensitized T220-DB one, would result in lower electron injection rates into TiO<sub>2</sub> and subsequently lead to a lower  $nE_F$  and hence lower  $V_{oc}$  at 1 sun.<sup>125-127</sup> Finally, the upward shift in the  $nE_F$  and the higher charge recombination resistance in the T220-DB co-sensitized cell well explain the higher cell efficiency and

the positive effect on the electron lifetime ( $\tau_n$  evaluated from the EIS experiments) as seen in Figure 29.



**Figure 28:** A) Charge transfer resistance values obtained from EIS and B) chemical capacitance values of T220, DB and the co-sensitized T220-DB cells.



**Figure 29:** Electron lifetime values obtained from EIS for the T220, DB and the co-sensitized T220-DB cells.

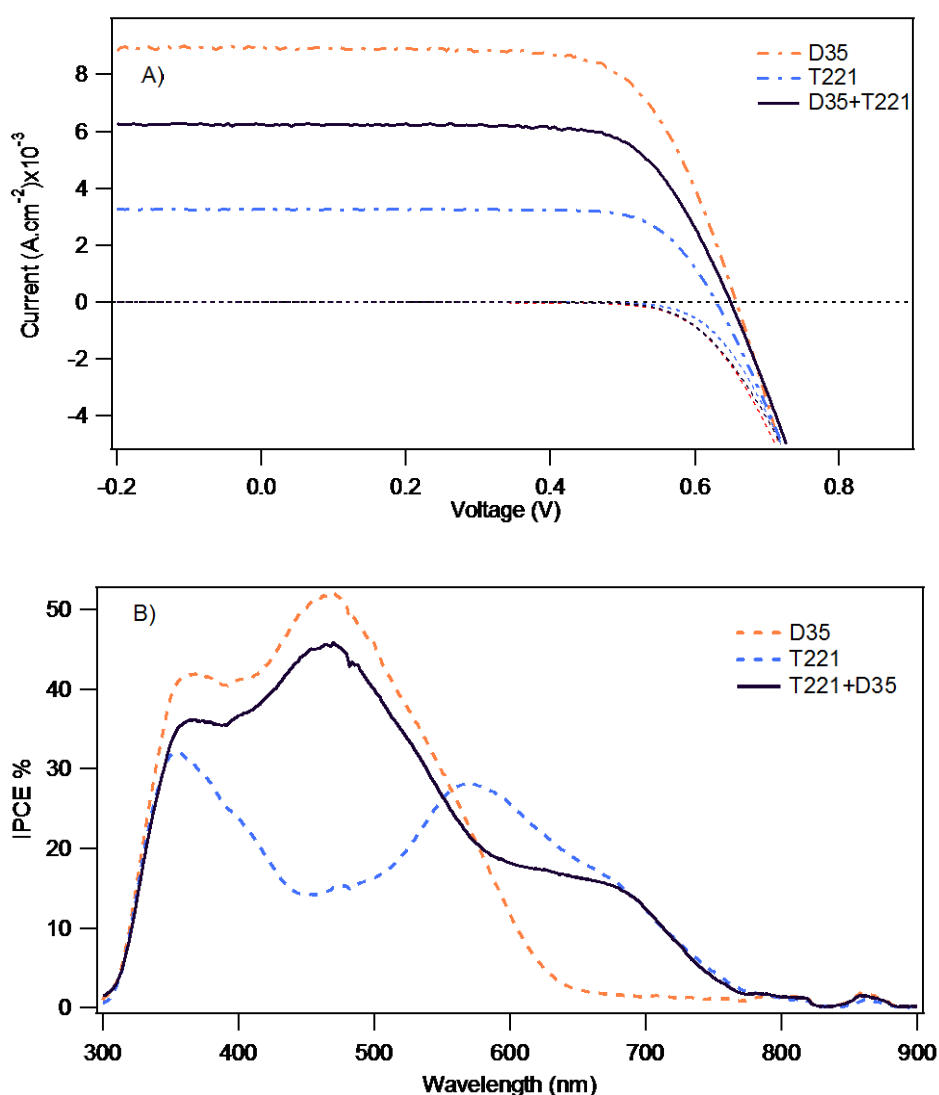
### 3. 9. Photovoltaic Performance

#### 3.9.1. Co-adsorbed T220 and D35 device

In a second study, the performance of our synthesized T221 blue dye and the commercially available cyanoacrylic-based D35 dye both having 0.2 mM concentrations, as well as the co-sensitization of these two dyes with the same concentrations were evaluated in fully assembled DSSCs using the same cobalt tris bipyridine electrolyte system with 0.2 M TBP. A 6  $\mu\text{m}$  thick active transparent  $\text{TiO}_2$  layer was printed with a 4  $\mu\text{m}$  thick scattering  $\text{TiO}_2$  layer. The current-voltage ( $I$ - $V$ ) characteristics as well as the IPCE plots are illustrated in figure 30 (A and B). The photovoltaic performances of these cells are listed in table 8.

From figure 30 B) the IPCE with D35 located in the range 300-750 nm is higher than the IPCE with T221, which is consistent with the higher short-circuit current value of D35 ( $J_{SC} = 8.8 \text{ mA}\cdot\text{cm}^{-2}$ ). The  $I$ - $V$  curves in figure 30 A) show that the short-circuit photocurrent density as well as the power conversion efficiency of the co-

sensitized T221-D35 based DSSC ( $6.2 \text{ mA}\cdot\text{cm}^{-2}$ , 2.67 %) is much lower than the device based on only D35 ( $8.8 \text{ mA}\cdot\text{cm}^{-2}$ , 2.67 %), but is higher than the individual T221 based cell ( $3.2 \text{ mA}\cdot\text{cm}^{-2}$ , 1.21 %). The lowering of the photovoltaic performance of the co-sensitized DSSC compared to the individual DSSCs might be due to a decrease in the electron injection efficiency during the transfer of electrons or the transfer of energy between the two different dyes. On the other hand, there is a slight increase in the  $V_{OC}$  value (728 mV) of the mixed DSSC compared to T221 (710 mV) alone.



**Figure 30:** A)  $I$ - $V$  curve of the DSSCs based on the individual T221, D35, and the co-sensitized T221-D35 under illumination and in darkness, B) incident photon-to-current conversion efficiency spectra.



**Table 8.** Photovoltaic performance of the T221, D35, and co-sensitized T221-D35 based devices obtained from the *I-V* curves

Dye	$J_{SC}$ (mA.cm <sup>-2</sup> )	$V_{OC}$ (mV)	FF	PCE (%) <sup>a</sup>
T221	3.2	710	0.53	1.20
D35	8.8	740	0.60	3.90
T221+D35	6.2	728	0.59	2.66

<sup>a</sup> Measured under 100 mW.cm<sup>-2</sup> simulated AM1.5 spectrum with an active area 0.5 x 0.5 cm<sup>2</sup> and a black mask (0.6 x 0.6 cm<sup>2</sup>); the electrolyte consisted of 0.25 M Co(II), 0.06 M Co(III), 0.1 M LiClO<sub>4</sub>, and 0.2 M TBP

On another note, it is important to mention that the short-circuit current (3.2 mA.cm<sup>-2</sup>) obtained for T221 using a 6 μm thick TiO<sub>2</sub> layer (Table 8) was less than the  $J_{SC}$  (6.7 mA.cm<sup>-2</sup>) obtained when using a 4 μm thick layer from table 4. It is known that a thicker TiO<sub>2</sub> layer increases the amount of dye coverage which in turn increases the light harvesting efficiency; however, this was not the case with the T221 devices. We speculate the decrease in photocurrent for the 6 μm thick TiO<sub>2</sub> layer to be due to the aggregation of T221 on the film as well as an increase in the recombination reaction as we increased the film's thickness. From the  $V_{OC}$  and  $J_{SC}$  values obtained for the co-sensitized T221-D35 device (Table 8) we can conclude that D35 is not the ideal sensitizer to co-sensitize with T221.

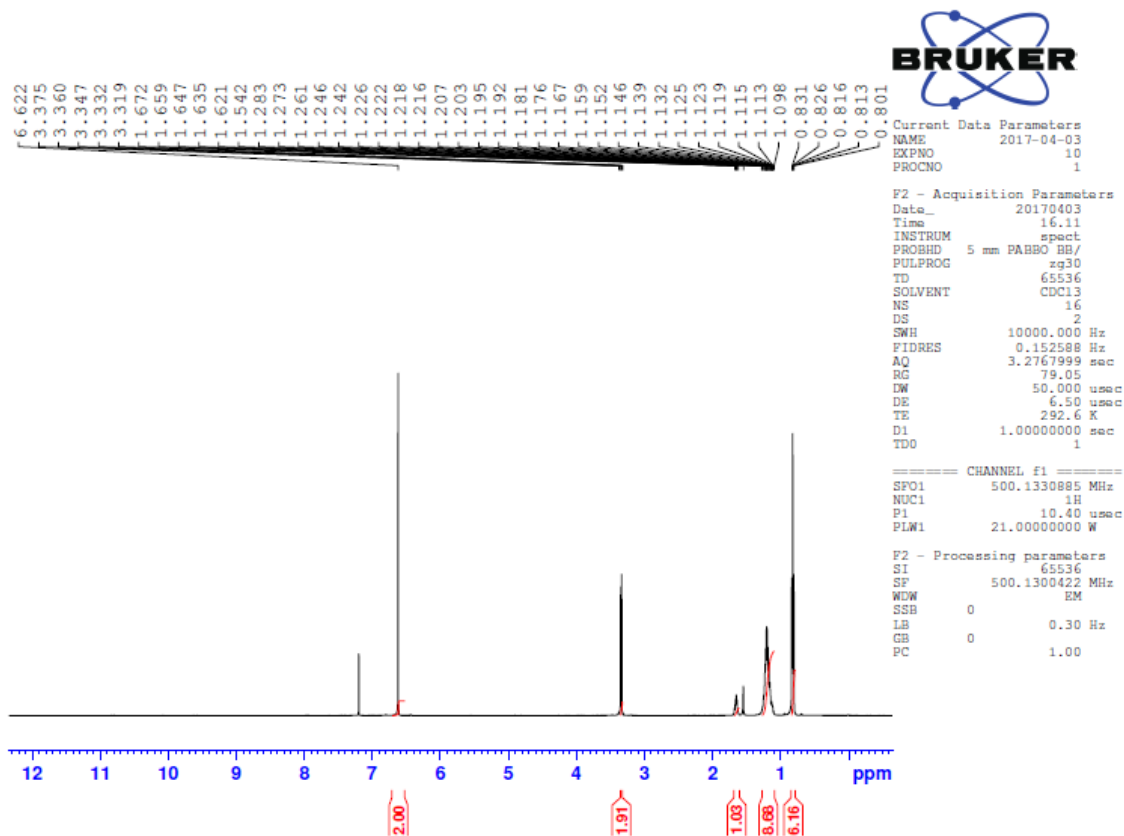
## CHAPTER 4

### CONCLUSION

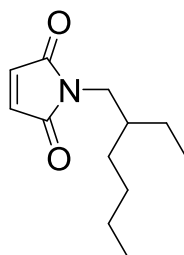
In conclusion, we were successful in synthesizing 3 novel pyridyl-based dyes, T220, T221 and T222 with absorptions ranging from blue to the red part of the visible spectrum. The photovoltaic performance of the individual dyes as sensitizers in fully operating cobalt-based DSSCs was evaluated, where the device employing T222 as a dye showed the poorest performance which was estimated to be due to its low LUMO level. We were also successful in co-sensitizing the pyridine anchored T220 dye with the carboxylic-based dye (Dyename Blue, DB). The dye loading measurements of the co-sensitized T220-DB film clearly demonstrated that both dyes do not compete for the same adsorption sites on TiO<sub>2</sub>. However, due to mismatching of their respective geometrical sizes T220 did not possess a suitable size and shape to fit appropriately the voids within the adsorbed DB dye molecules on the titania film. Nevertheless, the photovoltaic performance of the co-sensitized T220-DB cell showed enhancements in photo-current, photo-voltage and thus total efficiency when compared to the individual T220 and DB cells. Furthermore, the electrochemical impedance spectroscopy (EIS) measurements conducted on the devices were consistent with the increase in photovoltage for the co-sensitized cell. On the other hand, co-sensitizing T221 with the commercially available D35 proved to be ineffective. Power conversion efficiency for the co-sensitized cell of 2.66 % was obtained which is higher than the individual T221 cell (1.20 %) but lower than the individual D35 device (3.90 %). The low cell performance was due to the fact that T221 dye is prone to dye aggregation when a thick TiO<sub>2</sub> layer is employed.

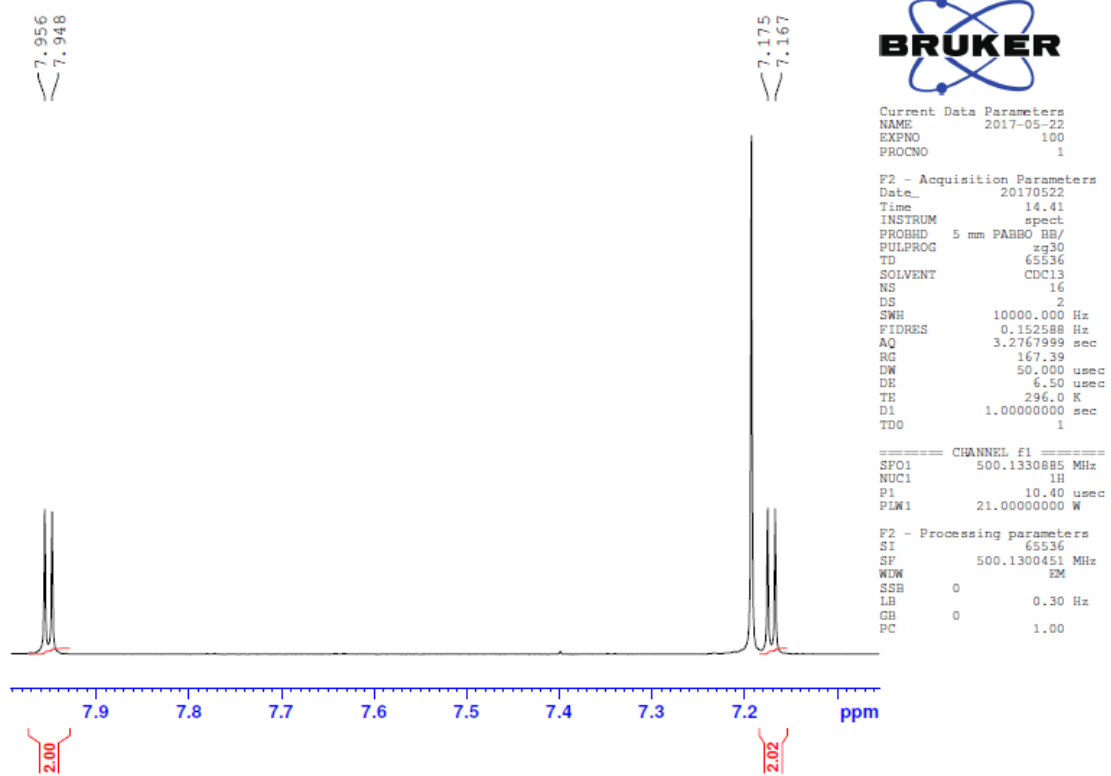
# SUPPORTING INFORMATION

## NMRs AND MS

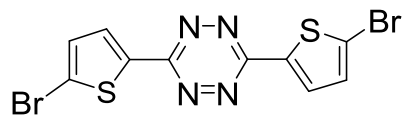


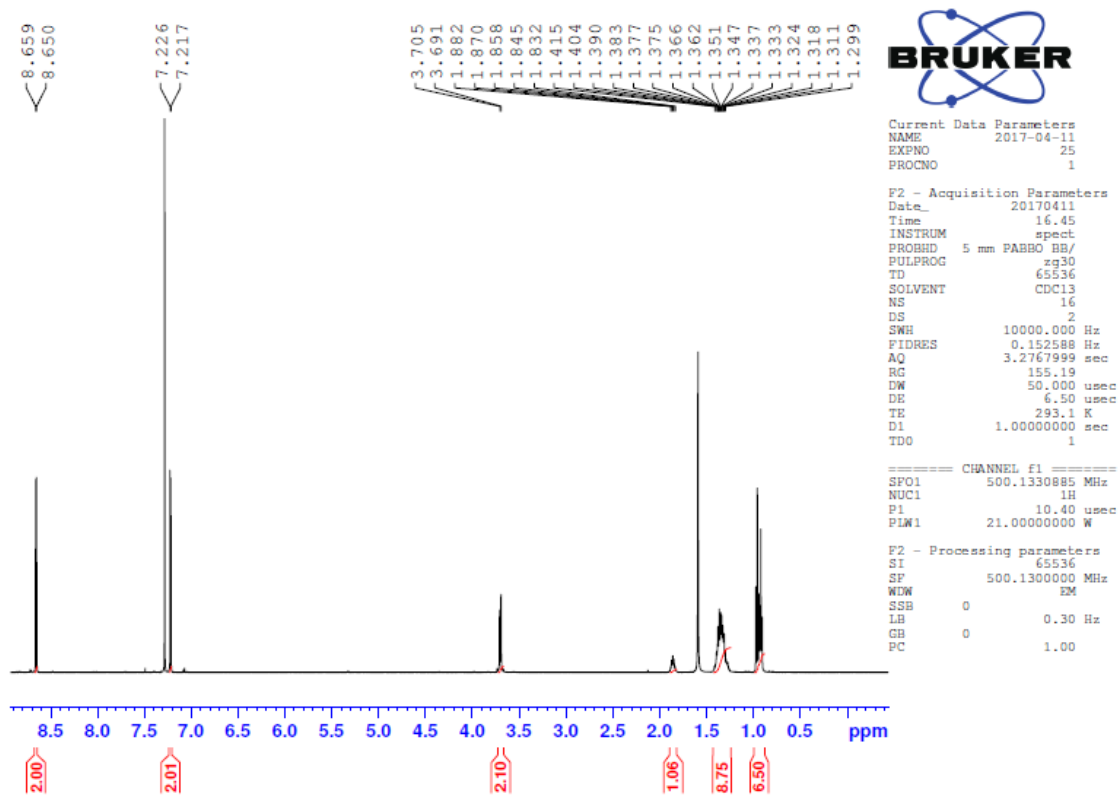
**Figure 31:**  $^1\text{H}$  NMR of 1-(2-ethylhexyl)-1H-pyrrole-2,5-dione in  $\text{CDCl}_3$  (**1**).



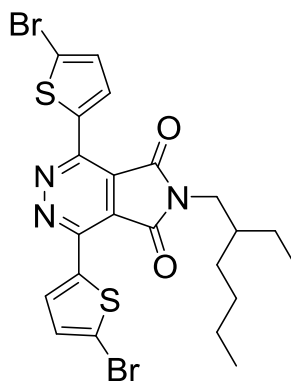


**Figure 32:**  $^1\text{H}$  NMR of 3, 6-Bis (5-bromo-2-thienyl)-1, 2, 4, 5-tetrazine in  $\text{CDCl}_3$  (2).





**Figure 33:**  $^1\text{H}$  NMR of 1,4-Bis(5-bromo-2-thienyl)-6-(2-octyldodecyl)-5H-pyrrolo[3,4-d]pyridazine-5,7(6H)-dione in  $\text{CDCl}_3$  (**3**).



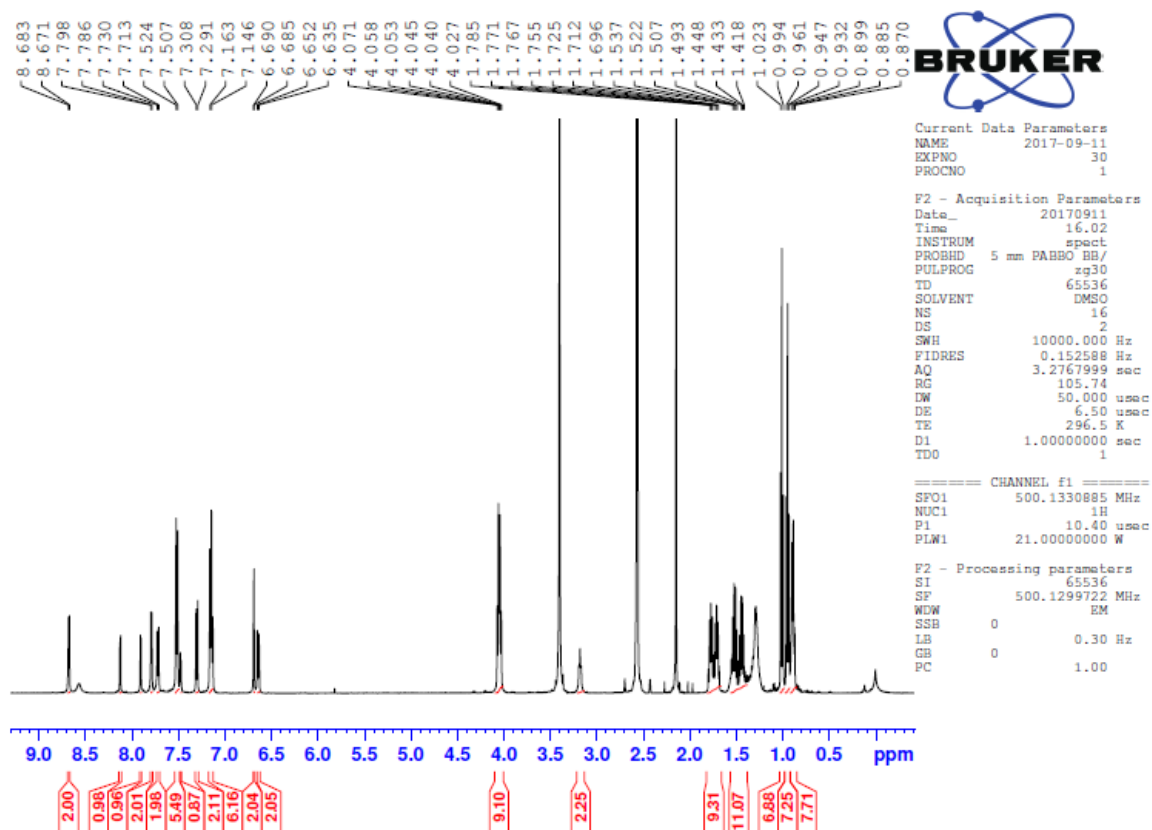
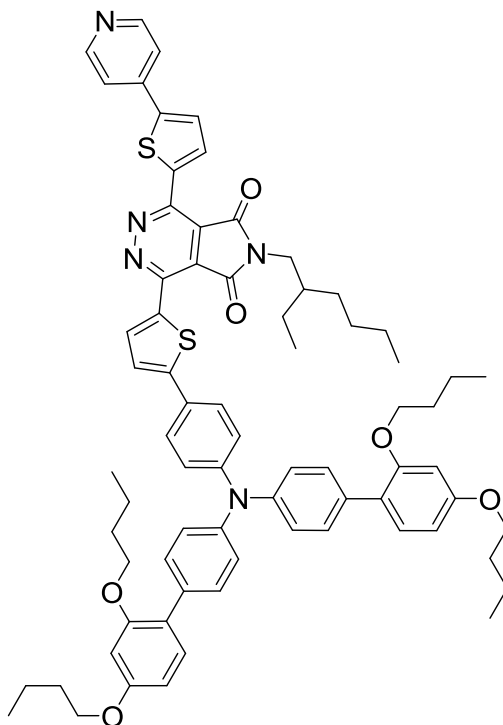
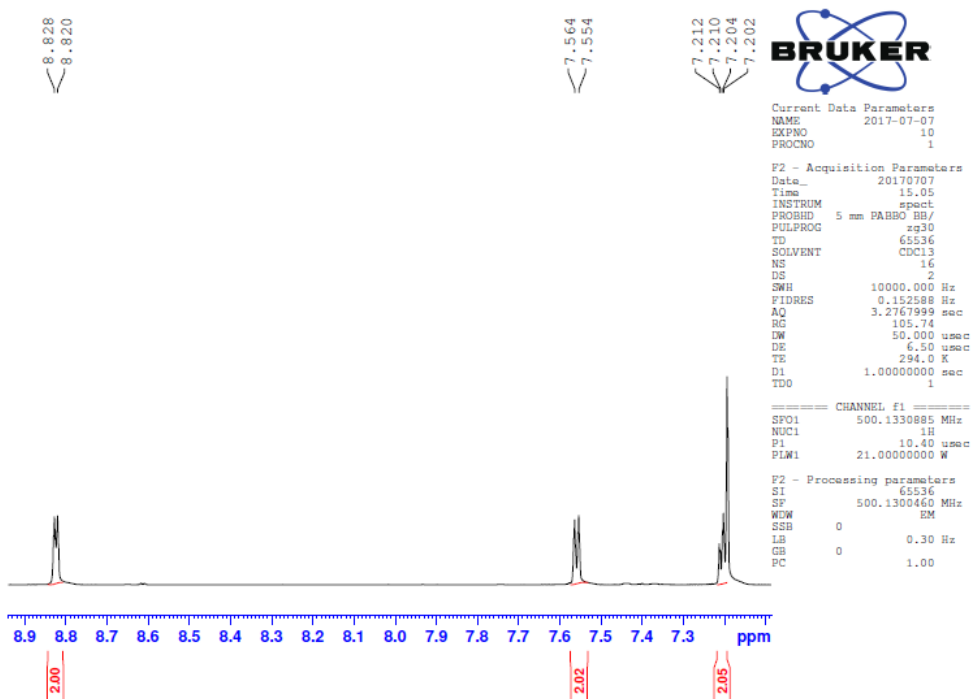
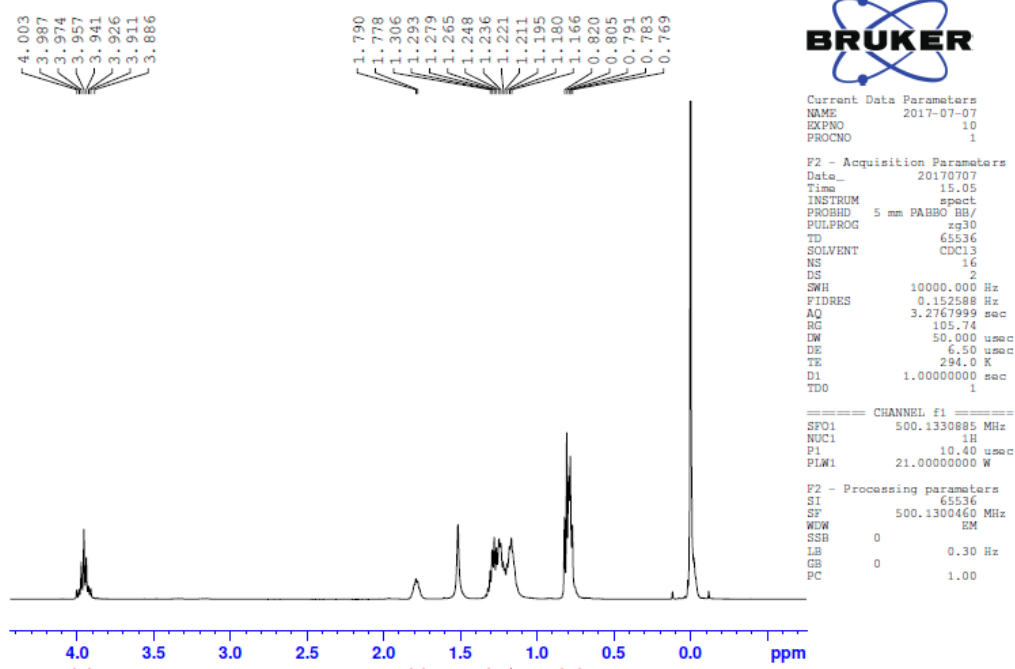
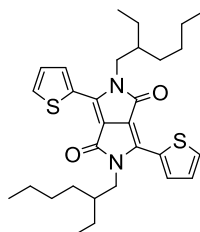


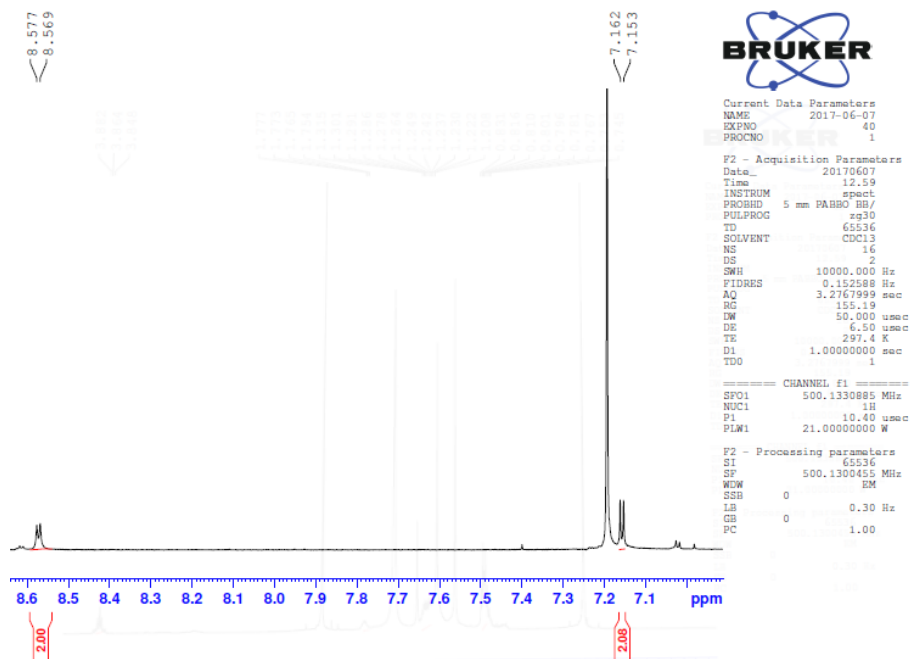
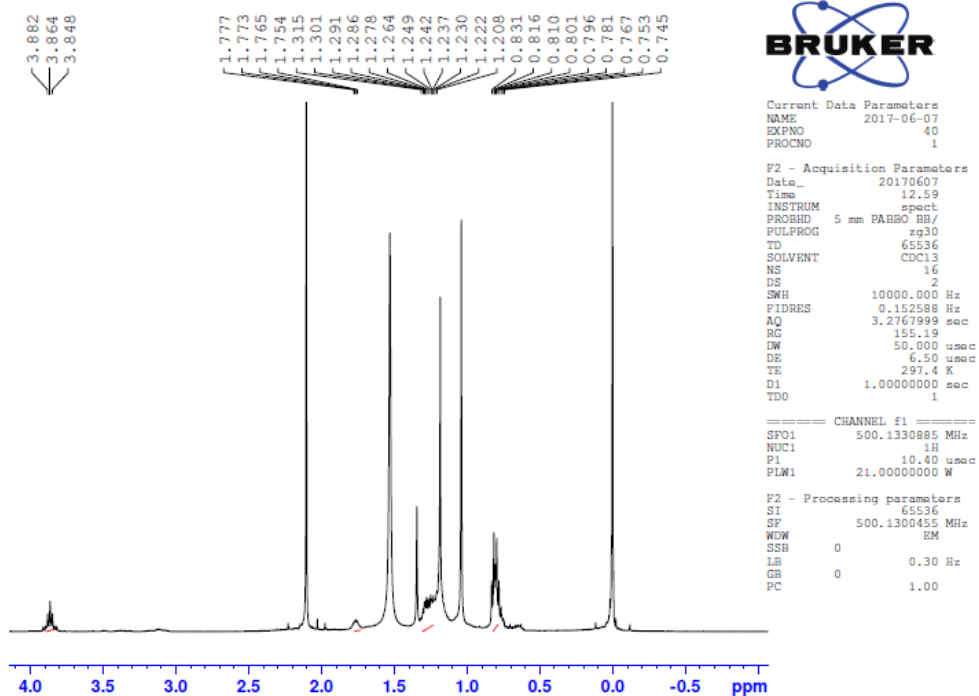
Figure 34:  $^1\text{H}$  NMR of T220 in DMSO.



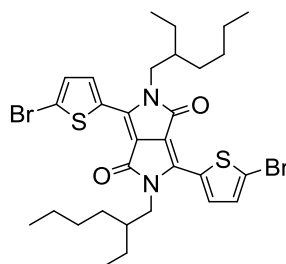


**Figure 35:**  $^1\text{H}$  NMR of 2, 5-Dihydro-3, 6-di-2-thienylpyrrolo [3, 4-c] pyrrole-1, 4-dione in  $\text{CDCl}_3$  (**5**).





**Figure 36:**  $^1\text{H}$  NMR of 2,5-Diethylhexyl-3,6-bis(5-bromothiophen-2-yl)pyrrolo[3,4-c]-pyrrole-1,4-dione in  $\text{CDCl}_3$  (**6**).





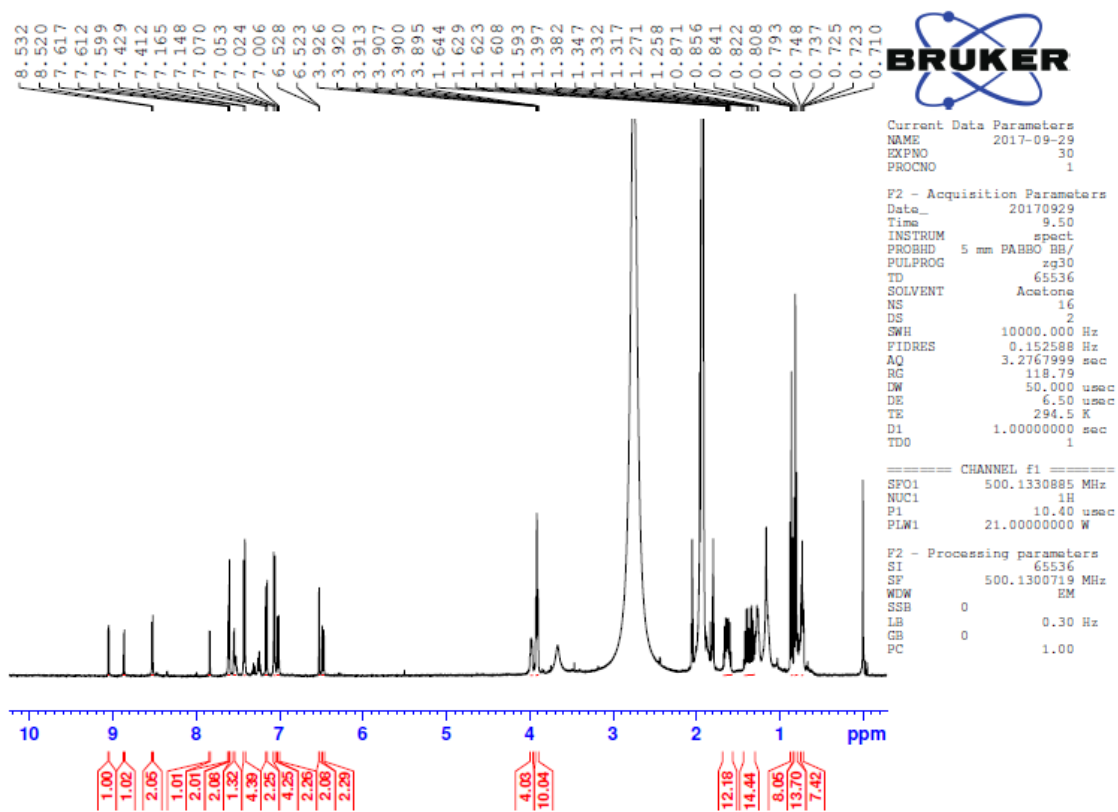
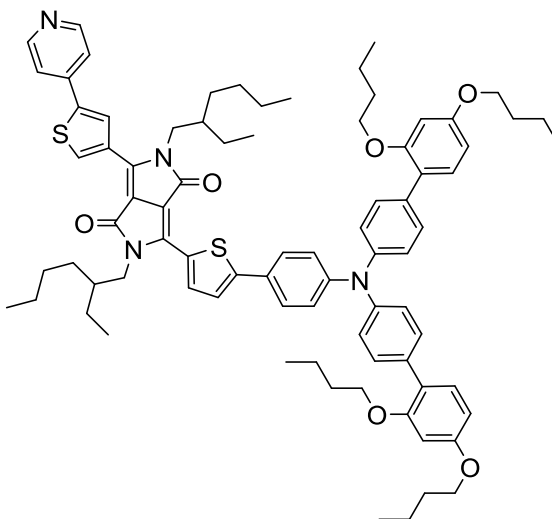
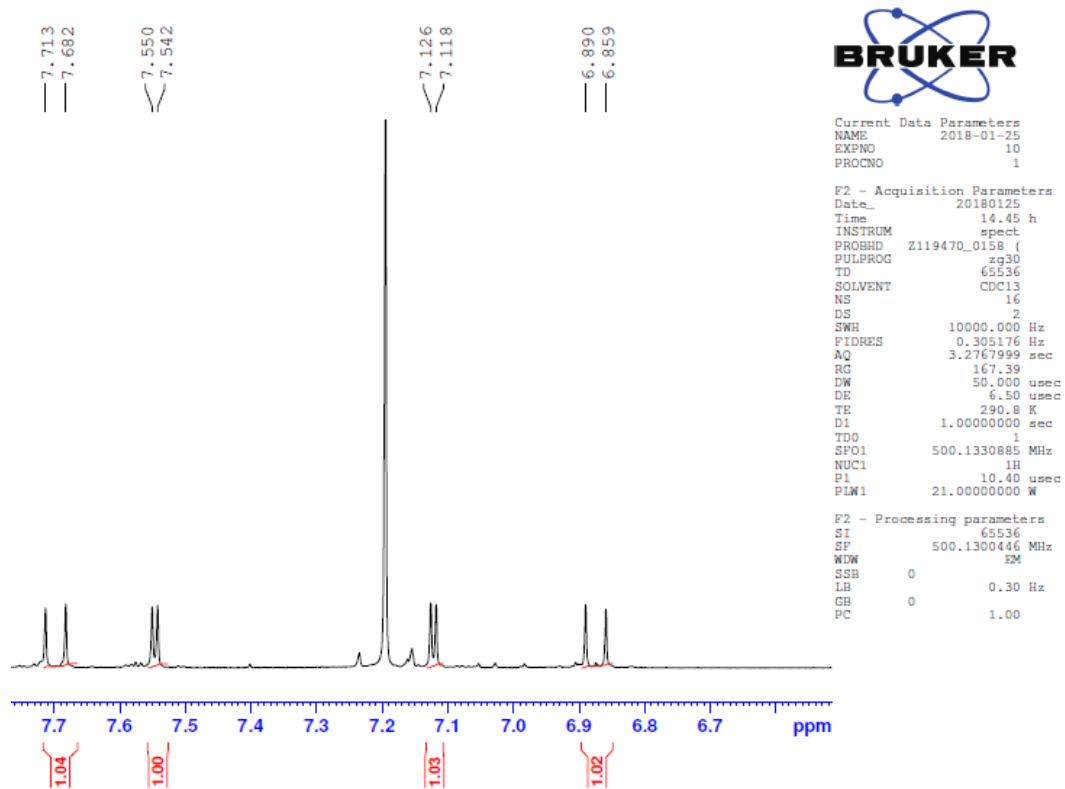
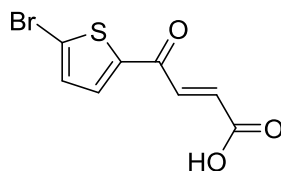


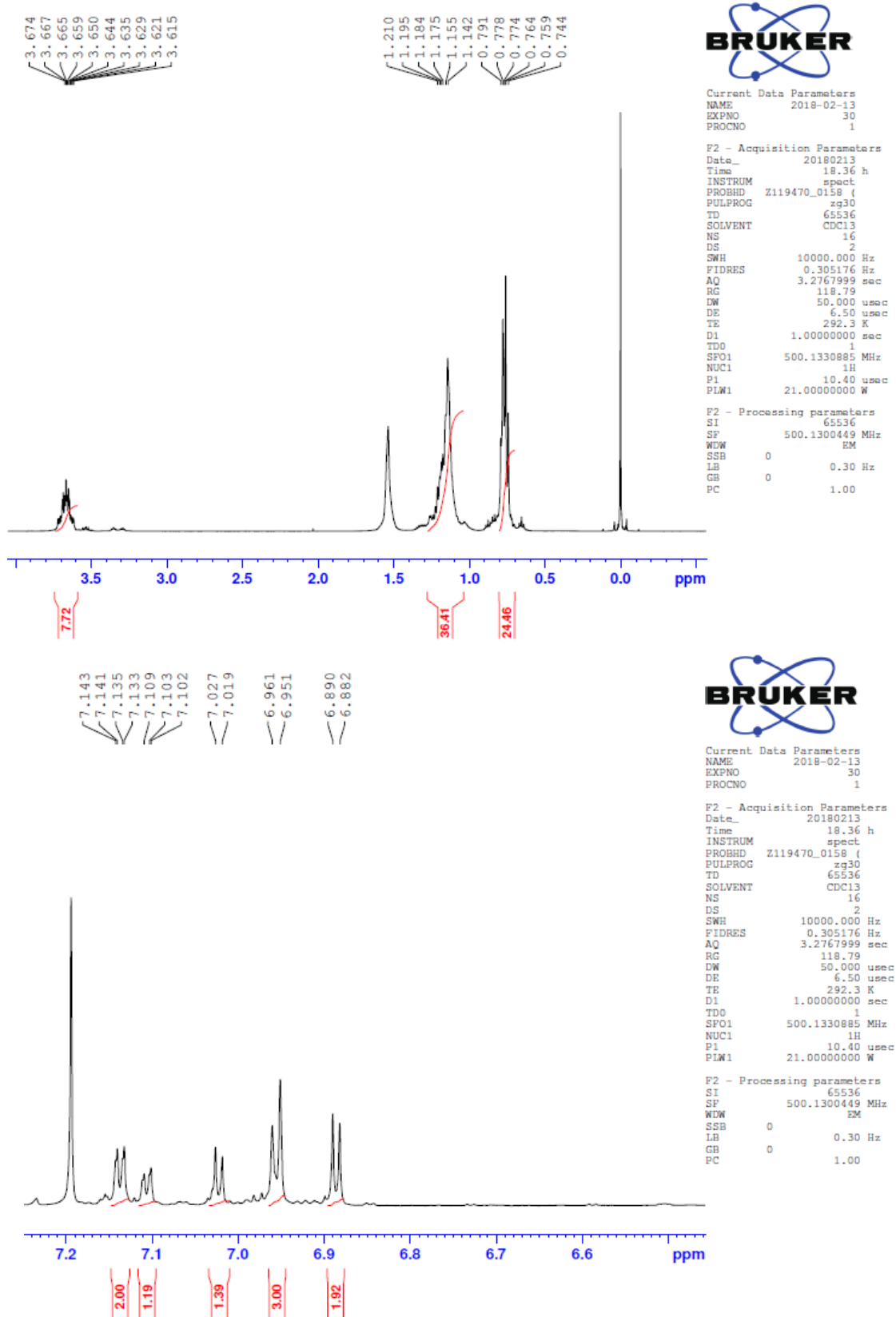
Figure 37:  $^1\text{H}$  NMR of T221 in Acetone- $d_6$ .





**Figure 38:**  $^1\text{H}$  NMR of (E)- 4-(5-Bromo-2-thienyl)-4-oxo-2-butenoic acid in  $\text{CDCl}_3$  (**7**).





**Figure 39:**  $^1\text{H}$  NMR of 2*H*-Pyrrol-2-one, 5-(5-bromo-2-thienyl)-3-[5-(5-bromo-2-thienyl)-1-(2-ethylhexyl)-1,2-dihydro-2-oxo-3*H*-pyrrol-3-ylidene]-1-(2-ethylhexyl)-1,3-dihydro-, (3*E*) in  $\text{CDCl}_3$  (**9**).

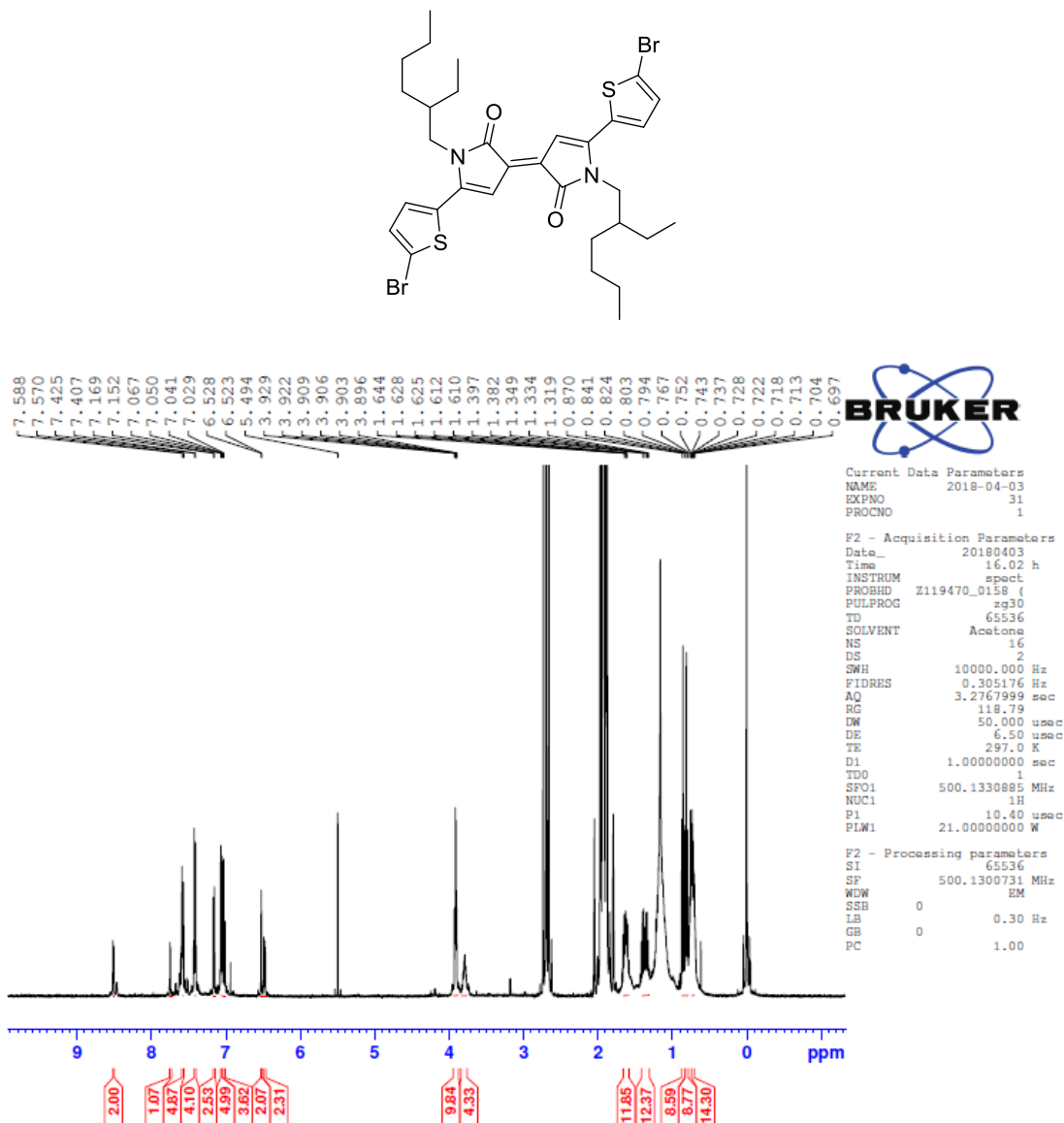
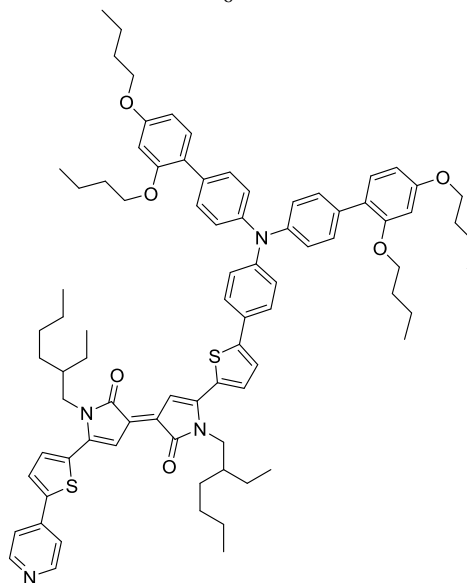


Figure 40: <sup>1</sup>H NMR of T222 in Acetone-d<sub>6</sub>.



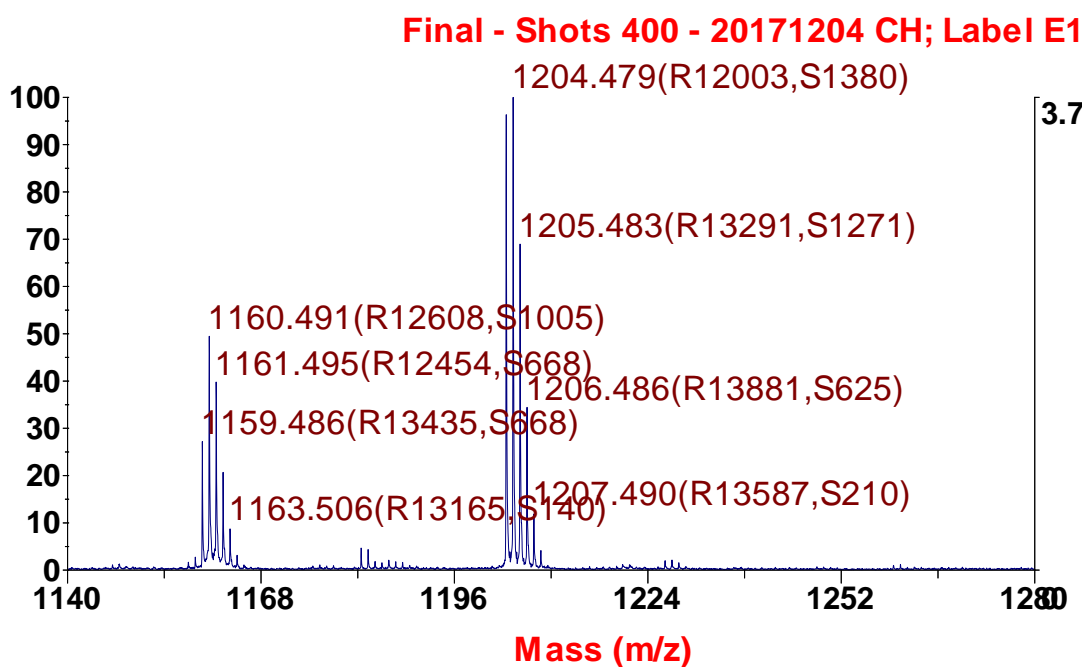


Figure 41: Mass spectrometry of T220.

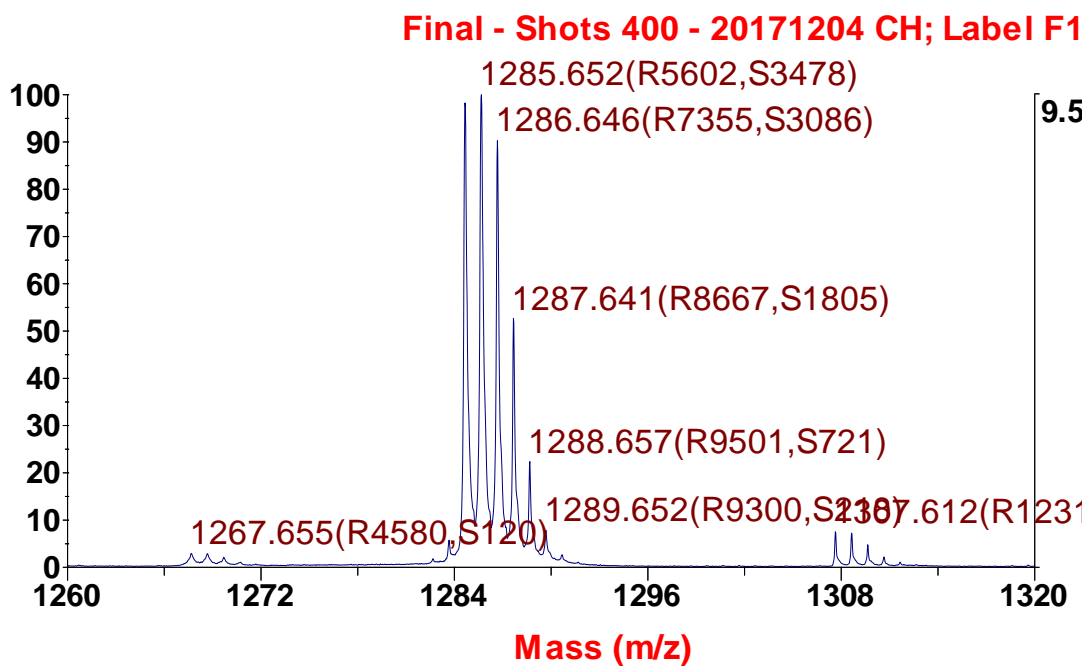
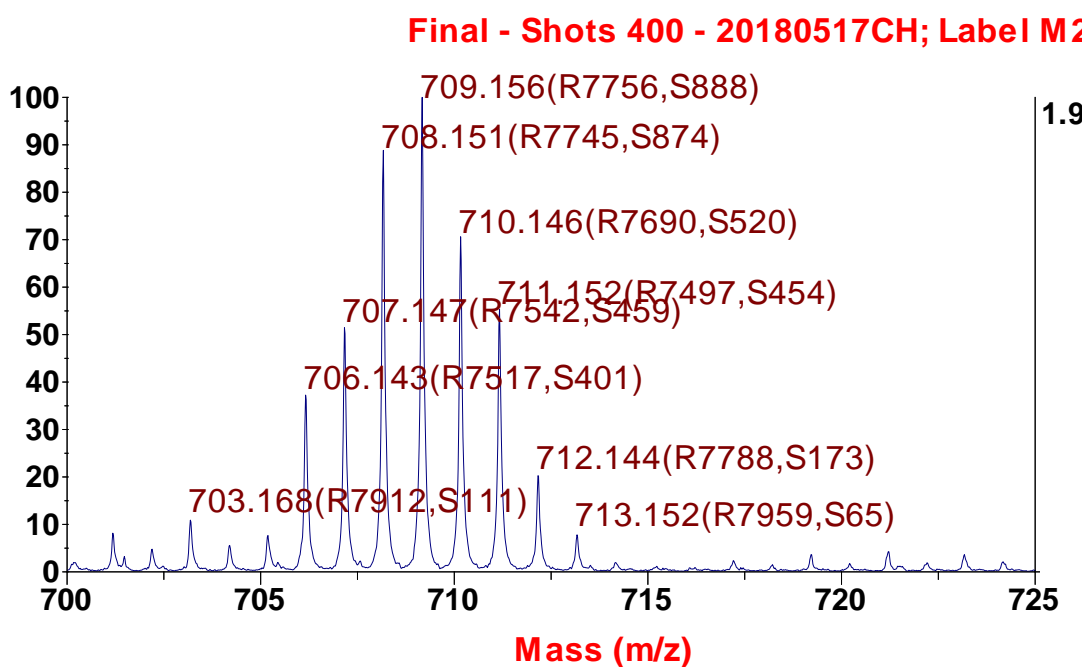
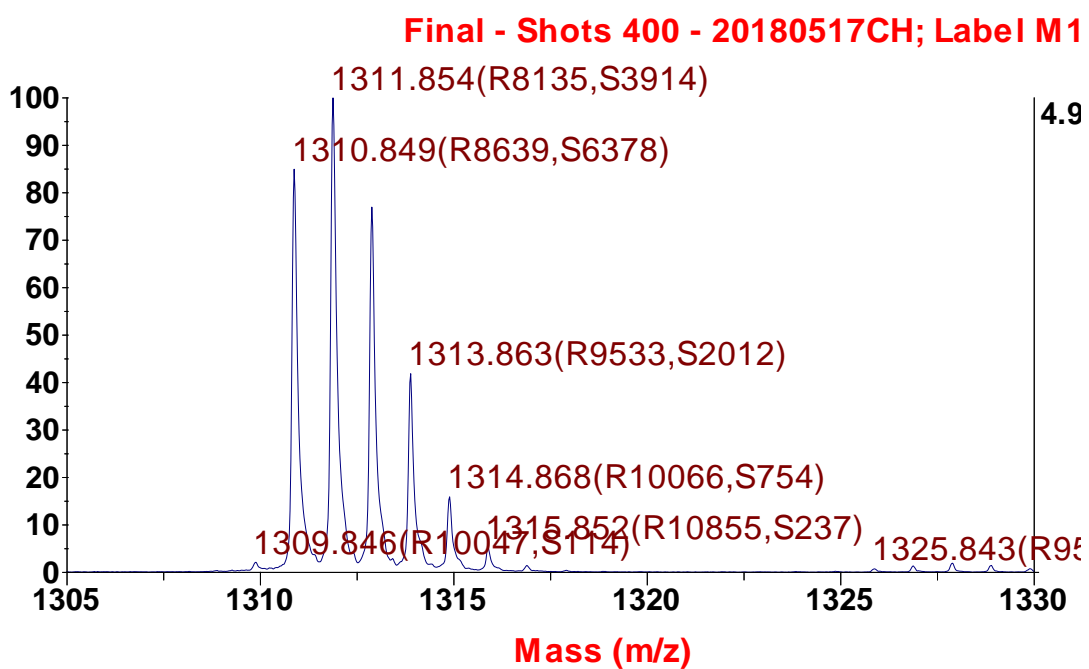


Figure 42: Mass spectrometry of T221.



**Figure 43:** Mass spectrometry of compound (9).



**Figure 44:** Mass spectrometry of T222.

## REFERENCES

1. Grätzel, M., Photoelectrochemical cells. *Nature* **2001**, *414*, 338.
2. Lewis, N. S. N., D. G., , Powering the planet: Chemical challenges in solar energy utilization. *Proceedings of the National Academy of Sciences* **2006**, *103* (43).
3. Grätzel, M., Solar Energy Conversion by Dye-Sensitized Photovoltaic Cells. *Inorganic Chemistry* **2005**, *44* (20), 6841-6851.
4. Green, M. A.; Emery, K.; Hishikawa, Y.; Warta, W., Solar cell efficiency tables (version 37). *Progress in Photovoltaics: Research and Applications* **2011**, *19* (1), 84-92.
5. Shockley, W.; Queisser, H. J., Detailed Balance Limit of Efficiency of p-n Junction Solar Cells. *Journal of Applied Physics* **1961**, *32* (3), 510-519.
6. Gerischer, H.; Michel-Beyerle, M. E.; Rebentrost, F.; Tributsch, H., Sensitization of charge injection into semiconductors with large band gap. *Electrochimica Acta* **1968**, *13* (6), 1509-1515.
7. O'Regan, B.; Grätzel, M., A low-cost, high-efficiency solar cell based on dye-sensitized colloidal TiO<sub>2</sub> films. *Nature* **1991**, *353*, 737.
8. Kakiage, K.; Aoyama, Y.; Yano, T.; Oya, K.; Fujisawa, J.-i.; Hanaya, M., Highly-efficient dye-sensitized solar cells with collaborative sensitization by silyl-anchor and carboxy-anchor dyes. *Chemical Communications* **2015**, *51* (88), 15894-15897.
9. Mathew, S.; Yella, A.; Gao, P.; Humphry-Baker, R.; Curchod, B. F. E.; Ashari-Astani, N.; Tavernelli, I.; Rothlisberger, U.; Nazeeruddin, M. K.; Grätzel, M., Dye-sensitized solar cells with 13% efficiency achieved through the molecular engineering of porphyrin sensitizers. *Nature Chemistry* **2014**, *6*, 242.
10. Yella, A.; Lee, H.-W.; Tsao, H. N.; Yi, C.; Chandiran, A. K.; Nazeeruddin, M. K.; Diao, E. W.-G.; Yeh, C.-Y.; Zakeeruddin, S. M.; Grätzel, M., Porphyrin-Sensitized Solar Cells with Cobalt (II/III)-Based Redox Electrolyte Exceed 12 Percent Efficiency. *Science* **2011**, *334* (6056), 629-634.
11. Gong, J.; Liang, J.; Sumathy, K., Review on dye-sensitized solar cells (DSSCs): Fundamental concepts and novel materials. *Renewable and Sustainable Energy Reviews* **2012**, *16* (8), 5848-5860.
12. Hagfeldt, A.; Grätzel, M., Molecular Photovoltaics. *Accounts of Chemical Research* **2000**, *33* (5), 269-277.
13. Asbury, J. B.; Hao, E.; Wang, Y.; Ghosh, H. N.; Lian, T., Ultrafast Electron Transfer Dynamics from Molecular Adsorbates to Semiconductor Nanocrystalline Thin Films. *The Journal of Physical Chemistry B* **2001**, *105* (20), 4545-4557.
14. Tachibana, Y.; Haque, S. A.; Mercer, I. P.; Moser, J. E.; Klug, D. R.; Durrant, J. R., Modulation of the Rate of Electron Injection in Dye-Sensitized Nanocrystalline TiO<sub>2</sub> Films by Externally Applied Bias. *The Journal of Physical Chemistry B* **2001**, *105* (31), 7424-7431.
15. Listorti, A.; O'Regan, B.; Durrant, J. R., Electron Transfer Dynamics in Dye-Sensitized Solar Cells. *Chemistry of Materials* **2011**, *23* (15), 3381-3399.
16. Fabregat-Santiago, F.; Bisquert, J.; Garcia-Belmonte, G.; Boschloo, G.; Hagfeldt, A., Influence of electrolyte in transport and recombination in dye-sensitized solar cells studied by impedance spectroscopy. *Solar Energy Materials and Solar Cells* **2005**, *87* (1), 117-131.

17. Nelson, J.; Chandler, R. E., Random walk models of charge transfer and transport in dye sensitized systems. *Coordination Chemistry Reviews* **2004**, *248* (13), 1181-1194.
18. Thompson, T. L.; Yates, J. T., Surface Science Studies of the Photoactivation of TiO<sub>2</sub>New Photochemical Processes. *Chemical Reviews* **2006**, *106* (10), 4428-4453.
19. Boschloo, G.; Hagfeldt, A., Characteristics of the Iodide/Triiodide Redox Mediator in Dye-Sensitized Solar Cells. *Accounts of Chemical Research* **2009**, *42* (11), 1819-1826.
20. Hirata, N.; Lagref, J. J.; Palomares, E. J.; Durrant, J. R.; Nazeeruddin, M. K.; Grätzel, M.; Di Censo, D., Supramolecular control of charge-transfer dynamics on dye-sensitized nanocrystalline TiO<sub>2</sub> films. *Chemistry* **2004**, *10* (3), 595-602.
21. Haque, S. A.; Handa, S.; Peter, K.; Palomares, E.; Thelakkat, M.; Durrant, J. R., Supermolecular control of charge transfer in dye-sensitized nanocrystalline TiO<sub>2</sub> films: towards a quantitative structure-function relationship. *Angewandte Chemie International Edition Engl* **2005**, *44* (35), 5740-4.
22. Cameron, P. J.; Peter, L. M.; Hore, S., How Important is the Back Reaction of Electrons via the Substrate in Dye-Sensitized Nanocrystalline Solar Cells? *The Journal of Physical Chemistry B* **2005**, *109* (2), 930-936.
23. Hagberg, D. P.; Yum, J.-H.; Lee, H.; De Angelis, F.; Marinado, T.; Karlsson, K. M.; Humphry-Baker, R.; Sun, L.; Hagfeldt, A.; Grätzel, M.; Nazeeruddin, M. K., Molecular Engineering of Organic Sensitizers for Dye-Sensitized Solar Cell Applications. *Journal of the American Chemical Society* **2008**, *130* (19), 6259-6266.
24. Boschloo, G.; Häggman, L.; Hagfeldt, A., Quantification of the Effect of 4-tert-Butylpyridine Addition to I<sup>-</sup>/I<sub>3</sub><sup>-</sup> Redox Electrolytes in Dye-Sensitized Nanostructured TiO<sub>2</sub> Solar Cells. *The Journal of Physical Chemistry B* **2006**, *110* (26), 13144-13150.
25. Nakade, S.; Kanzaki, T.; Kubo, W.; Kitamura, T.; Wada, Y.; Yanagida, S., Role of Electrolytes on Charge Recombination in Dye-Sensitized TiO<sub>2</sub> Solar Cell (1): The Case of Solar Cells Using the I<sup>-</sup>/I<sub>3</sub><sup>-</sup> Redox Couple. *The Journal of Physical Chemistry B* **2005**, *109* (8), 3480-3487.
26. Kalyanasundaram, K.-Dye-Sensitized Solar Cells-Taylor & Francis (2010).pdf.
27. Park, N. G.; van de Lagemaat, J.; Frank, A. J., Comparison of Dye-Sensitized Rutile- and Anatase-Based TiO<sub>2</sub> Solar Cells. *The Journal of Physical Chemistry B* **2000**, *104* (38), 8989-8994.
28. Zhang, Z.; Ito, S.; O'Regan, B.; Kuang, D.; Zakeeruddin, S. M.; Liska, P.; Charvet, R.; Comte, P.; Nazeeruddin, M. K.; Péchy, P.; Humphry-Baker, R.; Koyanagi, T.; Mizuno, T.; Grätzel, M., The Electronic Role of the TiO<sub>2</sub>Light-Scattering Layer in Dye-Sensitized Solar Cells. *Zeitschrift für Physikalische Chemie* **2007**, *221* (3), 319-327.
29. Hore, S.; Vetter, C.; Kern, R.; Smit, H.; Hinsch, A., Influence of scattering layers on efficiency of dye-sensitized solar cells. *Solar Energy Materials and Solar Cells* **2006**, *90* (9), 1176-1188.
30. Nazeeruddin, M. K.; Kay, A.; Rodicio, I.; Humphry-Baker, R.; Mueller, E.; Liska, P.; Vlachopoulos, N.; Graetzel, M., Conversion of light to electricity by cis-X<sub>2</sub>bis(2,2'-bipyridyl-4,4'-dicarboxylate)ruthenium(II) charge-transfer sensitizers (X = Cl<sup>-</sup>, Br<sup>-</sup>, I<sup>-</sup>, CN<sup>-</sup>, and SCN<sup>-</sup>) on nanocrystalline titanium dioxide electrodes. *Journal of the American Chemical Society* **1993**, *115* (14), 6382-6390.
31. Sommeling, P. M.; O'Regan, B. C.; Haswell, R. R.; Smit, H. J. P.; Bakker, N. J.; Smits, J. J. T.; Kroon, J. M.; van Roosmalen, J. A. M., Influence of a TiCl<sub>4</sub> Post-



Treatment on Nanocrystalline TiO<sub>2</sub> Films in Dye-Sensitized Solar Cells. *The Journal of Physical Chemistry B* **2006**, *110* (39), 19191-19197.

32. Koide, N.; Islam, A.; Chiba, Y.; Han, L., Improvement of efficiency of dye-sensitized solar cells based on analysis of equivalent circuit. *Journal of Photochemistry and Photobiology A: Chemistry* **2006**, *182* (3), 296-305.

33. Pysch, D.; Mette, A.; Glunz, S. W., A review and comparison of different methods to determine the series resistance of solar cells. *Solar Energy Materials and Solar Cells* **2007**, *91* (18), 1698-1706.

34. Zhang, B.; Wang, D.; Hou, Y.; Yang, S.; Yang, X. H.; Zhong, J. H.; Liu, J.; Wang, H. F.; Hu, P.; Zhao, H. J.; Yang, H. G., Facet-Dependent Catalytic Activity of Platinum Nanocrystals for Triiodide Reduction in Dye-Sensitized Solar Cells. *Scientific Reports* **2013**, *3*, 1836.

35. Gonçalves, L. M.; de Zea Bermudez, V.; Ribeiro, H. A.; Mendes, A. M., Dye-sensitized solar cells: A safe bet for the future. *Energy & Environmental Science* **2008**, *1* (6).

36. Wu, J.; Lan, Z.; Lin, J.; Huang, M.; Huang, Y.; Fan, L.; Luo, G., Electrolytes in Dye-Sensitized Solar Cells. *Chemical Reviews* **2015**, *115* (5), 2136-2173.

37. Yu, Z.; Vlachopoulos, N.; Gorlov, M.; Kloo, L., Liquid electrolytes for dye-sensitized solar cells. *Dalton Transactions* **2011**, *40* (40), 10289-10303.

38. Bella, F.; Gerbaldi, C.; Barolo, C.; Grätzel, M., Aqueous dye-sensitized solar cells. *Chemical Society Reviews* **2015**, *44* (11), 3431-73.

39. Fukui, A.; Komiya, R.; Yamanaka, R.; Islam, A.; Han, L., Effect of a redox electrolyte in mixed solvents on the photovoltaic performance of a dye-sensitized solar cell. *Solar Energy Materials and Solar Cells* **2006**, *90* (5), 649-658.

40. Lee, K.-M.; Suryanarayanan, V.; Ho, K.-C., Influences of different TiO<sub>2</sub> morphologies and solvents on the photovoltaic performance of dye-sensitized solar cells. *Journal of Power Sources* **2009**, *188* (2), 635-641.

41. Kawano, R.; Matsui, H.; Matsuyama, C.; Sato, A.; Susan, M. A. B. H.; Tanabe, N.; Watanabe, M., High performance dye-sensitized solar cells using ionic liquids as their electrolytes. *Journal of Photochemistry and Photobiology A: Chemistry* **2004**, *164* (1), 87-92.

42. Gorlov, M.; Kloo, L., Ionic liquid electrolytes for dye-sensitized solar cells. *Dalton Trans* **2008**, (20), 2655-66.

43. Kambe, S.; Nakade, S.; Kitamura, T.; Wada, Y.; Yanagida, S., Influence of the Electrolytes on Electron Transport in Mesoporous TiO<sub>2</sub>-Electrolyte Systems. *The Journal of Physical Chemistry B* **2002**, *106* (11), 2967-2972.

44. Huang, S. Y.; Schlichthörl, G.; Nozik, A. J.; Grätzel, M.; Frank, A. J., Charge Recombination in Dye-Sensitized Nanocrystalline TiO<sub>2</sub> Solar Cells. *The Journal of Physical Chemistry B* **1997**, *101* (14), 2576-2582.

45. Schlichthörl, G.; Huang, S. Y.; Sprague, J.; Frank, A. J., Band Edge Movement and Recombination Kinetics in Dye-Sensitized Nanocrystalline TiO<sub>2</sub> Solar Cells: A Study by Intensity Modulated Photovoltage Spectroscopy. *The Journal of Physical Chemistry B* **1997**, *101* (41), 8141-8155.

46. Kusama, H.; Arakawa, H., Influence of pyrazole derivatives in I<sup>-</sup>/I<sub>3</sub><sup>-</sup> redox electrolyte solution on Ru(II)-dye-sensitized TiO<sub>2</sub> solar cell performance. *Solar Energy Materials and Solar Cells* **2005**, *85* (3), 333-344.

47. Kusama, H.; Arakawa, H., Influence of pyrimidine additives in electrolytic solution on dye-sensitized solar cell performance. *Journal of Photochemistry and Photobiology A: Chemistry* **2003**, *160* (3), 171-179.
48. Kusama, H.; Arakawa, H., Influence of benzimidazole additives in electrolytic solution on dye-sensitized solar cell performance. *Journal of Photochemistry and Photobiology A: Chemistry* **2004**, *162* (2), 441-448.
49. Kopidakis, N.; Schiff, E. A.; Park, N. G.; van de Lagemaat, J.; Frank, A. J., Ambipolar Diffusion of Photocarriers in Electrolyte-Filled, Nanoporous TiO<sub>2</sub>. *The Journal of Physical Chemistry B* **2000**, *104* (16), 3930-3936.
50. Nistér, D.; Keis, K.; Lindquist, S.-E.; Hagfeldt, A., A detailed analysis of ambipolar diffusion in nanostructured metal oxide films. *Solar Energy Materials and Solar Cells* **2002**, *73* (4), 411-423.
51. Liu, Y.; Hagfeldt, A.; Xiao, X.-R.; Lindquist, S.-E., Investigation of influence of redox species on the interfacial energetics of a dye-sensitized nanoporous TiO<sub>2</sub> solar cell. *Solar Energy Materials and Solar Cells* **1998**, *55* (3), 267-281.
52. Zeng, W.; Cao, Y.; Bai, Y.; Wang, Y.; Shi, Y.; Zhang, M.; Wang, F.; Pan, C.; Wang, P., Efficient Dye-Sensitized Solar Cells with an Organic Photosensitizer Featuring Orderly Conjugated Ethylenedioxythiophene and Dithienosilole Blocks. *Chemistry of Materials* **2010**, *22* (5), 1915-1925.
53. Yu, Q.; Wang, Y.; Yi, Z.; Zu, N.; Zhang, J.; Zhang, M.; Wang, P., High-Efficiency Dye-Sensitized Solar Cells: The Influence of Lithium Ions on Exciton Dissociation, Charge Recombination, and Surface States. *ACS Nano* **2010**, *4* (10), 6032-6038.
54. Chiba, Y.; Islam, A.; Watanabe, Y.; Komiya, R.; Koide, N.; Han, L., Dye-Sensitized Solar Cells with Conversion Efficiency of 11.1%. *Japanese Journal of Applied Physics* **2006**, *45* (No. 25), L638-L640.
55. Anderson, A. Y.; Barnes, P. R. F.; Durrant, J. R.; O'Regan, B. C., Quantifying Regeneration in Dye-Sensitized Solar Cells. *The Journal of Physical Chemistry C* **2011**, *115* (5), 2439-2447.
56. Martinson, A. B.; Hamann, T. W.; Pellin, M. J.; Hupp, J. T., New architectures for dye-sensitized solar cells. *Chemistry* **2008**, *14* (15), 4458-67.
57. Tian, H.; Sun, L., Iodine-free redox couples for dye-sensitized solar cells. *Journal of Materials Chemistry* **2011**, *21* (29).
58. Feldt, S. M.; Gibson, E. A.; Gabrielsson, E.; Sun, L.; Boschloo, G.; Hagfeldt, A., Design of Organic Dyes and Cobalt Polypyridine Redox Mediators for High-Efficiency Dye-Sensitized Solar Cells. *Journal of the American Chemical Society* **2010**, *132* (46), 16714-16724.
59. Yum, J.-H.; Baranoff, E.; Kessler, F.; Moehl, T.; Ahmad, S.; Bessho, T.; Marchioro, A.; Ghadiri, E.; Moser, J.-E.; Yi, C.; Nazeeruddin, M. K.; Grätzel, M., A cobalt complex redox shuttle for dye-sensitized solar cells with high open-circuit potentials. *Nature Communications* **2012**, *3*, 631.
60. DeVries, M. J.; Pellin, M. J.; Hupp, J. T., Dye-Sensitized Solar Cells: Driving-Force Effects on Electron Recombination Dynamics with Cobalt-Based Shuttles. *Langmuir* **2010**, *26* (11), 9082-9087.
61. Klahr, B. M.; Hamann, T. W., Performance Enhancement and Limitations of Cobalt Bipyridyl Redox Shuttles in Dye-Sensitized Solar Cells. *The Journal of Physical Chemistry C* **2009**, *113* (31), 14040-14045.

62. Nelson, J. J.; Amick, T. J.; Elliott, C. M., Mass Transport of Polypyridyl Cobalt Complexes in Dye-Sensitized Solar Cells with Mesoporous TiO<sub>2</sub> Photoanodes. *The Journal of Physical Chemistry C* **2008**, *112* (46), 18255-18263.
63. Liberatore, M.; Petrocco, A.; Caprioli, F.; La Mesa, C.; Decker, F.; Bignozzi, C. A., Mass transport and charge transfer rates for Co(III)/Co(II) redox couple in a thin-layer cell. *Electrochimica Acta* **2010**, *55* (12), 4025-4029.
64. Cameron, P. J.; Peter, L. M.; Zakeeruddin, S. M.; Grätzel, M., Electrochemical studies of the Co(III)/Co(II)(dbbip)<sub>2</sub> redox couple as a mediator for dye-sensitized nanocrystalline solar cells. *Coordination Chemistry Reviews* **2004**, *248* (13), 1447-1453.
65. Kim, H. S.; Ko, S. B.; Jang, I. H.; Park, N. G., Improvement of mass transport of the [Co(bpy)<sub>3</sub>](II/III) redox couple by controlling nanostructure of TiO<sub>2</sub> films in dye-sensitized solar cells. *Chem Commun (Camb)* **2011**, *47* (47), 12637-9.
66. Safdari, M.; Lohse, P. W.; Häggman, L.; Frykstrand, S.; Högberg, D.; Rutland, M.; Asencio, R. A.; Gardner, J.; Kloo, L.; Hagfeldt, A.; Boschloo, G., Investigation of cobalt redox mediators and effects of TiO<sub>2</sub> film topology in dye-sensitized solar cells. *RSC Advances* **2016**, *6* (61), 56580-56588.
67. Yella, A.; Mathew, S.; Aghazada, S.; Comte, P.; Grätzel, M.; Nazeeruddin, M. K., Dye-sensitized solar cells using cobalt electrolytes: the influence of porosity and pore size to achieve high-efficiency. *Journal of Materials Chemistry C* **2017**, *5* (11), 2833-2843.
68. Freitag, M.; Daniel, Q.; Pazoki, M.; Sveinbjörnsson, K.; Zhang, J.; Sun, L.; Hagfeldt, A.; Boschloo, G., High-efficiency dye-sensitized solar cells with molecular copper phenanthroline as solid hole conductor. *Energy & Environmental Science* **2015**, *8* (9), 2634-2637.
69. Daeneke, T.; Kwon, T.-H.; Holmes, A. B.; Duffy, N. W.; Bach, U.; Spiccia, L., High-efficiency dye-sensitized solar cells with ferrocene-based electrolytes. *Nature Chemistry* **2011**, *3*, 211.
70. Wang, M.; Chamberland, N.; Breau, L.; Moser, J.-E.; Humphry-Baker, R.; Marsan, B.; Zakeeruddin, S. M.; Grätzel, M., An organic redox electrolyte to rival triiodide/iodide in dye-sensitized solar cells. *Nature Chemistry* **2010**, *2*, 385.
71. Clifford, J. N.; Martínez-Ferrero, E.; Viterisi, A.; Palomares, E., Sensitizer molecular structure-device efficiency relationship in dye sensitized solar cells. *Chemical Society Reviews* **2011**, *40* (3), 1635-1646.
72. Qin, Y.; Peng, Q., Ruthenium Sensitizers and Their Applications in Dye-Sensitized Solar Cells. *International Journal of Photoenergy* **2012**, *2012*, 1-21.
73. Chen, C.; Yang, X.; Cheng, M.; Zhang, F.; Sun, L., Degradation of cyanoacrylic acid-based organic sensitizers in dye-sensitized solar cells. *ChemSusChem* **2013**, *6* (7), 1270-5.
74. Ooyama, Y.; Inoue, S.; Nagano, T.; Kushimoto, K.; Ohshita, J.; Imae, I.; Komaguchi, K.; Harima, Y., Dye-sensitized solar cells based on donor-acceptor pi-conjugated fluorescent dyes with a pyridine ring as an electron-withdrawing anchoring group. *Angew Chem Int Ed Engl* **2011**, *50* (32), 7429-33.
75. Mishra, A.; Fischer, M. K.; Bauerle, P., Metal-free organic dyes for dye-sensitized solar cells: from structure: property relationships to design rules. *Angewandte Chemie International Edition Engl* **2009**, *48* (14), 2474-99.
76. Kim, S.; Lee, J. K.; Kang, S. O.; Ko, J.; Yum, J. H.; Fantacci, S.; De Angelis, F.; Di Censo, D.; Nazeeruddin, M. K.; Grätzel, M., Molecular Engineering of Organic

Sensitizers for Solar Cell Applications. *Journal of the American Chemical Society* **2006**, *128* (51), 16701-16707.

77. Liang, M.; Lu, M.; Wang, Q.-L.; Chen, W.-Y.; Han, H.-Y.; Sun, Z.; Xue, S., Efficient dye-sensitized solar cells with triarylamine organic dyes featuring functionalized-truxene unit. *Journal of Power Sources* **2011**, *196* (3), 1657-1664.

78. Choi, H.; Baik, C.; Kang, S. O.; Ko, J.; Kang, M. S.; Nazeeruddin, M. K.; Gratzel, M., Highly efficient and thermally stable organic sensitizers for solvent-free dye-sensitized solar cells. *Angewandte Chemie International Edition Engl* **2008**, *47* (2), 327-30.

79. Kitamura, T.; Ikeda, M.; Shigaki, K.; Inoue, T.; Anderson, N. A.; Ai, X.; Lian, T.; Yanagida, S., Phenyl-Conjugated Oligoene Sensitizers for TiO<sub>2</sub> Solar Cells. *Chemistry of Materials* **2004**, *16* (9), 1806-1812.

80. Ellis, H.; Eriksson, S. K.; Feldt, S. M.; Gabrielsson, E.; Lohse, P. W.; Lindblad, R.; Sun, L.; Rensmo, H.; Boschloo, G.; Hagfeldt, A., Linker Unit Modification of Triphenylamine-Based Organic Dyes for Efficient Cobalt Mediated Dye-Sensitized Solar Cells. *The Journal of Physical Chemistry C* **2013**, *117* (41), 21029-21036.

81. Lee, D. H.; Lee, M. J.; Song, H. M.; Song, B. J.; Seo, K. D.; Pastore, M.; Anselmi, C.; Fantacci, S.; De Angelis, F.; Nazeeruddin, M. K.; Grätzel, M.; Kim, H. K., Organic dyes incorporating low-band-gap chromophores based on  $\pi$ -extended benzothiadiazole for dye-sensitized solar cells. *Dyes and Pigments* **2011**, *91* (2), 192-198.

82. Burke, A.; Schmidt-Mende, L.; Ito, S.; Gratzel, M., A novel blue dye for near-IR 'dye-sensitized' solar cell applications. *Chem Commun (Camb)* **2007**, (3), 234-6.

83. Paek, S.; Choi, H.; Kim, C.; Cho, N.; So, S.; Song, K.; Nazeeruddin, M. K.; Ko, J., Efficient and stable panchromatic squaraine dyes for dye-sensitized solar cells. *Chem Commun (Camb)* **2011**, *47* (10), 2874-6.

84. Park, J.; Barolo, C.; Sauvage, F.; Barbero, N.; Benzi, C.; Quagliotto, P.; Coluccia, S.; Di Censo, D.; Gratzel, M.; Nazeeruddin, M. K.; Viscardi, G., Symmetric vs. asymmetric squaraines as photosensitizers in mesoscopic injection solar cells: a structure-property relationship study. *Chem Commun (Camb)* **2012**, *48* (22), 2782-4.

85. Shi, Y.; Hill, R. B.; Yum, J. H.; Dualeh, A.; Barlow, S.; Gratzel, M.; Marder, S. R.; Nazeeruddin, M. K., A high-efficiency panchromatic squaraine sensitizer for dye-sensitized solar cells. *Angewandte Chemie International Edition Engl* **2011**, *50* (29), 6619-21.

86. Yum, J. H.; Walter, P.; Huber, S.; Rentsch, D.; Geiger, T.; Nuesch, F.; De Angelis, F.; Gratzel, M.; Nazeeruddin, M. K., Efficient far red sensitization of nanocrystalline TiO<sub>2</sub> films by an unsymmetrical squaraine dye. *Journal of the American Chemical Society* **2007**, *129* (34), 10320-1.

87. Geiger, T.; Kuster, S.; Yum, J.-H.; Moon, S.-J.; Nazeeruddin, M. K.; Grätzel, M.; Nüesch, F., Molecular Design of Unsymmetrical Squaraine Dyes for High Efficiency Conversion of Low Energy Photons into Electrons Using TiO<sub>2</sub> Nanocrystalline Films. *Advanced Functional Materials* **2009**, *19* (17), 2720-2727.

88. Shibano, Y.; Umeyama, T.; Matano, Y.; Imahori, H., Electron-Donating Perylene Tetracarboxylic Acids for Dye-Sensitized Solar Cells. *Organic Letters* **2007**, *9* (10), 1971-1974.

89. Mao, J.; Yang, J.; Teuscher, J.; Moehl, T.; Yi, C.; Humphry-Baker, R.; Comte, P.; Grätzel, C.; Hua, J.; Zakeeruddin, S. M.; Tian, H.; Grätzel, M., Thiadiazolo[3,4-

- c]pyridine Acceptor Based Blue Sensitizers for High Efficiency Dye-Sensitized Solar Cells. *The Journal of Physical Chemistry C* **2014**, *118* (30), 17090-17099.
90. Ren, Y.; Sun, D.; Cao, Y.; Tsao, H. N.; Yuan, Y.; Zakeeruddin, S. M.; Wang, P.; Grätzel, M., A Stable Blue Photosensitizer for Color Palette of Dye-Sensitized Solar Cells Reaching 12.6% Efficiency. *Journal of the American Chemical Society* **2018**, *140* (7), 2405-2408.
91. Nielsen, C. B.; Turbiez, M.; McCulloch, I., Recent advances in the development of semiconducting DPP-containing polymers for transistor applications. *Advanced Materials* **2013**, *25* (13), 1859-80.
92. Qu, S.; Tian, H., Diketopyrrolopyrrole (DPP)-based materials for organic photovoltaics. *Chem Commun (Camb)* **2012**, *48* (25), 3039-51.
93. Farnum, D. G.; Mehta, G.; Moore, G. G. I.; Siegal, F. P., Attempted reformatkii reaction of benzonitrile, 1,4-diketo-3,6-diphenylpyrrolo[3,4-C]pyrrole. A lactam analogue of pentalene. *Tetrahedron Letters* **1974**, *15* (29), 2549-2552.
94. Qu, S.; Wang, B.; Guo, F.; Li, J.; Wu, W.; Kong, C.; Long, Y.; Hua, J., New diketo-pyrrolo-pyrrole (DPP) sensitizer containing a furan moiety for efficient and stable dye-sensitized solar cells. *Dyes and Pigments* **2012**, *92* (3), 1384-1393.
95. Warnan, J.; Favereau, L.; Pellegrin, Y.; Blart, E.; Jacquemin, D.; Odobel, F., A compact diketopyrrolopyrrole dye as efficient sensitizer in titanium dioxide dye-sensitized solar cells. *Journal of Photochemistry and Photobiology A: Chemistry* **2011**, *226* (1), 9-15.
96. Qu, S.; Qin, C.; Islam, A.; Wu, Y.; Zhu, W.; Hua, J.; Tian, H.; Han, L., A novel D-A-pi-A organic sensitizer containing a diketopyrrolopyrrole unit with a branched alkyl chain for highly efficient and stable dye-sensitized solar cells. *Chem Commun (Camb)* **2012**, *48* (55), 6972-4.
97. Zhang, F.; Jiang, K.-J.; Huang, J.-H.; Yu, C.-C.; Li, S.-G.; Chen, M.-G.; Yang, L.-M.; Song, Y.-L., A novel compact DPP dye with enhanced light harvesting and charge transfer properties for highly efficient DSCs. *Journal of Materials Chemistry A* **2013**, *1* (15).
98. Ganesan, P.; Yella, A.; Holcombe, T. W.; Gao, P.; Rajalingam, R.; Al-Muhtaseb, S. A.; Grätzel, M.; Nazeeruddin, M. K., Unravel the Impact of Anchoring Groups on the Photovoltaic Performances of Diketopyrrolopyrrole Sensitizers for Dye-Sensitized Solar Cells. *ACS Sustainable Chemistry & Engineering* **2015**, *3* (10), 2389-2396.
99. Chiu, K. Y.; Govindan, V.; Lin, L.-C.; Huang, S.-H.; Hu, J.-C.; Lee, K.-M.; Gavin Tsai, H.-H.; Chang, S.-H.; Wu, C.-G., DPP containing D- $\pi$ -A organic dyes toward highly efficient dye-sensitized solar cells. *Dyes and Pigments* **2016**, *125*, 27-35.
100. Hu, Y.; Robertson, N., Atypical organic dyes used as sensitizers for efficient dye-sensitized solar cells. *Frontiers of Optoelectronics* **2016**, *9* (1), 38-43.
101. Bahng, H.-W.; Hagfeldt, A.; Moser, J.-E., Donor Effect on the Photoinduced Interfacial Charge Transfer Dynamics of D- $\pi$ -A Diketopyrrolopyrrole Dye Sensitizers Adsorbed on Titanium Dioxide. *The Journal of Physical Chemistry C* **2018**, *122* (34), 19359-19369.
102. Yum, J. H.; Holcombe, T. W.; Kim, Y.; Rakstys, K.; Moehl, T.; Teuscher, J.; Delcamp, J. H.; Nazeeruddin, M. K.; Gratzel, M., Blue-coloured highly efficient dye-sensitized solar cells by implementing the diketopyrrolopyrrole chromophore. *Scientific Reports* **2013**, *3*, 2446.

103. Bijleveld, J. C.; Zoombelt, A. P.; Mathijssen, S. G. J.; Wienk, M. M.; Turbiez, M.; de Leeuw, D. M.; Janssen, R. A. J., Poly(diketopyrrolopyrrole-terthiophene) for Ambipolar Logic and Photovoltaics. *Journal of the American Chemical Society* **2009**, *131* (46), 16616-16617.
104. Yum, J. H.; Holcombe, T. W.; Kim, Y.; Yoon, J.; Rakstys, K.; Nazeeruddin, M. K.; Gratzel, M., Towards high-performance DPP-based sensitizers for DSC applications. *Chem Commun (Camb)* **2012**, *48* (87), 10727-9.
105. Hao, Y.; Saygili, Y.; Cong, J.; Eriksson, A.; Yang, W.; Zhang, J.; Polanski, E.; Nonomura, K.; Zakeeruddin, S. M.; Grätzel, M.; Hagfeldt, A.; Boschloo, G., Novel Blue Organic Dye for Dye-Sensitized Solar Cells Achieving High Efficiency in Cobalt-Based Electrolytes and by Co-Sensitization. *ACS Applied Materials & Interfaces* **2016**, *8* (48), 32797-32804.
106. Sacco, A., Electrochemical impedance spectroscopy: Fundamentals and application in dye-sensitized solar cells. *Renewable and Sustainable Energy Reviews* **2017**, *79*, 814-829.
107. Han, L.; Koide, N.; Chiba, Y.; Mitate, T., Modeling of an equivalent circuit for dye-sensitized solar cells. *Applied Physics Letters* **2004**, *84* (13), 2433-2435.
108. Wang, Q.; Moser, J.-E.; Grätzel, M., Electrochemical Impedance Spectroscopic Analysis of Dye-Sensitized Solar Cells. *The Journal of Physical Chemistry B* **2005**, *109* (31), 14945-14953.
109. Kern, R.; Sastrawan, R.; Ferber, J.; Stangl, R.; Luther, J., Modeling and interpretation of electrical impedance spectra of dye solar cells operated under open-circuit conditions. *Electrochimica Acta* **2002**, *47* (26), 4213-4225.
110. Sarker, S.; Ahammad, A. J. S.; Seo, H. W.; Kim, D. M., Electrochemical Impedance Spectra of Dye-Sensitized Solar Cells: Fundamentals and Spreadsheet Calculation. *International Journal of Photoenergy* **2014**, *2014*, 1-17.
111. Frisch, M. J.; al., e., *Gaussian 03; Gaussian, Inc.: Pittsburgh, PA, 2003*.
112. Cossi, M.; Barone, V., *J. Chem. Phys* **2001**, *115*, 4708-4717.
113. Li, J.; Xiong, Y.; Wu, Q.; Wang, S.; Gao, X.; Li, H., Synthesis and Physicochemical Properties of Strong Electron Acceptor 14,14,15,15-Tetracyano-6,13-pentacenequinodimethane (TCPQ) Diimide. *European Journal of Organic Chemistry* **2012**, *2012* (31), 6136-6139.
114. Hwang, D. K.; Dasari, R. R.; Fenoll, M.; Alain-Rizzo, V.; Dindar, A.; Shim, J. W.; Deb, N.; Fuentes-Hernandez, C.; Barlow, S.; Bucknall, D. G.; Audebert, P.; Marder, S. R.; Kippelen, B., Stable solution-processed molecular n-channel organic field-effect transistors. *Advanced Materials* **2012**, *24* (32), 4445-50.
115. Ye, Q.; Neo, W. T.; Cho, C. M.; Yang, S. W.; Lin, T.; Zhou, H.; Yan, H.; Lu, X.; Chi, C.; Xu, J., Synthesis of ultrahighly electron-deficient pyrrolo[3,4-d]pyridazine-5,7-dione by inverse electron demand Diels-Alder reaction and its application as electrochromic materials. *Organic Letters* **2014**, *16* (24), 6386-9.
116. Kobilka, B. M.; Hale, B. J.; Ewan, M. D.; Dubrovskiy, A. V.; Nelson, T. L.; Duzhko, V.; Jeffries-El, M., Influence of heteroatoms on photovoltaic performance of donor-acceptor copolymers based on 2,6-di(thiophen-2-yl)benzo[1,2-b:4,5-b']difurans and diketopyrrolopyrrole. *Polymer Chemistry* **2013**, *4* (20), 5329-5336.
117. Kantchev, E. A.; Norsten, T. B.; Tan, M. L.; Ng, J. J.; Sullivan, M. B., Thiophene-containing Pechmann dyes and related compounds: synthesis, and experimental and DFT characterisation. *Chemistry* **2012**, *18* (2), 695-708.

118. Cai, Z.; Guo, Y.; Yang, S.; Peng, Q.; Luo, H.; Liu, Z.; Zhang, G.; Liu, Y.; Zhang, D., New Donor–Acceptor–Donor Molecules with Pechmann Dye as the Core Moiety for Solution-Processed Good-Performance Organic Field-Effect Transistors. *Chemistry of Materials* **2013**, *25* (3), 471-478.
119. Kobilka, B. M.; Hale, B. J.; Ewan, M. D.; Dubrovskiy, A. V.; Nelson, T. L.; Duzhko, V.; Jeffries-El, M., Influence of heteroatoms on photovoltaic performance of donor–acceptor copolymers based on 2,6-di(thiophen-2-yl)benzo[1,2-b:4,5-b']difurans and diketopyrrolopyrrole. *Polymer Chemistry* **2013**, *4* (20).
120. Hilal, H. M.; El Bitar Nehme, M. A.; Ghaddar, T. H., Large Enhancement of Dye Sensitized Solar Cell Efficiency by Co-sensitizing Pyridyl- and Carboxylic Acid-Based Dyes. *ACS Applied Energy Materials* **2018**, *1* (6), 2776-2783.
121. Su, J.; Zhu, S.; Chen, R.; An, Z.; Chen, X.; Chen, P., Study on dye-loading mode on TiO<sub>2</sub> films and impact of co-sensitizers on highly efficient co-sensitized solar cells. *Journal of Materials Science: Materials in Electronics* **2016**, *28* (5), 3962-3969.
122. González-Pedro, V.; Xu, X.; Mora-Seró, I.; Bisquert, J., Modeling High-Efficiency Quantum Dot Sensitized Solar Cells. *ACS Nano* **2010**, *4* (10), 5783-5790.
123. Guillén, E.; Peter, L. M.; Anta, J. A., Electron Transport and Recombination in ZnO-Based Dye-Sensitized Solar Cells. *The Journal of Physical Chemistry. C* **2011**, *115* (45), 22622-22632.
124. Pazoki, M.; Lohse, P. W.; Taghavinia, N.; Hagfeldt, A.; Boschloo, G., The effect of dye coverage on the performance of dye-sensitized solar cells with a cobalt-based electrolyte. *Physical Chemistry Chemical Physics*. **2014**, *16* (18), 8503-8508.
125. Rühle, S.; Greenshtein, M.; Chen, S. G.; Merson, A.; Pizem, H.; Sukenik, C. S.; Cahen, D.; Zaban, A., Molecular Adjustment of the Electronic Properties of Nanoporous Electrodes in Dye-Sensitized Solar Cells. *The Journal of Chemistry. B* **2005**, *109* (40), 18907-18913.
126. Bisquert, J.; Cahen, D.; Hodes, G.; Rühle, S.; Zaban, A., Physical Chemical Principles of Photovoltaic Conversion with Nanoparticulate, Mesoporous Dye-Sensitized Solar Cells. *The Journal of Physical Chemistry. B* **2004**, *108* (24), 8106-8118.
127. Cahen, D.; Hodes, G.; Grätzel, M.; Guillemoles, J. F.; Riess, I., Nature of Photovoltaic Action in Dye-Sensitized Solar Cells. *The Journal of Physical Chemistry. B* **2000**, *104* (9), 2053-2059.